Controlled synthesis and properties of Neoglycoconjugates

Sebastian G. Spain

Controlled Synthesis and Properties of Neoglycoconjugates

Sebastian G. Spain

A Thesis presented for the degree of

Doctor of Philosophy

Department of Chemistry

University of Durham

England

March 2009

Dedicated to my parents, without whom I would neither be here nor the person I am

The ability to quote is a serviceable substitute for wit

W. Somerset Maugham (1874-1965)

Controlled Synthesis and Properties of Neoglycoconjugates

Sebastian G. Spain

Submitted for the degree of Doctor of Philosophy

March 2009

Abstract

Glucosyl and galactosyl bearing methacrylates were synthesised using a combination of well known carbohydrate chemistry and ultrasonic chemistry. Polymerisation of these monomers by aqueous reversible addition-fragmentation chain transfer polymerisation yielded glycosylated polymers in high yield with a high degree of control over molecular weight and narrow polydispersity. Polymers of varying levels of glycosylation could be achieved through addition of a comonomer. Block copolymers were synthesised through sequential monomer addition.

Binding studies of these polymers to *Ricinus communis* agglutinin 120 by both isothermal titration calorimetry and surface plasmon resonance found a high degree of molecular weight dependence on avidity. Studies also suggest that the increase in avidity through multivalency is due to both simultaneous binding to multiple receptors and the increased probability of binding due to the high local concentration of ligands.

Polymers synthesised have been used in the synthesis of glycosylated gold nanoparticles. Some degree of control over nanoparticle size was achieved through adjust-

ment of the gold:polymer ratio but was found to be limited. Agglutination assays show the particles display specific lectin binding but in vitro cell studies were unable to give conclusive information regarding the uptake of particles into cells.

Declaration

The work reported in this thesis is based on research carried out in the Department of Chemistry, University of Durham, England between October 2004 and December 2007. No part of this thesis has been submitted elsewhere for any other degree or qualification and it is all my own work unless referenced to the contrary in the text.

Acknowledgements

I wish to thank my supervisor Prof. Neil Cameron whose encouragement, expertise and, most importantly, patience has been near limitless in the writing of this thesis and throughout my time in the lab. I will always be pleased to consider Neil a friend and mentor. The Cameron lab was not always the happiest but without the people there it would have been a duller place. A special mention must be made of Matt 'Cotton Wool' Gibson, Luca 'Egon' Albertin, Francisco 'Paco' Fernandez-Trillo and Alex 'VPGVG' Dureault whose combined knowledge of organic synthesis and polymer chemistry was essential. To Weeman, the Johnson, Jon, Caroline, Greg, the Mikes (Big and Wee), Olivier, Geraldine, Carl and everyone else who shared CG156/169 over the years: we may not have always got on but I'm glad you were there. Thanks to Maria Bokhari for teaching me tissue culture and Stefan Przyborski and group for allowing me to use their lab for those experiments.

Appreciation must be shown to all the analytical and support staff in the Chemistry Department without whom it would fall apart. Particular thanks to Jean, Joan and the other lab attendents for polishing my bench and making me tea. Alan

Kenwright, Ian McKeag and Catherine Heffernan for the numerous long run NMRs (good use of the 700 MHz) and numerous conversations of about *nix. Lian Hutchings for all the help with the SECs and not being *that* angry when I accidently ran it dry and Doug Carswell for the TGAs. David Dixon for training and advice on ITC/SPR. Christine Richardson for the help with TEM.

To my friends, without you I don't know what I'd do, to list you all would take another page of inevitable anecdotes. I'll have a go: Pippa, John and Ben; Lucas, Faye, Dunwell, Taffy Nick, Crazy Marco, Scott, Will, Jules, Howard, Smurto, Helen, Emma, Jamie, Beckley, Smoggy, Jess, Kathryn, Aled, Dave W, Dave T, Pete and Carla, Cassie, Sophia, Ricky, Rachel, Joe, Shelley, Spikey, Barry, Ross C, Little Whittle, Amy, Tom, Kim, Ben. To all my friends outside of Durham Chemistry, I love you too but you'll never read this anyway. To the Oxford lot, thanks for letting me in to the (beer) club.

Finally I must thank my family. My Mum who, balancing patience and pestering, managed to make me finally finish this thesis and has always offered support. My Dad who may be gone but will always be the man I respect most. My brother and sister for always being there for me either with support or jibe.

Despite those mentioned above, my sanity over the last three years has been kept due to my undying love of music. Remember, "I'm only working here 'cos I need the fucking money" Million Dead - *To whom it may concern.*

Contents

List of Figures

List of Tables

Abbreviations

Aβ	amyloid β-peptide
AcGalEA	2-(2',3',4',6'-tetra-*O*-acetyl-β-D-galactosyloxy)ethyl acrylate
AcGalEMA	2-(2',3',4',6'-tetra-*O*-acetyl-β-D-galactosyloxy)ethyl methacrylate
AcGlcEA	2-(2',3',4',6'-tetra-*O*-acetyl-β-D-glucosyloxy)ethyl acrylate
AcGlcEMA	2-(2',3',4',6'-tetra-*O*-acetyl-β-D-glucosyloxy)ethyl methacrylate
ACPA	4,4'-azobis(4-cyanopentanoic acid)
AD	Alzheimer's disease
AIDS	acquired immunodeficiency syndrome
ASGPR	asialoglycoprotein receptor
ATRP	atom transfer radical polymerisation
AuNP	gold nanoparticle
BA	*n*-butyl acrylate
BBB	blood brain barrier
Con A	Concanavalin A

CPADB	(4-cyanopentanoic acid)-4-dithiobenzoate
CRD	carbohydrate recognition domain
CRP	controlled radical polymerisation
CTA	chain transfer agent
DDS	drug delivery system
DLS	dynamic light-scattering
DMAc	*N*,*N*-dimethyl acetamide
DMAEMA	2-(dimethylamino)ethyl methacrylate
DMEM	Dulbecco's modified Eagle's medium
DMF	*N*,*N*-dimethyl formamide
DMSO	dimethyl sulfoxide
DP_n	degree of polymerisation
ES^+	electrospray (positive ionisation mode)
FGF-2	fibroblast growth factor 2
FGFR-1	fibroblast growth factor receptor 1
GalEMA	2-(β-D-galactosyloxy)ethyl methacrylate
GlcEMA	2-(β-D-glucosyloxy)ethyl methacrylate
glycoNP	glycosylated gold nanoparticle
HA	hæmagglutinin
HAI	hæmagglutinin inhibitor
HEA	2-hydroxyethyl acrylate
HEMA	2-hydroxyethyl methacrylate
HIV	human immunodeficiency virus

HPLC	high performance liquid chromatography
HPMA	*N*-(2-hydroxypropyl)methacrylamide
ITC	isothermal thermal (micro)calorimetry
IUPAC	International Union of Pure and Applied Chemistry
IV	intravenous
LDL	low density lipoprotein
MADIX	macromolecular design through the interchange of xanthates
MMA	methyl methacrylate
MWCO	molecular weight cut-off
NA	neuraminidase
NAS	*N*-(acryloyloxy)succinimide
NIPAM	*N*-isopropyl acrylamide
NMP	nitroxide-mediated polymerisation
PEO/PEG	poly[ethylene oxide]/poly[ethylene glycol]
PLGA	poly[L-glutamic acid]
PNA	*Peanut agglutinin*
RAFT	reversible addition-fragmentation chain transfer
RALS	right angle light scattering
RCA_{120}	*Ricinus communis* agglutinin 120
RI	refractive index
RIP	ribosome-inactivating protein
RME	receptor-mediated endocytosis
RNA	ribose nucleic acid

ROMP	ring-opening metathesis polymerisation
SA	sialic acid a.k.a. *N*-acetyl neuraminic acid
SD	standard deviation
SEC	size exclusion chromatography
SEM	standard error measurement
SPR	surface plasmon resonance
TEM	transmission electron microscopy
TLC	thin layer chromatography
UHQ	ultra high quality

Results! Why, man, I have gotten a lot of results. I know several thousand things that won't work.

Thomas Edison (1847–1931)

1

Introduction

1.1 Carbohydrates and Glycobiology

Carbohydrates are ubiquitous throughout Nature. Although traditionally defined by the general formula $C_n(H_2O)_m$, carbohydrates are now considered to be a far wider ranging family of compounds as defined by IUPAC. [1]

> "...includes monosaccharides, oligosaccharides and polysaccharides as well as substances derived from monosaccharides by reduction of the carbonyl group (alditols), by oxidation of one or more terminal groups to carboxylic acids, or by replacement of one or more hydroxy group(s) by a hydrogen atom, an amino group, a thiol group or similar heteroatomic groups. It also includes derivatives of these compounds. The term 'sugar' is frequently applied to monosaccharides and lower oligosaccharides."

The study of carbohydrates has been central to both biological and chemical research for over a century, but early research was generally limited to the elucidation of the structure of simple sugars and the role of polysaccharides as in vivo energy sources (glycogen and starch) or structural materials (cellulose and chitin). In the latter half of the twentieth century important discoveries, such as Watkins and Morgan's recognition that blood group antigens were oligosaccharides, [2] led to carbohydrates being held in higher regard in biochemical fields. Today the biological significance of carbohydrates is well realised and carbohydrates are known to be involved in biological processes as diverse as their structures including, but not limited to, fertilisation and embryogenesis, [3] protein folding, [4–6] cell-cell recognition and the proliferation and organisation of cells in tissues. The latter was demonstrated most elegantly by Popescu and Misevic by the aggregation of coloured sponges in a

Figure 1.1: Self recognition in glyconectins: (a) Discrete aggregation of 3 species of marine sponge in the presence of Ca^{2+} ions: (b) aggregation of coloured beads coated in different glyconectins; (c) Control experiment where all beads are coated in the same glyconectin. Reprinted with permission from Macmillan Publishers Ltd: Nature, 1997. [7]

species specific manner via a Ca^{2+}-mediated carbohydrate-carbohydrate recognition process (Fig. 1.1). [7]

1.1.1 The 'Glycocode'

The prevalence of carbohydrates throughout complex biological roles, particularly those involving recognition, can be attributed to the vast quantity of information that can be conveyed within their structures. Other biopolymers, the nucleic acids and proteins, only possess one linkage type between a pair of residues; the phosphodiester and amide links respectively. Conversely carbohydrates can form 1→2, 1→3, 1→4 and 1→6 glycosidic linkages, thus introducing the possibility of branching, in both α and β configurations. The huge complexity of structure is well demonstrated when you consider the number of possible structures for a hexamer of nucleotides,

amino acids or saccharides; for nucleic acids (base set = 4) there are 4096 structures, for peptides (base set = 20) there are 6.4×10^7, but for carbohydrates there are in excess of 1.05×10^{12}. This figure is for a hexasaccharide featuring only hydroxyl groups, add to this the permutations available through modification of a hydroxyl group, through sulfation, alkylation, phosphorylation or acylation and the figures start to become unfathomable. [8] This information is the language of carbohydrate structure and has come to be known as the *glycocode*.

1.1.2 Lectins and multivalency

Like all ciphers, the glycocode requires a method of interpretation and such a role is chiefly performed by a group of carbohydrate complexing proteins known as lectins. Like carbohydrates, lectins are ubiquitous throughout nature being present in almost all organisms and viruses. Traditionally, lectins have been categorised based upon their source and/or carbohydrate specificity. Improved analytical techniques have allowed the determination of several hundred lectin amino acid sequences as well as tens of crystallographic structures, subsequently lectins may now be grouped by similarities in their structure: simple, mosaic (or multidomain) and macromolecular assemblies. These groups may be further sub-divided into discrete families which share particular sequence and structural motifs. Such subdivisions are not necessarily linked to genetic similarities between the parent organisms with seemingly unrelated species, such as plants and animals, producing lectins with high structural similarity. [9]

Simple lectins are currently the biggest family; including almost all plant lectins

and the galectins, a sub-family of β-galactoside binding mammalian proteins. Simple lectins consist of a small number of subunits, that may or may not be identical, with molecular weights $\lesssim 40$ kDa and may contain a domain that is not involved in carbohydrate-binding. Mosaic, or multidomain, lectins are a diverse family where the lectins are composed of several differing subunits only one of which contains a carbohydrate recognition domain (CRD). Typically they are monovalent, but are often membrane bound to form multivalent arrays such as those of influenza hæmagglutinin. Macromolecular assembly lectins are commonly found in bacteria and consist of a large number of individual protein subunits that assemble into helical *fimbriæ* with CRDs arranged at specific intervals.

Typically lectin–carbohydrate binding is rather weak, K_d is usually 10^{-3} - 10^{-6} M, when compared to other biological avidities. Avidin–biotin, for example, displays one of the strongest interactions found in Nature with $K_d \sim 10^{-15}$ M. [10,11] At first glance the weak interaction between lectins and carbohydrates appears to make it a poor cousin compared to others found in Nature. Their weakness may be attributed to the typically shallow nature of the carbohydrate recognition domain, which leaves it prone to exposure to solvent, resulting in few direct lectin–carbohydrate contacts. Despite this low affinity lectins display remarkable selectivity with respect to the saccharide moieties they bind and it is rare, for example, to find a lectin that binds both glucose and galactose or mannose and galactose. Some structural variation is tolerated, particularly around C-2, so it is fairly common for lectins to bind both galactose and N-acetylgalactosamine. [12]

Lectin–carbohydrate recognition has been identified as potentially useful for the

targeting of drugs. [13] If the specificity of lectin–carbohydrate interactions are to be exploited for such means then an increase in avidity is required. Here, as is often the case, Nature has already provided us with a solution – multivalency – lectins and their corresponding carbohydrate ligands are usually presented on cell surfaces in clusters of high valency. The increased avidity through multivalency is unusual as the relationship is non-linear and thus not an artefact of increased local concentration. This was well illustrated by Lee et al. who found that lectin binding of lactosamine derivatives increased 10^6-fold when the number of lactosamine moieties rose from 1 to 4. This unusual non-linear avidity increase has been dubbed the *cluster glycoside effect*. [14] Similarly lectins are often oligomeric, each subunit having a carbohydrate recognition domain, and these oligomers may also aggregate, further increasing their capacity for binding. [15] A good example is influenza hemagglutinin of which approximately 500 trimers are found on the virus surface. [16] Similar effects have also been demonstrated in non-carbohydrate systems; Whitesides et al. demonstrated an avidity increase of 10 orders of magnitude between a trivalent vancomycin derivative and trivalent dipeptide compared to a monovalent analogue. The resulting binding, $K_d = 4\times10^{-17}$ M, is stronger than that of avidin–biotin. [17]

1.1.3 Receptor-mediated endocytosis

Eucaryotic cells use two main methods for the assimilation of molecules: diffusion through the lipid bilayer, which may or may not be facilitated by membrane proteins, and endocytosis. Endocytosis is the act of a cell enveloping external material by deformation of the cell membrane allowing hydrophilic molecules, which are of-

ten important but cannot diffuse through the cell membrane easily, to enter the cell. In order to maintain the cell size the opposite process, exocytosis, occurs simultaneously. There are three forms of endocytosis: phagocytosis, pinocytosis and receptor-mediated endocytosis (RME) (Fig. 1.2). Phagocytosis, or 'cellular-eating',

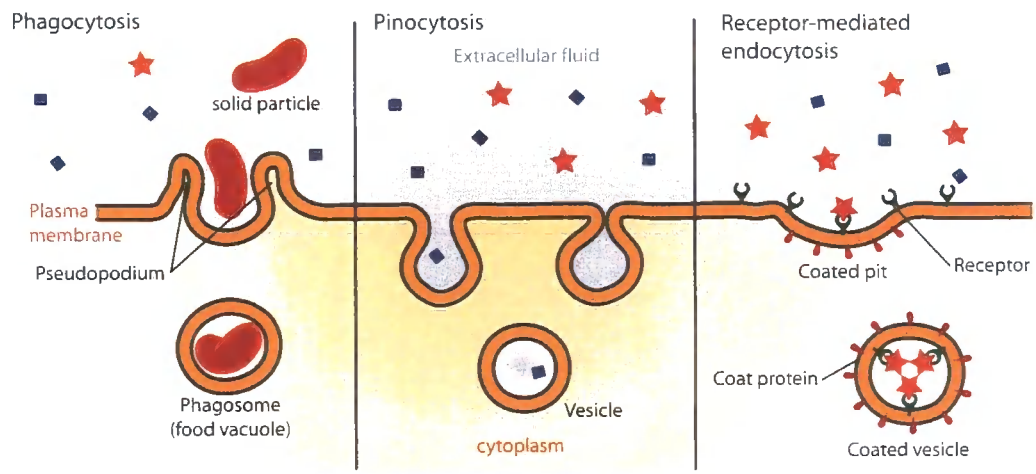

Figure 1.2: Schematic representation of the three forms of endocytosis: phagocytosis, pinocytosis and receptor-mediated endocytosis. Modified with permission from ref. [18]

is confined to certain cell lines, typically those involved in immune response, and allows a cell to consume large particles, such as a whole bacterium, and then destroy them within the cell. Pinocytosis, or 'cellular-drinking', is where the cell membrane indiscriminately internalises small vesicles of extracellular fluid and delivers them to the lysosome for digestion. Receptor-mediated endocytosis is similar to pinocytosis but only internalises molecules that bind specifically to a membrane surface receptor. [19] The addition of specificity to the process means that receptor-mediated endocytosis is a good candidate for targeted delivery of drugs to specific cell lines.

Examples of receptor-mediated endocytosis include the uptake of cholesterol to cells and the clearance of old erythrocytes, red blood cells, from the bloodstream. Cholesterol is an extremely hydrophobic steroid that is required by animal cells to produce plasma membrane. Its insolubility means that it must be transported by the bloodstream as particles known as *low density lipoproteins* (LDL) which bind to receptors in clathrin-coated pits on the cell surface. From here they are internalised via RME and then degraded in the lysosome to yield free cholesterol; the LDL receptors are returned to the cell membrane. Asialoglycoprotein receptors (ASGPRs), found on hepatocytic cells and elsewhere, are galactose-binding lectins that are responsible for the removal of desialylated glycoproteins. For example, as erythrocytes age they become increasingly desialylated resulting in exposure of galactosyl residues. ASGPRs bind the resulting galactosides, internalise the cell, thus removing it from the circulatory system, and destroy it. This is also a further example of the usefulness of multivalency: older cells present more galactosides and thus have an increased likelihood of being bound and destroyed.

1.2 Neoglyconjugates: Elucidating and exploiting the glycocode

With such varied and complex roles in vivo, combined with the unfathomable number of potential structures that carbohydrates can form, tools are required to allow science to probe glycofunction further and potentially exploit it for biomedical gain. Extraction and purification of glycoconjugates from natural sources can be a labo-

rious task often resulting in minute quantities of materials that may or may not be pure. This is further complicated by microheterogeneity within these products. This heterogeneity is prevalent in glycoproteins where it is common to find several *glycoforms* which share identical protein components but differ in the site or nature of glycosylation. [20] Synthetic, *neoglycoconjugates* allow for true uniformity of structure where required and the production of (relatively) large quantities of material. One of the more obvious but oft overlooked benefits of neoglycoconjugates is the ability to augment binding affinity through multivalency and the cluster glycoside effect. Additionally during synthesis it is possible to add further functionality as required; for example, a fluorescent marker may be incorporated for easy detection via fluorescence/confocal microscopy.

The potential applications of neoglycoconjugates are as vast and varied as the field of glycoscience itself. Here, one class of neoglycoconjugates will be concentrated upon – glycopolymers. Glycopolymers are synthetic polymers, typically with a carbon backbone, featuring pendant and/or terminal saccharide moieties. [21] Previously, glycopolymers have been linked to many applications in biosciences including; macromolecular drugs [22–25] and drug-delivery systems, [26–29] biocatalytic [30] and biosensitive [31] hydrogels and matrices for controlled cell culture. [32–34] Some of these applications are expanded upon below.

1.2.1 Glycopolymeric drugs

Considering the biological significance of carbohydrates it should be unsurprising that polymers featuring multiple saccharide residues along their backbones could

act as drugs. The ubiquitous nature of lectins within recognition and binding events suggests great potential for their exploitation as drug targets and at least one review on the subject has already be published. [13] Several targets for glycopolymeric drugs have been identified including influenza, Alzheimer's disease and some cancers.

1.2.1.1 Influenza hæmagglutinin and neuraminidase inhibitors

One class of disease-carrying agent that has received considerable attention as a target for glycopolymeric treatments are the influenza viruses. Considering their abundance and the number of fatalities that these viruses can cause, tens of thousands of deaths are attributed to influenza each year in the USA alone, [35] the search for effective treatments is unsurprising.

Influenza infection is a multistep process: initially the virus binds to α-sialic acid (N-acetylneuraminic acid) residues on the target cell via hæmagglutinin (HA) fingers on its capsid and the virus enters the cell via endocytosis. Within the endosome the virus releases its RNA and other molecules into the cytoplasm which are then transported into the nucleus and the process of virus replication begins. If initial binding of the virus to the cell can be prevented subsequent uptake and replication can also be halted. A molecule that could block HA binding efficiently could prove a useful prophylactic during influenza epidemics. Influenza hæmagglutinin, like most lectins, has a shallow binding site and its interaction with monovalent sialosides is typically weak ($K_d \sim 2$ mM) [36] and thus multivalent ligands should provide improved avidity. To complicate matters further the surface of influenza viruses also present neuraminidase (NA) and consequently hæmagglutinin inhibitors need to be stable with respect to neuraminidase action.

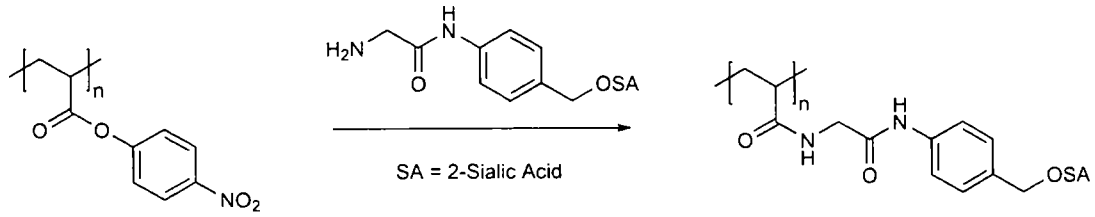

Figure 1.3: Synthesis of polymeric multivalent sialosides as used by Bovin et al. [37]

The first example of an influenza hæmagglutinin inhibitor (HAI) based around a glycopolymer was reported by Bovin et al. in 1990. Polymeric sialosides of varying carbohydrate densities were synthesised by the reaction between poly[4-nitrophenylacrylate] with monosialosides with amino-terminated linkers (Fig. 1.3). As would be expected little or no inhibition was seen for monovalent sialosides, β-sialosides, or polymers carrying low quantities of α-sialoside residues (~5 %). Upon increasing the sialoside density from 10 through to 30 % a maximum in inhibition was seen at 20 % with 30 % having a lower inhibitory effect than the 10 % sialylated polymer. [37]

The main contributors to the field of glycopolymeric HAIs are Whitesides and collaborators. Throughout the 1990s Whitesides et al. published several studies on the inhibition activity of polymeric sialosides synthesised by both polymerisation of sialylated monomers and post-polymerisation functionalisation of reactive polymers. [22, 38–43] Initial studies involved copolymers of acrylamido α-*O*-sialoside **1.2** with various *N*-substituted acrylamides. As Bovin et al. had seen previously, [37] a maximum level of inhibition was seen at intermediate levels of sialylation. This may be rationalised by the competition between cooperative and efficient binding of the sialic acid groups: at low SA levels the groups are well separated and thus binding

of one residue does not increase the likelihood of a subsequent groups binding, with high SA levels binding may be limited as the steric bulk of the groups overcrowd one another. It was also noted that bulky or charged groups on the comonomer tended to reduce the binding efficiency and, in turn, inhibition. [38,40] Although copolymers of **1.2** resulted in highly effective HAIs, inhibition constants (K_i^{HAI}) were typically 10^4–10^5 fold greater than monomeric equivalents on a per sugar basis, the *O*-linked SA made them susceptible to cleavage by neuraminidases. In order to alleviate this problem acrylamido α-*C*-sialoside **1.1** was synthesised and copolymerised with acrylamide. Polymers with *C*-linked SA groups were found to have a maximum inhibitory effect comparable to that of their *O*-linked equivalents and had a far greater effect at low SA concentrations, probably due to their ability to interact with neuraminidase without deactivation. [39]

Despite high levels of inhibition displayed by polymers synthesised from sialylated monomers they were still less efficient than either non-polymeric synthetic HAIs, such as sialylated liposomes, [44] or naturally occurring HAIs, such as equine α_2-macroglobulin, [45] whose $K_i^{HAI} \sim$ 100–200 nM; instead Whitesides et al. turned their attention to the sialylation of reactive polymer backbones. The reasons for this are three-fold: firstly, due to differing monomer reactivities, it is unlikely that sialosides will be statistically placed along a polymer based upon feed ratio. If the comonomer is of higher reactivity it is likely that, especially at the low feed level of SA monomers, the resulting polymer chains will be more like block copolymers with a short gradient section between blocks. Secondly, if the polymer can be too heavily functionalised, as appears to be the case, then sterics should prevent over function-

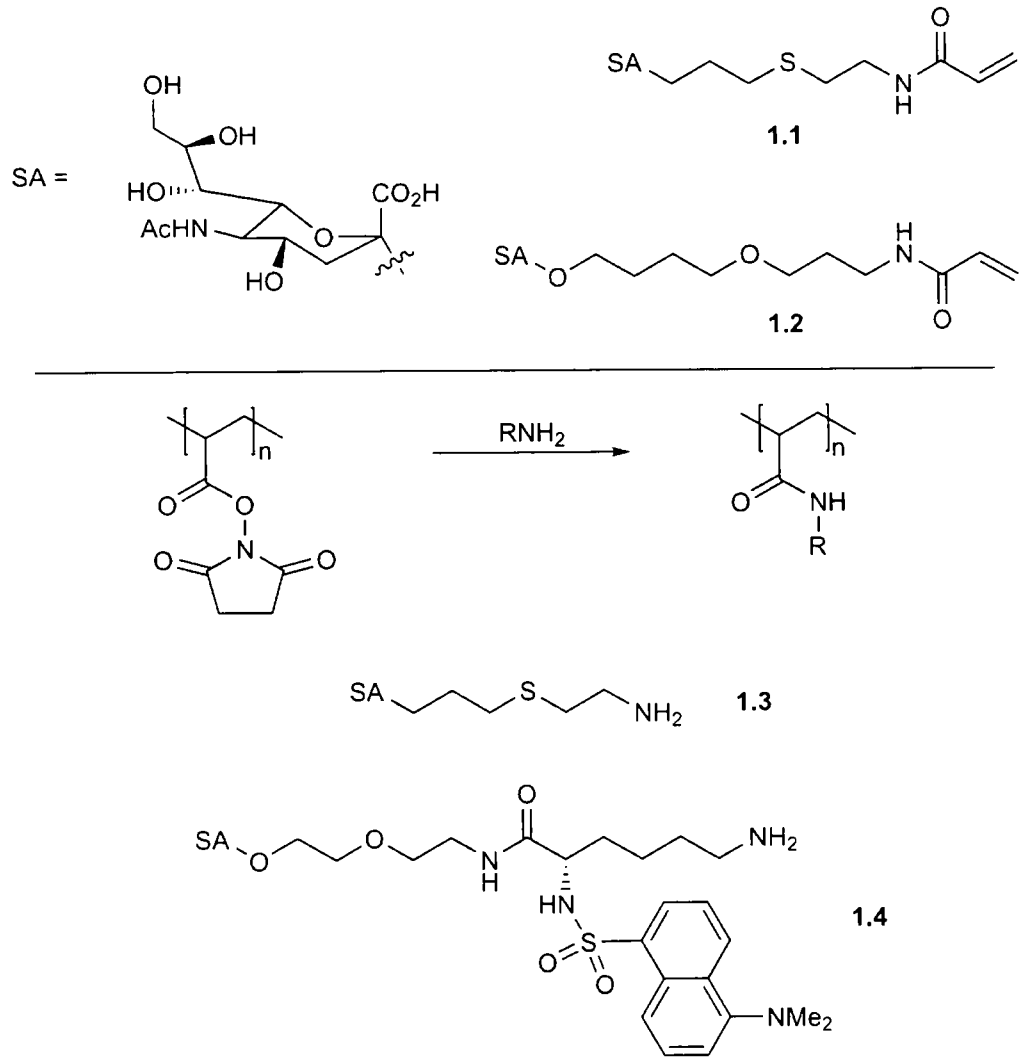

Figure 1.4: Sialic acid derived monomers and amines as used by Whitesides et al. in the synthesis of glycopolymeric influenza hæmagglutinin inhibitors.

alisation of a reactive polymer as reactive sites become crowded out by their already functionalised neighbours. Finally, polymers may be more directly compared; a single batch of a precursor polymer results in all derivative polymers having the same polydispersity and degree of polymerisation.

The precursor polymers of choice were those featuring activated esters, such as poly[*N*-(acryloyloxy)succinimide] (pNAS) or poly[acrylic anhydride] (pAAn), which

were reacted with amino-terminated sialosides including **1.3** and **1.4**. pNAS was treated with a varying number of equivalents of **1.3** from 0.2–1.2 with respect to the number of succinimide groups; the level of sialoside incorporation was found to correlate directly with the number of sialoside equivalents up the maximum value of 1. After reaction of the sialoside, any remaining succinimide groups were functionalised by addition of an excess of a second amine or ammonia to yield copolymers of various *N*-substituted acrylamides. As was seen with the previous polymers, addition of charged groups had a negative effect on the inhibition, particularly positive charges where a singly positively charged side group has a more detrimental effect than a triply negatively charged side group; neutral, polar side groups also reduced inhibition with increasing steric bulk. Hydrophobic side groups increased or decreased inhibition depending on the steric bulk. Benzylamine, for example, was found to improve efficacy as its level of incorporation was increased; presumably through increased hydrophobic–hydrophobic interactions between the polymer and virus surface. Conversely, hexylamine resulted in reduced inhibition. [41] Overall polymers with sub-nanomolar values of K_i^{HAI} could be produced. Polymers synthesised by similar methods from pAAn gave similar results. [22] It was also determined that a synergistic treatment combining *C*-sialoside-acrylamide copolymers and low molecular monomeric neuraminidase inhibitors resulted in even greater inhibition of hæmagglutination. Although the mechanism of this synergy was not confirmed it is thought that the NA inhibitor displaces the polymer from the NA sites either allowing more SA residues to bind to HA sites or increasing the overall steric bulk of the polymer around the virus. [42]

In addition to hæmagglutinins the neuraminidases are also targets for influenza treatment; in fact the currently preferred influenza antivirals, such as oseltamivir (Tamiflu®, Hoffman-La Roche) and zanamivir (Relenza®, GlaxoSmithKline), act as transition state analogues of sialic acid cleavage. [46] The presence of NAs on influenza at first seems counterproductive for the virus, NAs cleave sialic acid residues which would, in effect, reduce the chances of viral binding to the cell surface. In fact the neuraminidases are essential for spread of the virus and infection of further host cells. Once a replicated virus has matured and budded off from the cell it once again binds to the cell surface via the hæmagglutinin molecules, the neuraminidases cleave the cell surface sialic acid groups releasing the new virus. [47] Multivalent sialosides that are resistant to NAs have the potential of binding to these receptors and preventing the release of the virus from the host cell and therefore limiting the infection.

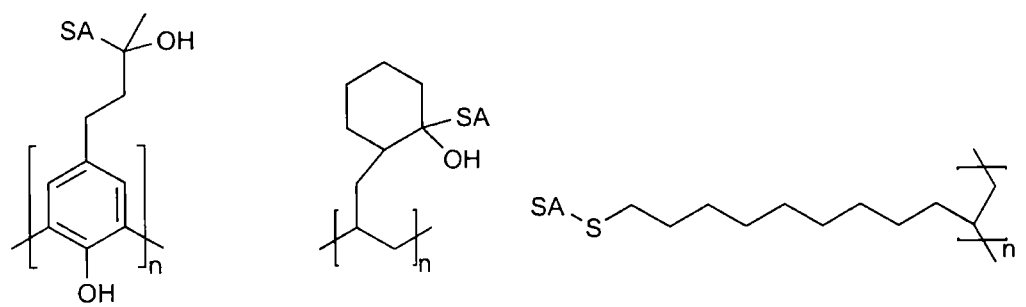

1.5 **1.6** **1.7**

Figure 1.5: Polymeric neuraminidase inhibitors as synthesised by Linhardt et al. (**1.5** and **1.6**) and Matsuoka et al (**1.7**). SA = α-sialoside.

Linhardt et al. synthesised *C*-linked glycopolymers **1.5** and **1.6** (fig. 1.5 and tested them with respect to their ability to inhibit neuraminidase from *Clostridium*

perfringens, a common bacterium. **1.5** was synthesised by enzymatic polymerisation of the monomeric aromatic by soy bean peroxidase in the presence of hydrogen peroxide; **1.6** was synthesised by radical polymerisation of an allyl precursor. **1.5** was seen to inhibit neuraminidase 10-fold greater than monomeric equivalents. [48] Matsuoka et al. synthesised **1.7** as a copolymer by radical polymerisation of an acetate-protected vinyl precursor with vinyl acetate; after treatment with NaOH sialylated poly[vinyl alcohol] was isolated. In preliminary tests polymers were shown to have an inhibitory effect against influenza neuraminidases in the millimolar range. [49] Dendritic sialosides synthesised by the same group display similar levels of inhibition. [50]

1.2.1.2 Human immunodeficiency virus

Human immunodeficiency virus (HIV) infection is now a major international pandemic and is estimated to have killed 25 million people through progression to acquired immunodeficiency syndrome (AIDS). It is estimated that between 33 and 46 million people are currently infected with HIV and between 3.4 and 6.4 million people were infected in 2005 alone. [51] One area of interest for the development of improved HIV treatments is the use of anionic polysaccharides which have been shown to prevent HIV binding to the CD-4 receptor, and thus its entrance to the host cell, in vitro. [52] Yoshida et al. synthesised methacrylate polymer **1.8** with maltoheptaose pendant groups by polymerisation of the peracetylated monomer followed by deacetylation and sulfation with either piperidine-*N*-sulfonic acid or SO_3-DMF complex. The polymers were assayed for the their ability to inhibit the infection of MT-4 cells by HIV and as blood anti-coagulant. HIV inhibition was seen to increase

with increasing polymer chain length and degree of sulfation for homopolymers but was poor compared to naturally derived polysaccharides such as dextran and curdlan sulfates. Copolymers with methyl methacrylate (MMA) increased in inhibitory effect as the number of maltoheptaose groups was reduced. At approximately 80 % MMA the copolymers displayed inhibition in the same order of magnitude as the polysaccharides. Although the level of inhibition is still 2 orders of magnitude worse than that of AZT these materials display reduced cytotoxicity in comparison and may have potential in the future. [24]

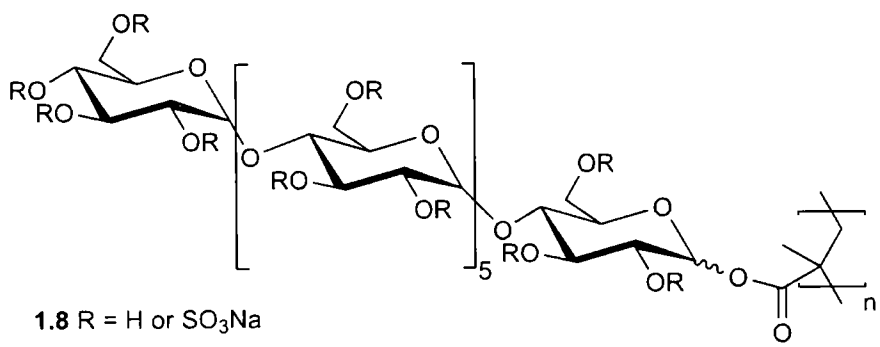

1.8 R = H or SO_3Na

Figure 1.6: Sulfated maltoheptaose derived methacrylate glycopolymers as synthesised by Yoshida et al.

1.2.1.3 Alzheimer's Disease

Alzheimer's disease (AD) is a neurodegenerative disorder that is the leading cause of dementia of which there are an estimated 24 million sufferers worldwide, a figure that is expected to rise to over 80 million by 2040. [53] Alzheimer's disease is characterised pathologically by the accumulation of 'senile plaques' – insoluble aggregates of misfolded amyloid β-peptide (Aβ). One of the current hypotheses for

the progression of AD is that these plaques, [54] or smaller soluble precursors, [55] are neurotoxic resulting in atrophy of brain tissue; Aβ itself is harmless. Prevention of amyloid-β aggregation may slow, or stop, brain degeneration. Although the underlying cause and mechanism of Aβ misfolding and plaque formation is still the subject of debate there have been several reports of glycoconjugates, such as gangliosides and glycosaminoglycans accelerating aggregation of Aβ potentially by acting as templates on which the process may occur. [56–60] In an attempt to understand further the interaction between glycosaminoglycans and Aβ, Miura et al. synthesised glycopolymeric mimics by copolymerisation of glycomonomers **1.9** and **1.10** with acrylamide. Polymers containing relatively small quantities of monomer **1.10** (10–30 %) were seen to reduce the level of Aβ aggregation and the morphology of those aggregates that did form; no appreciable effect was observed for polymers of **1.9**. Cytotoxicity of Aβ to HeLa cells was found to be significantly reduced by addition of a copolymer containing 11 % of **1.10**; the polymer itself was found to be non-cytotoxic. [61]

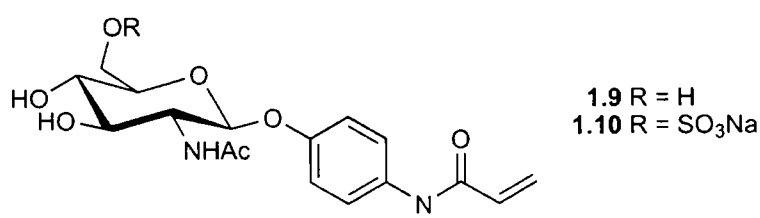

Figure 1.7: Glucosamine based glycomonomers as synthesised by Miura et al.

1.2.2 Glycopolymeric drug-delivery

One of the greatest problems facing pharmaceutical development is the production of an efficacious drug that does not produce undesirable side effects; patient death being the least desirable of all. Side effects are usually the product of a drug having little or no selectivity with regard to its site of action, the drug can affect more than the desired target, or poor pharmacokinetics, the drug is cleared from the body too quickly requiring either larger doses or regular administration in order to keep the treatment at an adequate level. Poor pharmacokinetics are a particular problem with anti-tumour drugs which, by their very nature, are usually cytotoxic and thus doses must be accurately controlled in order to destroy the tumour without disrupting healthy cells. The importance of dosage is clear when one considers methotrexate, a widely used anti-tumour drug, the use of which often requires the subsequent administration of a 'rescue drug', folinic acid or its salts, to prevent methotrexate toxicity. [62] Another major obstacle in drug delivery is the blood-brain barrier (BBB), which is remarkably efficient at preventing the diffusion of molecules into the brain. The walls of the majority of the capillaries in the body consist of endothelial cells with small pores between, known as fenestræ, which allow small molecules to diffuse between the blood stream and surrounding tissues and vice versa. The capillary walls of the blood brain barrier have no such fenestræ and consequently transport through the BBB must be via the lipid membrane or some form of transport protocol. This is well demonstrated in fig. 1.8 which shows a full body radiogram of a mouse 30 min. after injection with radiolabelled histamine; the histamine enters all organs of the body except the brain and spinal column. [63]

Glycosylation has recently been shown to be effective at enabling drugs to cross the BBB. [64] In order to combat these problems methodologies for site-specific delivery of drugs are required.

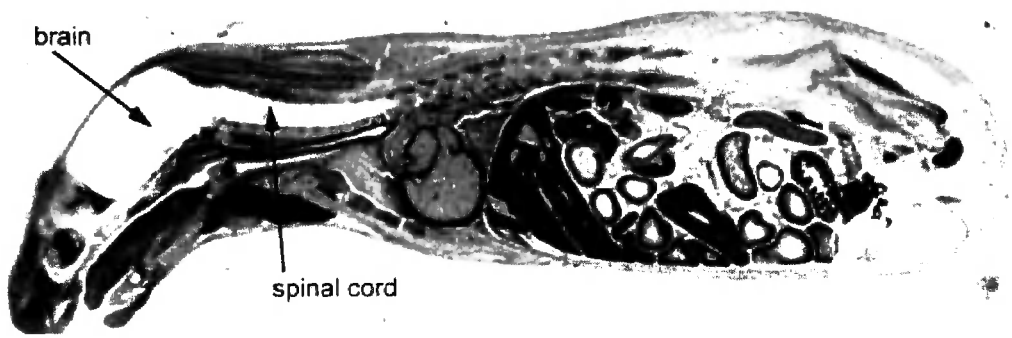

Figure 1.8: Autoradiogram of an adult mouse 30 min. after intravenous injection of radiolabelled histamine. The dark regions show where the histamine is located - none is detected in the brain and spinal cord regions. Reprinted with permission from ref. [63].

1.2.2.1 Carbohydrate targeting

In the mid-1970s Ringsdorf introduced a simplistic model for the polymeric delivery of drugs, a so-called 'magic bullet' method. The Ringsdorf model is remarkably simple. Attached to a polymer backbone are three types of group: a targeting moiety, a solubilising moiety and, via a cleavable linker, the drug to be delivered (see fig. 1.9). [65] In the case of glycopolymers the carbohydrate moieties may act as both the targeting vector, specific to a lectin on the surface of the tissue to be treated, as well as aiding solubility. There are now approximately 20 drugs either on the market or in clinical trials based upon this type of model. [66]

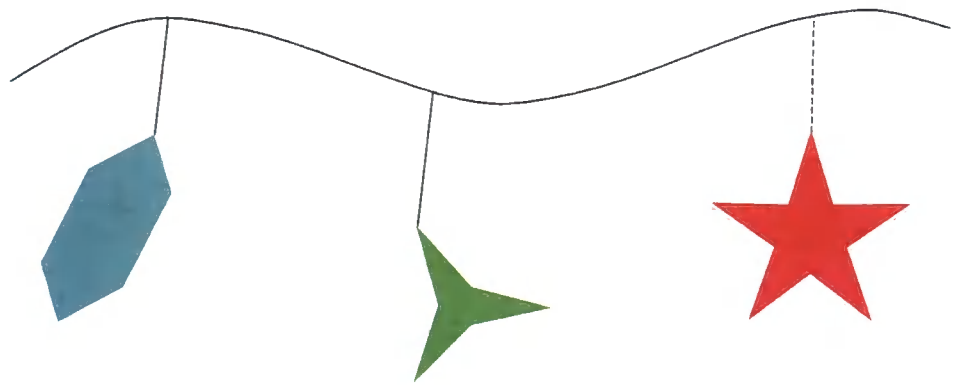

Figure 1.9: The Ringsdorf model for drug delivery by polymers. The model features three species of pendant group on a polymer backbone: a targeting species (blue), a solubilising species (green) and the drug itself (red) attached by a cleavable linker (- - -).

The field of glycopolymers as targeting vectors for drug delivery has been dominated by work of Duncan and Kopeček. Typically, they synthesised copolymers of *N*-(2-hydroxypropyl)methacrylamide (HPMA) and a second monomer featuring an active ester, such as a *p*-nitrophenyl ester, as a pendant group; the active ester was linked to the polymerisable moiety by a peptide linker. Gly-Gly or Gly-Phe-Leu-Gly for example. These polymers were then reacted with the 'drug' to be delivered and a glycosamine in order to provide targeting. Initial studies used model drug compounds such as tyrosinamide which were radiolabelled to allow easy detection of their relative biodistribution. The radiolabelled polymers were administered intravenously to rats and blood radioactivity levels were measured at regular intervals. After a set time (1 or 5 hours) the rats were sacrificed and radioactivity levels of individual organs assayed. When the polymers beared galactosamine moieties, 90 % clearance of the polymer from the bloodstream was seen within 1 hour and nearly

70 % was seen to be present in the liver. Polymers featuring gluco- or mannosamine moieties, or control polymers with a simple amine, were seen to be cleared from the bloodstream more slowly with ~10 % accumulating in the liver. For all polymers, after 5 h $\geq$ 80 % of radioactivity was to be found in the urine and faeces. [67, 68]

This approach was developed further by replacing tyrosinamide with anti-tumour drugs such as daunomycin and doxorubicin, the resulting polymers being candidates in phase I clinical trials for the treatment of hepatic tumours. Poly[HPMA] featuring pendant galactosamine and doxorubicin, as well as trace quantities of ^{123}I-labelled tyrosinamide, were administered to patients with liver malignancies. Blood and urine samples were analysed to determine the level of polymer-bound and free doxorubicin and metabolites; distribution of the polymer was determined by full body imaging of ^{123}I using single photon emission computed tomography. The galactosamine-polymer-doxorubicin conjugate was seen to be rapidly cleared from the bloodstream with 15–20 % of the administered dose accumulating in the liver after 24 h. A control polymer, identical except for the absence of galactosamine residues, was seen to remain in the bloodstream for longer and was found to have a general body distribution with no organ specificity. Despite a large accumulation of the polymer in the liver the majority was found in healthy hepatic cells rather than in the tumours themselves, although the accumulation was still significant compared to background. The reduced uptake to cancerous cells was rationalised by the reduced levels of ASGPR that hepatoma cells are known to express compared to their healthy counterparts. [69–72] The increased uptake compared to other tissues may instead be due to the enhanced permeability and retention effect and not a result of

lectin targeting. [73]

Although attempts at specifically targeting hepatic tumours were not a complete success the ability to target normal hepatocytes may allow the targeted treatment of other liver diseases such as cirrhosis or viral hepatitis. An example of such a treatment has been demonstrated by Hashida et al. in mice. The K vitamins are a family of hydrophobic molecules required for the synthesis of the proteins involved in blood coagulation. [74] The denotation of 'K' vitamins derives from the German naming *koagulations vitamin*, [75] consequently vitamin K deficiency may lead to hemorrhaging. It is common for expectant mothers and newborns to be administered vitamin K as a prophylatic but this has found controversy due to its administration having been linked to childhood cancers and other side effects. [76] The majority of coagulating proteins are synthesised in the liver and thus targeted delivery of vitamin K to the liver may allow suitable prophylaxis with reduced side effects. Hashida et al. synthesised terpolymers based upon a poly[L-glutamic acid] (PLGA) backbone (fig. 1.10) by reaction with ethylenediamine followed by 2-imino-2-methoxyethyl 1-thiogalactoside to produce galactosylated PLGA. In turn, this was reacted with vitamin K_5, a synthetic K vitamin analogue, to yield a galactosyl-PLGA-vit. K_5 conjugate. The anti-hemorhaggic effect of such polymers was determined in mice models by comparison of the prothrombin time, a measure of coagulation efficiency, after systemic treatment with warfarin. As expected, in all cases prothrombin time was increased for warfarin treated mice compared with untreated. Warfarin treated mice that received intravenous, unconjugated vitamin K only had a statistically significant reduction in prothrombin time 4 h after treatment, those

receiving IV galactose-PLGA-K_5 conjugate had a significant reduction at 2, 3 and 4 h time points. [77]

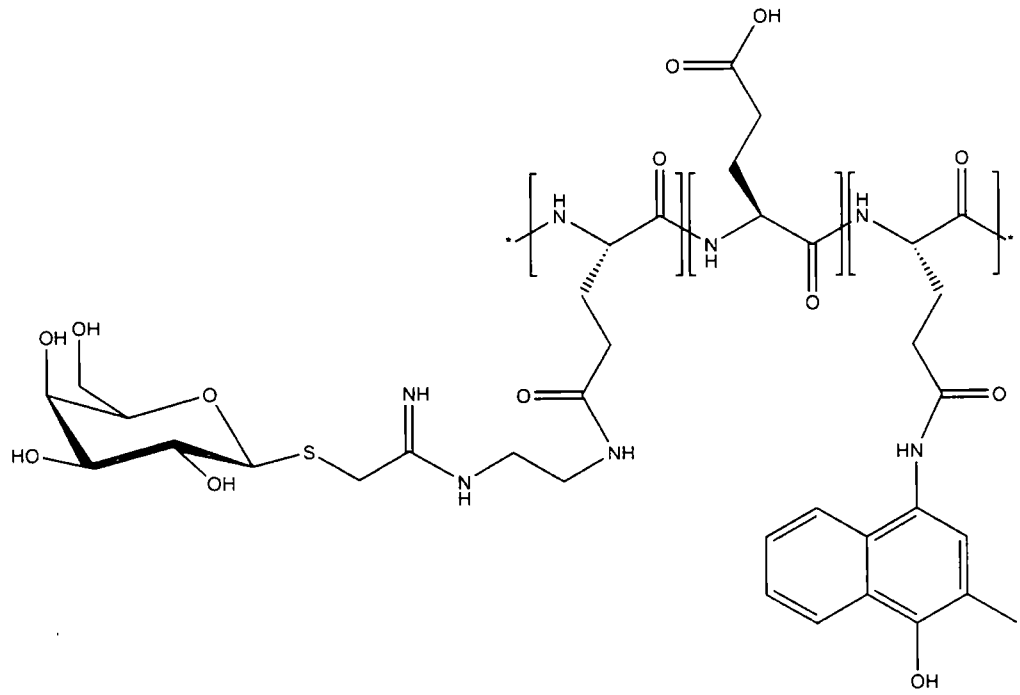

Figure 1.10: Anti-hemorhaggic, poly[L-glutamic acid] based terpolymers as synthesised by Hashida et al.

Similarly Fleming et al. have targeted boar spermatozoa, which are known to display a galactose-binding lectin with great similarity to the hepatic ASGPR, with galactosyl polymers in vitro. They synthesised terpolymers of 2-(β-D-galactosyloxy)ethyl methacrylate, 2-(dimethylamino)ethyl methacrylate (DMAEMA) and a methacrylate featuring an α-tocopherol functionality. The resulting polymers were incubated with spermatozoa in an attempt to deliver the α-tocopherol, an antioxidant, to the cells to reduce oxidative damage during storage. Although the polymers appeared to have some protective effect to confirm their entrance into the cells, rather than acting as an extra-cellular protectant, the α-tocopherol monomer

was replaced by a fluorescent monomer, hostasol methacrylate, and the polymer inside the cell visualised by confocal microscopy (fig. 1.11). [78]

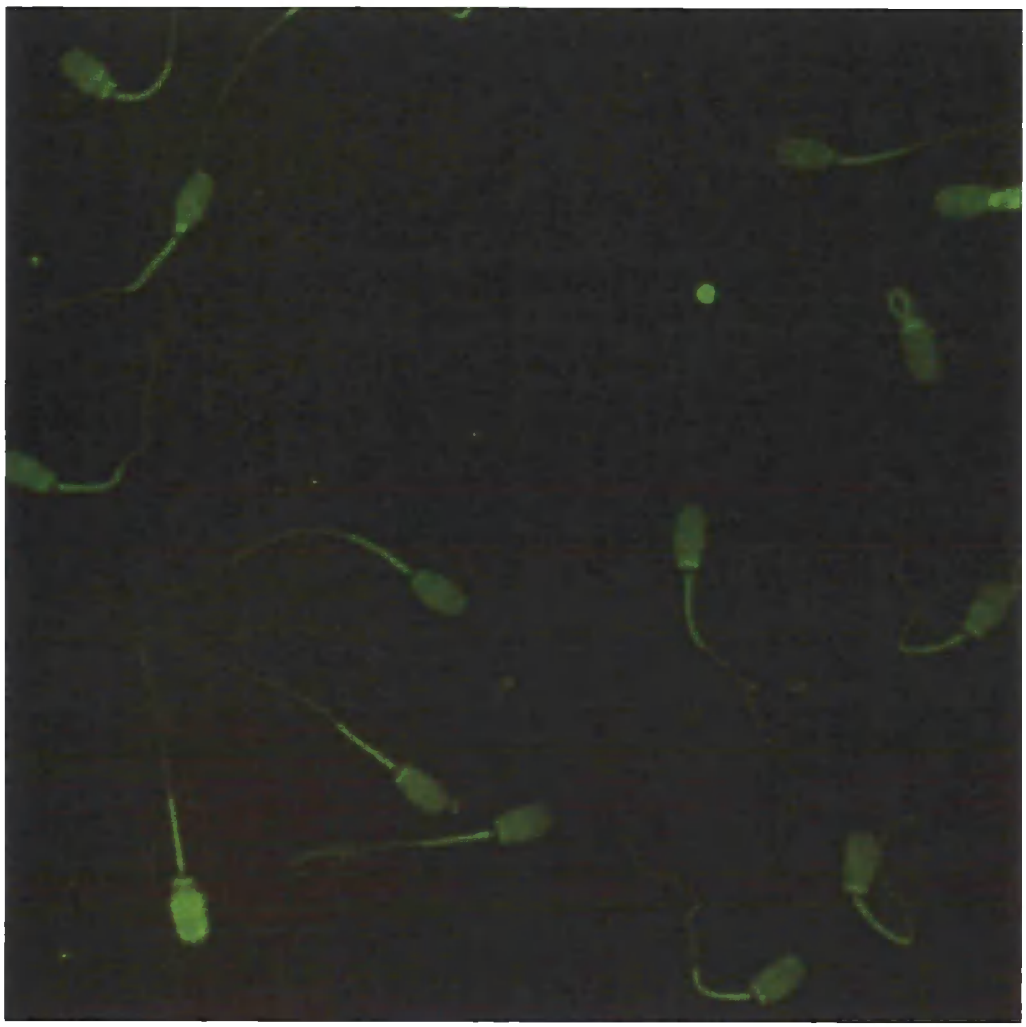

Figure 1.11: Confocal micrograph of boar spermatozoa after incubation with a poly[GalEMA-DMAEMA-hostasol methacrylate] terpolymer. [78] Image provided by the author.

1.2.2.2 Glycopolymeric Chaperones

The difficulties in effective drug-delivery are apparent when the payload to be delivered is a protein or nucleic acid for which the immune system is a veritable minefield. Ideally, a suitable drug-delivery system for such molecules would provide protection from degradation and a means of targeting the payload to a specific site. The simplest method of introducing a gene or other biomolecule into a cell is direct microinjection but this is hardly practical for the treatment of large multicellular organisms such as humans. The use of viruses, modified to carry the nucleic acid sequence of choice, allows efficient delivery but involves the use of potentially pathogenic precursors and nucleic acid strand length may be limited. Non-viral delivery vectors have the potential to replace viral vectors with non-immunogenic, low cost and easily produced materials. [79]

The use of glycopolymers as molecular chaperones for proteins has been demonstrated by Chaikof et al. They utilised cyanoxyl-mediated polymerisation [80,81] for the synthesis of several biomimetic glycopolymer species from alkenyl, acryloyl and acrylamido glycomonomers, often in their sulfated form (fig. 1.12). [82–85] Several of these polymers were tested with respect to their ability to act as mimics of heparan sulfates. [84] In vivo, fibroblast growth factor 2 (FGF-2) is bound by heparan sulfate, an anionic polysaccharide, which acts as a molecular chaperone protecting FGF-2 from deactivation and facilitating its binding to FGF receptor-1 (FGFR-1). [86] Binding assays found that polymers featuring *N*-acetylglucosamine residues did bind, but weakly compared to heparan sulfate, the linker length was seen to have no effect. Sulfated sugars bound more strongly than their non-sulfated equivalents,

particularly for polymers featuring pendant lactose groups. Further investigation into the FGF-2 chaperone role of glycopolymers featuring lactose sulfate residues found that low molecular weight (~10 kDa) polymers containing ca. 10 % of the glycomonomer were nearly as effective as heparin in dimerising FGF-2 and binding it to FGFR-1. The chaperone qualities of the polymer were also demonstrated by the extra stability that it gave FGF-2 with respect to degradation by acid, heat and trypsin. [87] The glycosyl functionalised polymers were also compared to heparin in anticoagulant activity assays. Polymers featuring monosaccharides had no anticoagulant activity, those featuring lactosyl groups displayed interesting anticoagulant activity dependent on polymer composition and functionalisation. Non-sulfated polymers, like the monosaccharide polymers, had no activity, sulfated polymers were active but homopolymers less so than copolymers with acrylamide.

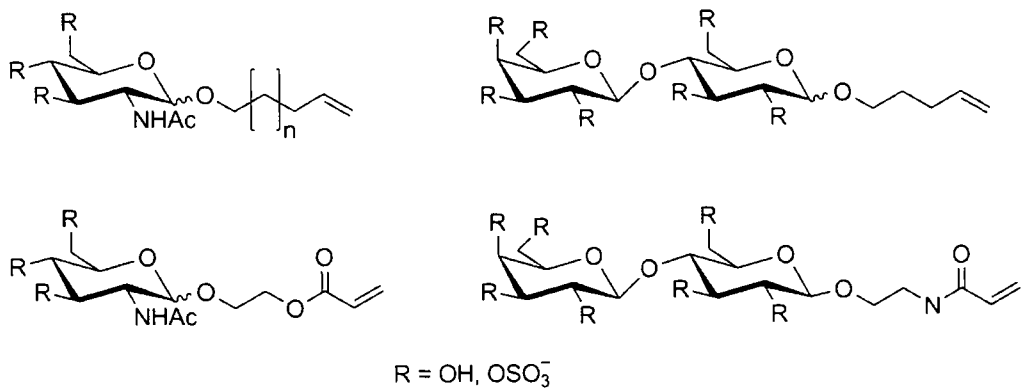

Figure 1.12: Glycosylated monomers as used by Chaikof et al. for the synthesis of heparin mimics via cyanoxyl-mediated polymerisation.

1.2.3 Glycohydrogels

Glycohydrogels, chemically or physically crosslinked polymeric materials, have been linked to a variety of therapeutic and drug-delivery applications. Nakamae et al. synthesised glycohydrogels by polymerising the glycosylated monomer 2-(β-D-glucosyloxy)ethyl methacrylate in the presence of a divinyl crosslinker and the lectin concanavalin A (Con A). In addition to the chemical crosslinking provided by the divinyl monomer, physical crosslinking is provided by Con A. The presence of Con A leads to gels displaying sensitivity to glucose (and mannose) with swelling increasing with glucose concentration as this displaces the polymeric ligand from the Con A binding site resulting in a loss of crosslinking. Consequently, such materials display promise as either glucose sensors or as drug-delivery devices for insulin as increased glucose levels would promote the release of the drug. [88, 89]

Wang et al. have produced glycohydrogels for the treatment of norovirus infection, one of the main causes of gastroenteritis. Noroviruses have been demonstrated to bind to the surface glycans on erythrocytes that determine the blood group. They synthesised the monomer 1-acrylamido-3,6-dioxa-8-octyl-*O*-(α-L-fucopyranosyl)-(1→2)-*O*-(α-D-galactopyranosyl)-(1→3)-β-D-galactoside (**1.11**) and subsequently polymerised it in the presence of acrylamide, diallyldimethylammonium chloride and *N,N'*-methylene bisacrylamide to yield hydrogels of the type shown in fig. 1.13. The entrapment ability of the glycohydrogels with respect to norovirus was determined using recombinant virus-like particles, virus particles that carry no payload, and ELISA assays. Glycohydrogels were seen to reduce dramatically the solution virus concentration compared to hydrogels prepared in the absence of the glycosy-

lated monomer. [90]

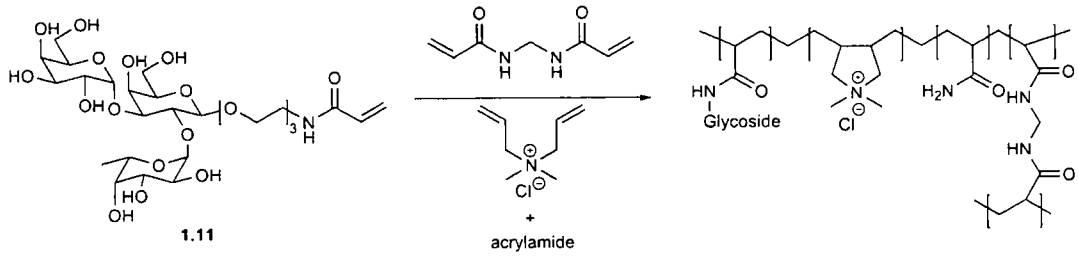

Figure 1.13: Synthesis of glycohydrogels capable of binding norovirus as synthesised by Wang et al.

Novick and Dordick synthesised biocatalytic glycohydrogels by polymerisation of acrylamido-functionalised enzymes with sucrose 1'-acrylate in the presence of 1,2-dihydroxyethylene-bis-acrylamide crosslinker. Here, the carbohydrate residues are not used for their bioactivity. Instead, they are utilised to impart a high degree of hydophilicity whilst minimising the non-specific adsorption of biomolecules; a potential problem that is often seen with the charged groups that are often used. The resulting gels were seen to improve the thermal stability of the contained enzymes as well as enhancing their catalytic ability. [30]

Akashi et al. investigated glycohydrogels featuring glucosyl moieties and their sulfated derivatives as potential substrates for cell culture. The role of heparin mimics in the stabilisation of fibroblast growth factors has already been discussed and sulfated glycosyl hydrogels may act similarly. Glycohydrogels were swollen in a solution of basic fibroblast growth factor (bFGF) and, although the matrices were unable to allow slow release of bFGF over time, they were seen to increase cell viability and adhesion compared to standard tissue culture plastic suggesting an

increase in bFGF activity. [34]

1.3 Reversible addition-fragmentation chain transfer polymerisation

1.3.1 Controlled radical polymerisation

Free-radical polymerisation is of great industrial importance, being used for the manufacture of tons of polymers per annum. Its ubiquity throughout industry is due to its ability to polymerise an almost limitless number of monomers, aided by its compatibility with many functional groups, and its tolerance to a wide range of polymerisation conditions and impurities. Despite its widespread use, free radical polymerisation has, until recently, had limited application in the synthesis of well-defined polymeric materials.

Free radical polymerisations are known to proceed by a mechanism that may be divided into three distinct stages: initiation, propagation and termination. Initiation involves the production of active radical centres. This is a two-step process, involving the formation of free radicals followed by addition of these radicals to a monomer species to produce an initial propagating radical. The first step may be achieved in several ways including thermal, redox and photochemical reactions. Most commonly these primary radicals are produced by homolytic bond cleavage of a peroxide or azo compound to form a pair of radicals. Homolytic cleavage is usually slow compared to addition to monomer and is consequently rate limiting.

Propagation is the successive addition of monomer molecules to a radical that is

not initiator derived. Each addition results in a radical identical to the previously except that it the chain is longer by one monomer unit. Propagation is extremely rapid.

Termination is the irreversible reaction of a propagating polymer chain that results in the loss of its radical. This usually occurs by one of two mechanisms: recombination whereby a pair of propagating chains react to form a single chain of their combined lengths, and disproportionation whereby one propagating chain abstracts a hydrogen from another resulting in two terminated chains, one with an unsaturated end-group, the other saturated.

Although these stages are often written separately, in reality they all occur simultaneously soon after the beginning of the polymerisation. The fast rate of propagation compared to initiation results in long chain lengths even at low monomer conversion which, combined with termination processes, results in polymers poorly defined in molecular weight and polydispersity – controlled free radical polymerisations aim to alleviate these problems.

Controlled polymerisation has recently been defined as a process to produce polymers that are well-defined with respect to:

- macromolecular architecture, e.g. linear, star, comb, etc.,
- terminal functionality
- monomer composition

and must also have molecular weights predetermined by the ratio of the monomer and initiator feed concentrations and narrow, unimodal molecular weight distributions. [91]

Controlled radical polymerisations all share one theme; they reduce the immediate radical concentration thus reducing the rate of propagation and any other radical reactions. This has a particular effect on the rate of bimolecular termination as:

$$R_t \propto [Radicals]^2 \tag{1.1}$$

If the rate of propagation can be reduced to below that of initiation then all polymer chains can be considered to have been initiated simultaneously, and all have an equal chance of growing, resulting in product of definable molecular weight and narrow polydispersity. To reduce the radical concentration a mediating agent is added to the polymerisation. The role of this agent is to allow propagating polymer chains to be reversibly capped, creating an equilibrium between reactive propagating chains and unreactive 'dormant' chains. In a well controlled system this equilibrium is weighted towards the dormant chains, resulting in a greatly reduced immediate radical concentration and thus drastically reduced termination at the expense of a reduced rate of propagation.

The earliest attempt at controlled radical polymerisation (CRP) was introduced by Otsu in the early 1980s. [92] Otsu's *iniferter* (*ini*tiator-trans*fer* agent-*ter*minator) concept involved the use of some compound, the iniferter, that was capable of thermal (or photo-) initiation and also able to react reversibly with the propagating chain end; thus, by choosing the iniferter carefully end-functionalisation could be achieved. Reversible chain capping also allowed for the synthesis of block copolymers by sequential monomer addition. [93] Overall control by iniferters was, unfortunately, limited and it took a further ten years before CRP really began to gain recognition

as a useful technique to the polymer chemist. Although many systems have been developed, with varying degrees of success, three main systems have dominated the field, namely nitroxide-mediated polymerisation (NMP), [94] atom transfer radical polymerisation (ATRP) [95] and reversible addition-fragmentation chain transfer (RAFT) polymerisation. [96]

Reversible addition-fragmentation chain transfer polymerisation is the most recently developed CRP system to have gained widespread popularity. Developed by Chiefari et al. in the late 1990s, [97] RAFT polymerisations are generally performed under standard free radical conditions with the addition of a chain transfer agent (CTA or RAFT agent); usually thiocarbonylthio compounds such as dithioesters, dithiocarbamates, trithiocarbonates and xanthates. In the latter case the technique is usually referred to as MADIX: MAcromolecular Design through the Interchange of Xanthates. Considering its relative youth, the use of RAFT has grown rapidly (see fig. 1.14). Such rapid adoption can be attributed to RAFT's incredible versatility with respect to both reaction conditions and monomer functionalities. Styryl, (meth)acryloyl and (meth)acrylamido monomers are readily polymerised and polymers featuring a range of functional side groups, including CO_2H, SO_3Na, OH and NR_2, can be synthesised with only minor or no adjustments to the reaction conditions. [97–103] Even highly reactive monomers, such as vinyl acetate, can be polymerised in a controlled manner through careful selection of an appropriate RAFT agent. [104,105] As well as common bulk and solution phase polymerisation, RAFT may be conducted in emulsions [106] and a variety of more esoteric solvents such as ionic liquids, [107] supercritical CO_2 [108,109] and aqueous solutions. [110] Careful

selection of CTA and initiator allows reaction temperature to be reduced to ambient [111, 112] and microwave-aided synthesis has been demonstrated for several monomers. [113, 114]

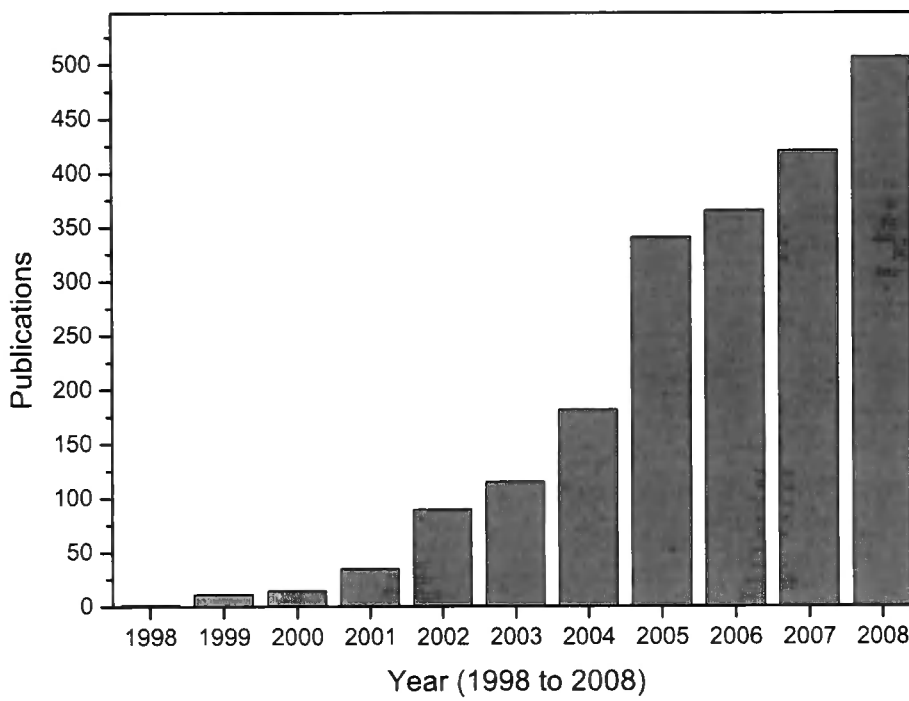

Figure 1.14: Number of scientific publications on RAFT/MADIX polymerisation (Source: Scifinder®)

1.3.2 Mechanism and subsequent considerations

The mechanism of RAFT polymerisation is considerably different to that of the other common controlled radical polymerisation techniques, namely ATRP and NMP, which operate via reversible homolytic bond cleavage. In a RAFT system chain

growth is regulated by exchange of the chain transfer agent (CTA) between a low concentration of propagating chains and a higher concentration of 'dormant' chains; the accepted mechanism is shown in fig. 1.15.

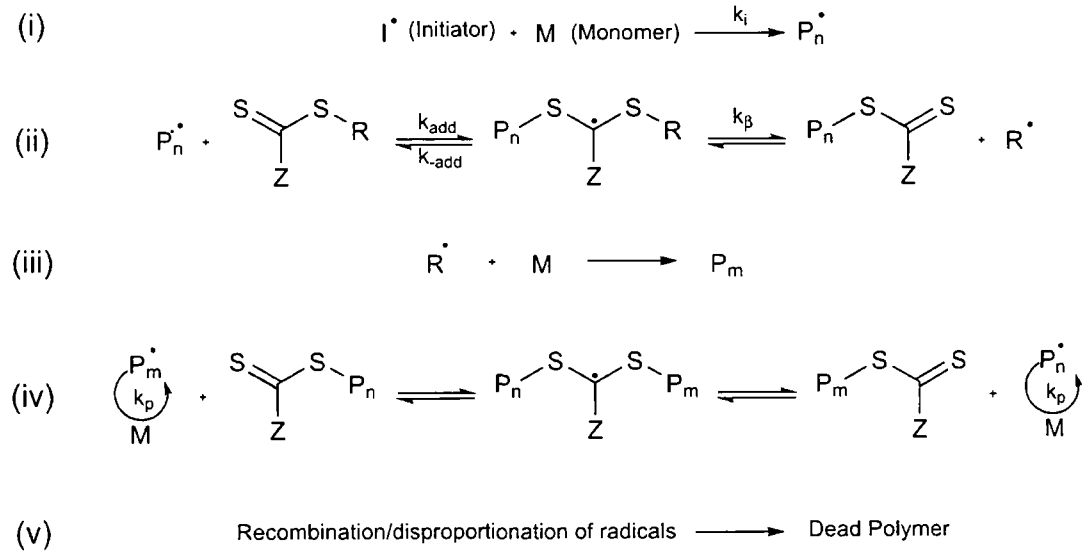

Figure 1.15: General mechanism of reversible addition fragmentation chain transfer polymerisation.

Standard free radical initiation and propagation (i) are followed by rapid addition of the propagating chain to the C=S bond of the CTA to give a radical adduct that may fragment to either reform the CTA and propagating radical, or to form a macro-CTA and a new initiating radical R• (ii). The new radical may then reinitiate polymerisation by addition to monomer, resulting in a new propagating chain (iii), or react back on the macro-CTA. Once all of the original CTA is consumed and only the macro-CTA moieties are present the reaction enters equilibrium (iv). This is the main equilibrium in the system and, when the exchange between active and dormant chains is rapid, all chains have an equal probability of growth and thus a

narrow molecular weight distribution. As with all radical polymerisation systems some bimolecular termination via recombination or disproportionation of radicals is inevitable (v); although, if conditions are chosen carefully, this may be kept to negligible levels. The number of chains in a RAFT polymerisation is equal to the total number of radicals derived from both the fragmentation of the RAFT agent and those from the initiator. To keep the number of initiator derived, and consequently dead, chains to a minimum, the ratio of the RAFT agent to consumed initiator in the reaction timescale must be kept high. Assuming that the fraction of initiator derived chains is kept low, then the molecular weight of the polymers formed is given by:

$$M_n = M_M \cdot \chi \cdot \frac{[M]_0}{[RAFT]_0} + M_{RAFT} \tag{1.2}$$

where M_n, M_M, M_{RAFT} are the molecular weights of the polymer, monomer and RAFT agent respectively; $[M]_0$ and $[RAFT]_0$ are the initial monomer and RAFT agent concentrations and χ is the monomer conversion. At the end of the polymerisation all chains will be end-capped with the thiocarbonylthio moiety, except those terminated by initiator derived radicals. The end-capped chains can then be used as macroRAFT agents in the polymerisation of a second monomer resulting in block copolymers by sequential monomer addition.

1.3.3 RAFT agent selection

The series of equilibria in the RAFT mechanism means that the structure of the RAFT agent can have a great effect on the control in a polymerisation. All RAFT agents may generally be represented as Z-(C=S)-S-R, where the Z-group improves

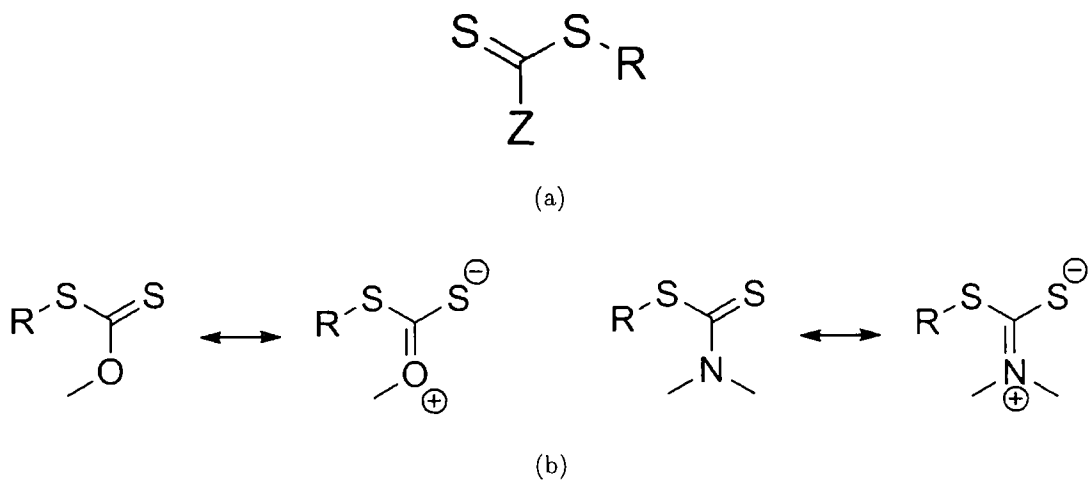

Figure 1.16: (a) General structure of a RAFT agent and (b) canonical forms of xanthates and dithiocarbamates.

stability of the radical intermediate (fig. 1.15, step ii.) and R is a fragment capable of acting as a reinitiating radical.

1.3.3.1 Effect of the Z-group

The choice of Z-group has a large influence on the stability of the intermediate radical adduct, thus it follows that a good stabilising group will increase the reactivity of the C=S bond towards a propagating radical. Unfortunately, Z-group selection is not as straight-forward as choosing a strongly stabilising group as, if the intermediate radical is too stable, it will not fragment to expel an initiating radical. Several systematic studies into Z-group choice have been published and, in the vast majority of cases, a phenyl group has been found to be suitable. With a benzyl group the intermediate stability is reduced. For more reactive monomers, such as acrylates and acrylamides, this results in increased polymerisation rates; for bulkier monomers, such as methacrylates, the reduced intermediate stability results in a loss of control

over the polymerisation.

When the Z-group is bonded through a heteroatom, such O (xanthates) or N (dithiocarbamates), a lone pair is delocalised with the C=S bond, increasing its stability and reducing its reactivity towards radical addition (see fig. 1.16b). For the majority of monomers this results in poor control over the polymerisation and an ill-defined product. For highly reactive monomers, such as vinyl acetate, the low C=S reactivity is beneficial as control is achieved without large retardation of the polymerisation rate.

The other class of CTAs are those where the Z-group is bonded through a sulfur atom, trithiocarbonates. In this case the C=S bond is reactive enough for intermediate formation but fragments quickly enough to give little or no induction period on the polymerisation; unfortunately the C=S bond is usually too unreactive to control the polymerisation of methacrylates. [96]

1.3.3.2 Effect of the R-group

The R-group, like the Z-group, has an effect on the stability of the intermediate radical but this effect is generally negligible in comparison. Consequently the R-group should be chosen such that it is both a good leaving group compared to the propagating polymer chain and a good re-initiating species for the monomer being polymerised. As with Z-group selection this requires a compromise, now between having a radical that is stable enough to make a good leaving group but reactive enough to re-initiate polymerisation. Equally, the R-group can be used to tailor the CTA to the reaction conditions required by, for example, improving solubility. Because of these factors it is unsurprising that many of the fragments used as the

R-group bear more than a passing resemblance to the initiating fragments of azo initiators (see fig. 1.17).

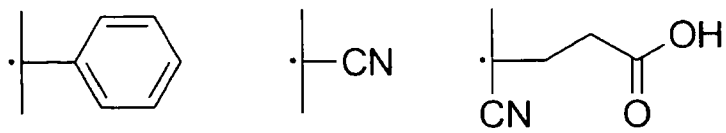

Figure 1.17: Common radical fragments used as RAFT agent R-groups. Cumyl radical, cyanoisopropyl radical, 4-cyanopentanoic acid radical.

In addition to providing efficient reinitiating radicals the use of such fragments can also simplify understanding of the polymerisation system as, if the appropriate initiator is used, chains will all be initiated by the same radical fragment whether CTA derived or not. Fig. 1.17 shows the structures of some common radical fragments used as RAFT agent R-groups. Both cumyl and cyanoisopropyl groups are commonly used as the initiating fragment of radical initiators as the radical is reactive enough to initiate polymerisation but stable enough not to abstract hydrogen indiscriminantly; the result of which is usually polymer branching or termination. The 4-cyanopentanoic acid radical is fundamentally a cyanoisopropyl radical with an additional functionality and is commonly used, in the form of (4-cyanopentanoic acid)-4-dithiobenzoate, as the CTA in aqueous polymerisation; the carboxyl group improving solubility.

1.4 Conclusions

Despite its relative youth the field of glycobiology is of increasing importance and further understanding is required to exploit it to its full potential. Glycopolymers have great potential as both drug delivery systems and as therapeutics themselves. Many of these applications rely on the cluster glycoside effect. To further define the factors that are important for this effect greater control over the synthesis of glycopolymers is required. Reversible addition-fragmentation chain transfer polymerisation ability to polymerise highly functional monomers in a controlled manner makes it an ideal choice for the synthesis of polymeric neoglycoconjugates.

A tidy laboratory means a lazy chemist.

Jöns Jakob Berzelius (1779–1848), Swedish Chemist and originator of the term *polymer*

2

Neoglycoconjugates: Controlled Synthesis and Properties

2.1 Introduction

The potential uses of glycopolymers has already been outlined in section 1.2. In order to investigate further and improve upon these applications, methods of synthesising glycopolymers that are controlled with respect to i) the carbohydrate moiety – both its type and anomeric configuration; ii) the length and macromolecular architecture of the polymeric backbone and iii) the site and density of glycosylation, are required. The first of these requires knowledge of carbohydrate chemistry to provide regio- and stereoselective synthesis of any glycosylated precursors. The second requires advanced polymerisation techniques that allow control over molecular weight and architecture. The third is the most challenging and will not be dealt with here.

The synthesis of glycopolymers falls into two main groups: polymerisation of a glycosylated monomer (glycomonomer), with or without a comonomer(s), or post-polymerisation glycosylation of a reactive polymer; [115, 116] several examples of both techniques have been mentioned previously. Historically, the former method of synthesis has been the most widespread as quantitative glycosylation of large macromolecules is not facile. However, recent advances in organic synthesis, such as 'click' chemistry, [117] and the realisation that complete glycosylation is not necessarily advantageous has resulted in an increase in post-polymerisation functionalisation.

The polymerisation of glycosylated monomers has been achieved using all common techniques including ionic, ring-opening metathesis, free radical and controlled radical polymerisations. It has previously been demonstrated that the polymerisation of protected glycomonomers followed by post-polymerisation deprotection can lead to products with ill-defined saccharide moieties; [118] consequently the use of

unprotected monomers is preferable. Hereby, ionic polymerisations are unsuitable as the nature of the propagating polymers requires the use of protected monomers as well as stringent control over reaction conditions. [119–124] Similar problems were initially encountered with the use of ring-opening metathesis polymerisations [125] but were quickly overcome through careful selection of catalyst and reaction conditions. [126, 127] Unfortunately, due to the use of heavy metal catalysts, glycopolymers synthesised via ROMP would require thorough purification before they can be used for many biomedical applications. The recent development of controlled radical polymerisation techniques has increased the armoury of the polymer chemist drastically. The ability to produce polymers of predictable molecular weight and low polydispersity, under relatively facile conditions, has resulted in a wealth of interesting polymers being reported. The three most common controlled radical polymerisation techniques, namely nitroxide-mediated, [94] atom transfer [95] and reversible addition-fragmentation chain transfer polymerisations, [96] have all been applied to the synthesis of glycopolymers with varying degrees of success. [115]

Here it was desired that glycopolymers were synthesised from anomerically pure, biologically active, glycosylated monomers. Polymerisations were to be performed under facile conditions, preferably in aqueous solution, without the requirement of protecting group chemistry. Consequently a combination of glycosylated methacrylates and RAFT polymerisation was chosen.

2.1.1 Previous syntheses of methacrylate glycomonomers

(Meth)acrylate based glycomonomers have been reported several times previously. Kitazawa et al. synthesised galactosyl, glucosyl, mannosyl and xylosyl monomers by the glycosylation of 2-hydroxyethyl (meth)acrylate (HE(M)A) with their respective methyl glycosides. These reactions were performed at high temperatures ($\geq$ 100 °C) in chlorobenzene with phosphomolybdic acid as a promoter; the resulting monomers were obtained as anomeric mixtures ranging between 2/1 to 4/1 α/β. [128] Nakaya et al. synthesised anomerically pure glucosyl methacrylates with differing methylene linker chain lengths using the methodology of Helferich and Weis. ω-Hydroxyalkyl methacrylates, the alkyl chains having between 2 and 9 carbons, were glycosylated with α-D-acetobromoglucose with $Hg(CN)_2$ or Ag_2O as promoters; yields ranged from 20–60 %. [129] 2-(2',3',4',6'-tetra-*O*-acetyl-β-D-glucosyloxy)ethyl acrylate (AcGlcEA) was synthesised similarly by Li et al. via glycosylation of HEA with α-D-acetobromoglucose in the presence of $HgBr_2$. Yoshida et al. synthesised anomeric mixtures of 1-*O*-methacryloyl maltoheptaoside (**1.8** on page 17). Peracetylated maltoheptaose was obtained by acetylosis of β-cyclodextrin and the reducing end deacetylated by benzylamine; the resulting hydroxyl group was reacted with methacryoyl chloride to yield peracetylated 1-*O*-methacryloyl maltoheptaoside; complete deacetylation was only reported post-polymerisation. [24] Stereoselective synthesis of 2-(β-D-galactosyloxy)ethyl methacrylate (GalEMA) has previously been achieved by both enzymatic [130, 131] and chemical routes. Enzymatically, a β-D-galactosidase was used for transglycosylation of HEMA with either *para*-nitrophenyl-β-D-galactose or lactose as the glycosyl donor. Although these syntheses result in

β-anomer selectivity, and remove the need for protecting group chemistry, extended reaction times (up to 8 days) coupled with low conversions ($\sim$ 40 %) and exotic enzymes makes enzymatic synthesis less than desirable. Chemically, the coupling of α-D-acetobromo-sugars to HEMA with silver triflate as the promoter results in a high yields (80 %) and β-stereoselectivity, but requires extended reaction times (48 h) at low temperatures (-40 °C). [118] Alternatively β-D-galactose pentaacetate in the presence of $BF_3.Et_2O$ at 0 °C results in β-stereoselectivity but yields are typically low ($\leq$ 45 %). [78] In both cases deprotection was achieved with sodium methoxide prior to polymerisation. Davis et al. synthesised methacryoyl monomers (**2.5** and **2.6**), featuring a 1-*O*-methyl gluco- or manno-pyranose residue, using an enzymatic lipase-catalysed synthesis; consequently the carbohydrate moiety is 6-*O*-substituted rather than at the anomeric centre. [132]

2.1.2 Glycopolymers via RAFT polymerisation

The concept of RAFT polymerisation has already been introduced in section 1.3. RAFT's high tolerance to both reaction conditions and monomer functionality make it a near perfect choice for the synthesis of glycopolymers and several reports have been published. In 2003, Lowe et al. polymerised the commercially available monomer, 2-methacryloxyethyl glucoside (**2.10**), under aqueous conditions with (4-cyanopentanoic acid)-4-dithiobenzoate (CPADB, **2.1**) as the chain transfer agent and 4,4'-azobis(4-cyanopentanoic acid) (ACPA, **2.2**) as the initiator; a small amount of 1.0 M NaOH was required to improve their solublity. Polymerisations were seen to proceed in a controlled manner, with pseudo first order kinetics and a near lin-

ear relationship between conversion and M_n; values of M_n are also very near the theoretical ones at lower conversion, but deviate as the polymerisation nears completion. Further evidence for the level of control is seen in the values of M_w/M_n, which stay below 1.07 throughout the polymerisation. Chain extension and block copolymer formation (with 3-sulfopropyl methacrylate (SPMA)) were demonstrated using poly[**2.10**] as a macro-CTA (M_n = 14.2 kDa; M_w/M_n = 1.07). In both cases the reactivation of the thiocarbonylthio groups appears quantitative, with no detectable low molecular weight peak in the SEC, however polydispersities increased above 1.5 and some high molecular weight termination products were seen. When SPMA was used for macro-CTA synthesis (M_n = 35 kDa; M_w/M_n = 1.04) which, in turn, was used for polymerisation of **2.10**, the product copolymer retained its low polydispersity (final polymer M_n = 68.2 kDa; M_w/M_n = 1.18). [133]

Davis et al. polymerised **2.5** and **2.6** using the same CTA/initiator combination as Lowe et al., but the CTA and initiator were dissolved in EtOH prior to addition. The use of EtOH aids the solubility of the CTA and initiator without resorting to the use of a base and thus reduces the rate of CTA hydrolysis. [134] After a short inhibition period, polymerisations were seen to proceed with pseudo-first order kinetics and had molecular weights that increase linearly with conversion, albeit with values lower than those predicted; polydispersities were consistently low throughout. Block copolymers with HEMA were demonstrated with little increase in PDI. [132] The same group used a similar method for the synthesis of a glucopyranose substituted vinyladipoyl monomer (**2.8**), which was subsequently polymerised using both dithiocarbamate (**2.3**) and xanthate (**2.4**) CTAs in water and MeOH, respectively.

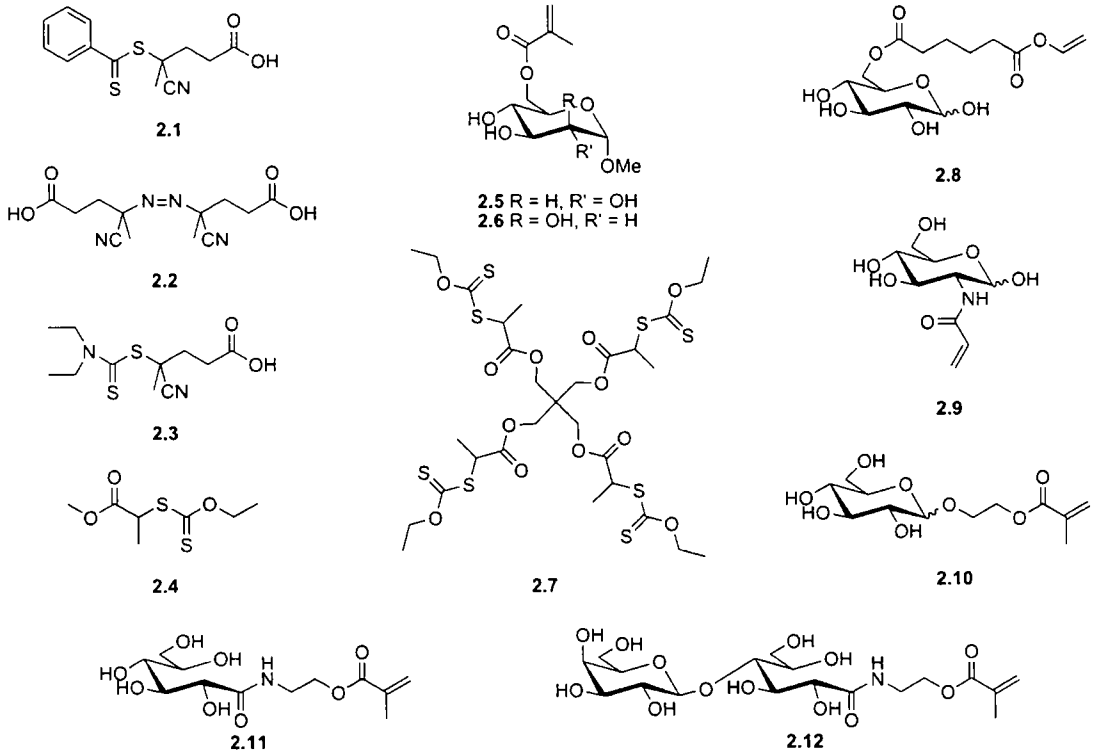

Figure 2.1: Structures of monomers and chain transfer agents used in the synthesis of glycopolymers via RAFT polymerisation. **2.1**. (4-cyanopentanoic acid)-4-dithiobenzoate (CPADB); **2.2**. 4,4'-azobis(4-cyanopentanoic acid) (ACPA); **2.3**. 4-cyano-4-diethylthiocarbamoylsulfanyl-4-methyl-butyric acid; **2.4**. 2-thiopropionyl-sulfanyl-propionic acid methyl ester; **2.5**. methyl 6-*O*-methacryloyl-α-D-glucoside; **2.6**. methyl 6-*O*-methacryloyl-α-D-mannoside; **2.7**. tetra-functional RAFT agent used by Stenzel et al.; **2.8**. 6-*O*-vinyladipoyl-D-glucopyranose; **2.9**. *N*-acryloyl glucosamine; **2.10**. 2-(D-glucosyloxy)ethyl methacrylate; **2.11**. 2-gluconamidoethyl methacrylate; **2.12**. 2-lactobionamidoethyl methacrylate.

Polymerisations in both solvents gave low polydispersities, particularly in MeOH, but conversions were extremely low at 27 % and 14 % for the aqueous and methanolic systems respectively. [135] The same monomer was used by Stenzel et al. for the

synthesis of glycostars by polymerisation in the presence of tri- or tetrafunctional xanthates, attached to a core via either the R- or Z-group (**2.7**, see section 1.3 for more information on RAFT agent structure). Polymerisations were performed in DMAc at 70 °C using ACPA as the initiator. As was seen with the synthesis of linear polymers conversions were low, reaching only 35 % after 4 h and a limiting conversion of 50 % after 9 h. Molecular weights are seen to increase with conversion but are higher than predicted for any given conversion. This may have been due to the inadequacies of the SEC calibrants, but is also likely to be contributed to by side reactions. [136]

Ting et al. combined RAFT polymerisation with 'click' chemistry in order to synthesise block copolymers of 6-*O*-methacryloyl mannose and vinyl acetate. Due to the difference in reactivity of the monomers each block was synthesised with a different RAFT agent; a dithioester for the methacrylate and a xanthate for vinyl acetate. The two blocks were then coupled together via the Cu-catalysed Huisgen 1,3-dipolar cycloaddition reaction. [137]

Stenzel et al. have also described the synthesis of thermoresponsive glycopolymers of various architectures using *N*-isopropyl acrylamide (NIPAM) and *N*-acryloyl glucosamine (**2.9**) Block copolymers were synthesised using mono- and tri-functional trithiocarbonate CTAs. To improve the solubility of the trifunctional CTA in the reaction media a short hydroxyethyl acrylate block was synthesised prior to the polymerisation of the glycomonomer and NIPAM; considering the complex nature of the system control was good (M_w/M_n = 1.3–1.6). [138] Thermosensitive brushes were synthesised in a similar manner by submerging a trithiocarbonate functionalised Si

substrate in a solution of the appropriate monomer, ACPA and a small quantity of the trithiocarbonate; the free RAFT agent suppresses any termination reactions when the polymers are unattached to the surface, resulting a greater degree of control. [139] The molecular weight of the polymer in solution increases linearly with conversion, agreeing closely with theoretical values. Similarly, the brush thicknesses, as measured by ellipsometry, increased with monomer conversion. [140]

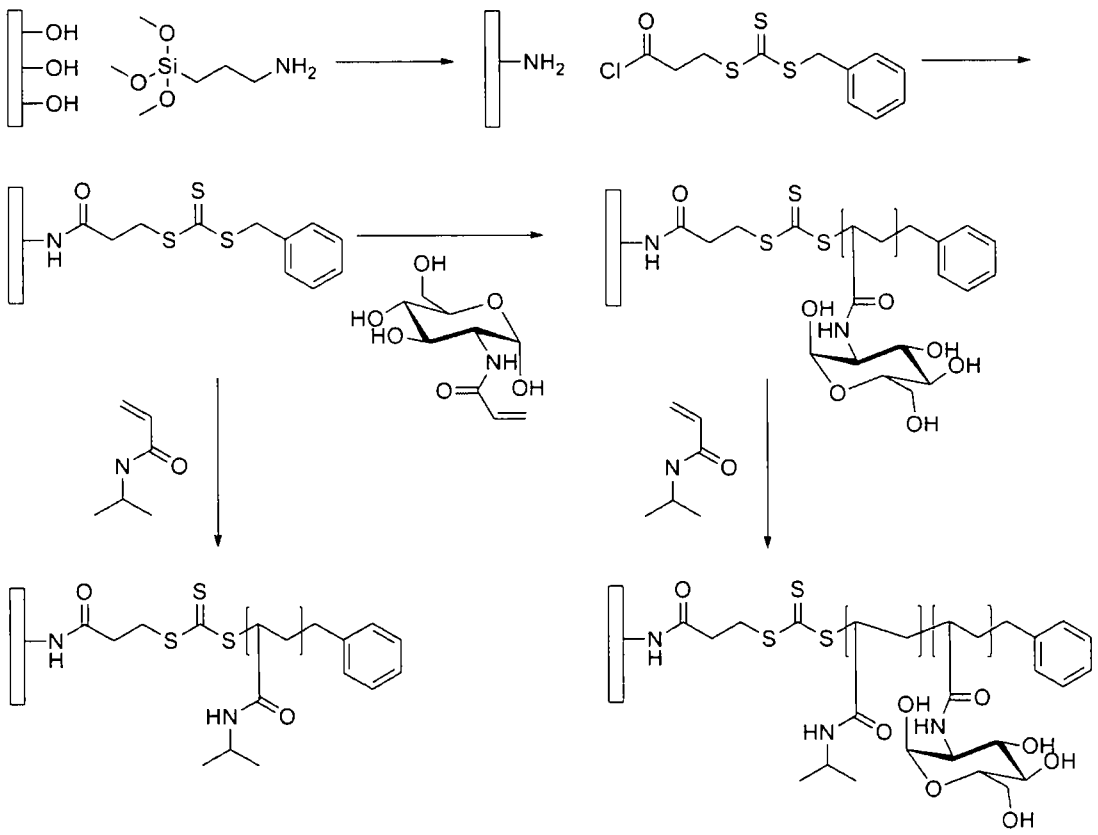

Figure 2.2: Schematic of the synthesis of thermoresponsive glycopolymer brushes by RAFT polymerisation as described by Stenzel et al.

Narain et al. recently reported the polymerisation of monomers **2.11** and **2.12** using *S,S'*-bis-(α,α'-dimethyl-α"-acetic acid)-trithiocarbonate or 2-dodecylsulfanyl-thiocarbonylsulfanyl-2-methyl propionic acid as the RAFT agent and ACPA or 2,2'-

azobis(2-methylpropionamide) dihydrochloride as initiator. Polymerisations were performed in aqueous conditions containing 15–40 % organic solvent (MeOH or DMF) at 60–65 °C. Polymers formed were of relatively low polydispersity (< 1.5) but little can be determined about molecular weight control as the data has not been published. [141] The same group used a biotinylated RAFT agent or *tert*-butyl dithiobenzoate for the synthesis of poly[*N*-acryloylmorpholine] from which block copolymers were synthesised with 6-*O*-acrylamido-6-deoxy-1,2:3,4-di-*O*-isopropylidene-α-D-galactopyranose; the carbohydrate moiety was deprotected post-polymerisation with TFA. [142]

2.1.3 Synthetic methodology

In this study methacrylate glycomonomers featuring β-D-glucosyl and β-D-galactosyl moieties (**2.14**) have been synthesised by glycosylation of the 2-hydroxyethyl methacrylate with the respective peracetylated glycoside in the presence of $BF_3.Et_2O$ followed by removal of the acetyl groups with either NaOMe or K_2CO_3. Polymerisations were achieved using RAFT techniques with the commonly used (4-cyanopentanoic acid)-4-dithiobenzoate and 4,4'-azobis(4-cyanopentanoic acid) as the RAFT agent and initiator respectively in an approximately 8:2 mixture of water and ethanol at 70 °C.

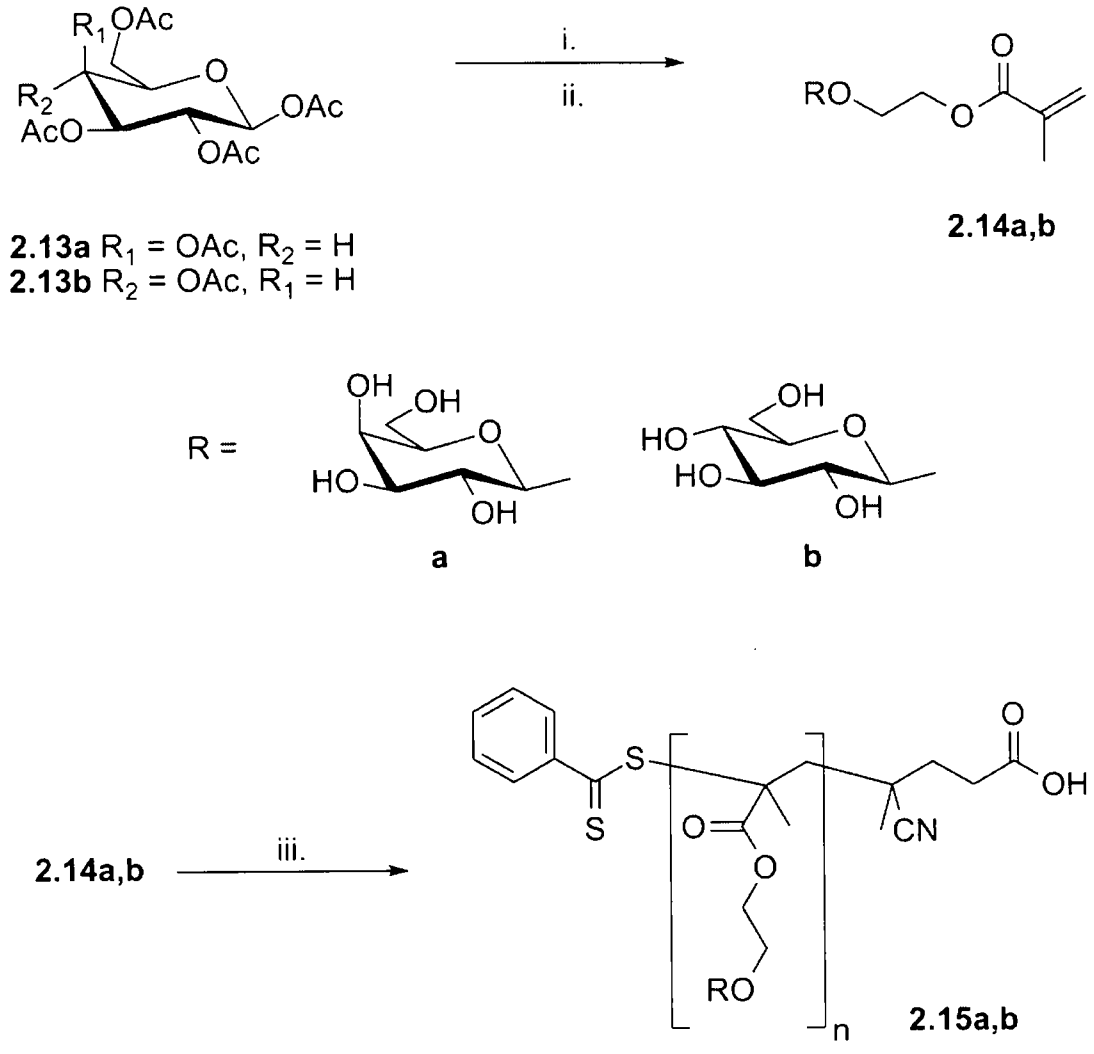

Figure 2.3: Synthesis and RAFT polymerisation of 2-(D-glycosyloxy)ethyl methacrylates: i. 2-hydroxyethyl methacrylate, $BF_3.Et_2O$, DCM, N_2 25 °C, sonication; ii. NaOMe or K_2CO_3, MeOH; iii. (4-cyanopentanoic acid)-4-dithiobenzoate, 4,4'-azobis(4-cyanopentanoic acid), water:EtOH 8:2, N_2, 70 °C.

2.2 Results and Discussion

2.2.1 Synthesis of 2-(D-glycosyloxy)ethyl methacrylates

The synthesis of 2-(D-glycosyloxy)ethyl methacrylates was achieved via a two-step synthesis using readily available and relatively cheap starting materials. Firstly, 2-(2',3',4',6'-tetra-*O*-acetyl-β-D-glycosyloxy)ethyl methacrylates were synthesised by the coupling of peracetylated glycosyl donors (**2.13**) to glycosyl acceptor 2-hydroxyethyl methacrylate (HEMA) via a boron trifluoride diethyl etherate promoted glycosylation reaction. [78] As with many Lewis acid catalysed glycosylation reactions, this proceeds via an S_N1 type nucleophilic substitution at the anomeric carbon. Activation of the glycosyl donor by the boron trifluoride diethyl etherate results in formation of a glycosyl oxocarbenium ion, which is stabilised by neighbouring group participation of the 2-*O*-acetyl group (anchimeric assistance, see fig. 2.4). In the case of glucosyl and galactosyl species, the carbonyl oxygen of the 2-*O*-acetyl group can attach to the anomeric carbon from the underside of the ring, resulting in a *cis*-1,2-acetoxonium species. Attack of the nucleophilic alcohol (HEMA) at *C*-1 can therefore only occur on the top face, *trans* to the neighbouring group, in an S_N2 type reaction yielding the *trans*-1,2-glycoside. For D-galacto- and D-glucosylation, where the 2-*O*-acyl group is equatorial, this results in exclusive formation of the β-glycoside.

Glycosyl 2-*O*-acetates are considered to be "disarmed", that is they are relatively poor glycosyl donors, and consequently require long reaction times to achieve high levels of glycosylation. Conversely, 2-*O*-benzyl sugars are considered to be "armed" and make excellent glycosyl donors. The armed–disarmed effect was first observed

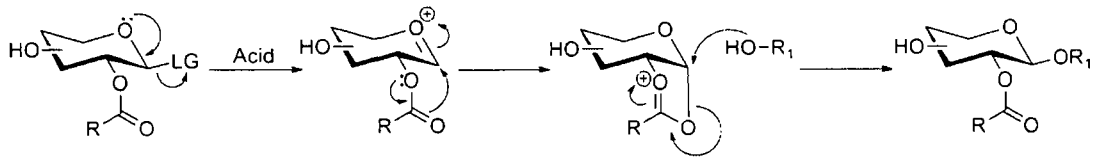

Figure 2.4: General mechanism for β-selective *trans*-1,2-glycosylation by neighbouring group participation of a 2-*O*-acyl group.

Table 2.1: Data for synthesis of anomerically pure 2-(D-glycosyloxy)ethyl methacrylates

Monomer	Yield[a] (%)	δ ^{13}C (*lit.*)[b] (ppm)		δ ^{13}C (*exp.*)[b] (ppm)	J[c] (Hz)	Anomer
		α	β			
GalEMA	40–50	98.8	103.4	104.1	7.5	β
GlcEMA	40–50	96.6	103.8	102.8	7.8	β

[a] Overall yield for both glycosylation and deprotection steps; [b] ^{13}C chemical shift for the anomeric carbon, literature values from ref. [128]; [c] H-1, H-2 vicinal coupling from ^{1}H NMR spectroscopy.

in glycosylations by *n*-pentenyl glycosides; the transition state requires nucleophilic attack of the anomeric oxygen prior to ejection of the leaving group and formation of the oxocarbenium ion. When the substituent in the 2-*O* position is a an electron withdrawing group, such as an acetate ester, the anomeric oxygen has reduced potential to act as a nucleophile. [143] Similarly, in BF_3 promoted glycosylation, the anomeric oxygen must first bond datively to the boron centre prior to formation of the oxocarbenium ion. Its reduced electron density reduces the rate at which this occurs, making this the limiting step of the reaction. Chang et al. recently reported increased reaction rate and yield in many common organic reactions, including BF_3

promoted glycosylations, by the use of sonication. [144] Using such methods the reaction time was reduced dramatically from 36 h to 45 min; after this time the mixture was worked-up and treated as usual. Sonication introduces a large amount of energy into the reaction compared to conventional mixing and consequently a significant increase in temperature was observed during the reaction; enough to produce a gentle reflux by the end of the reaction. Despite the increased temperature and short reaction times no detrimental effect on the α/β stereoselectivity was seen; as confirmed by ^{13}C and ^{1}H NMR spectroscopy. In both cases the ^{13}C resonance for the anomeric carbon is in good agreement with literature values (table 2.1). [128] From the ^{1}H NMR spectrum it is possible to confirm the configurations from the size of the H1-H2 vicinal coupling for the carbohydrate moiety. For galactosyl and glucosyl structures, $J_{(H1,H2)}$ is typically $\sim$ 8 Hz for the β configuration and $\sim$ 4 Hz for the α; here they are 7.5 Hz and 7.8 Hz respectively, confirming both are β-anomers (see table 2.1). [145] No resonances for the α-glycosides were observed by either ^{1}H or ^{13}C NMR spectroscopy (Fig. 2.5).

$BF_3.Et_2O$ is moisture sensitive and consequently the use of dry solvent and atmosphere is essential to prevent its decomposition to fluoroboric and boric acids. [146] Consequently previous syntheses via the BF_3 method have typically used an additional drying agent, such as molecular sieves, to help maintain the dry reaction conditions. Here their addition was found to be unnecessary as the reduced reaction times, combined with dry solvent and a constant flow of dry N_2 through the apparatus, all but eliminates the possibility of the introduction of water. Performing the glycosylation in the absence of molecular sieves also simplifies work-up by remov-

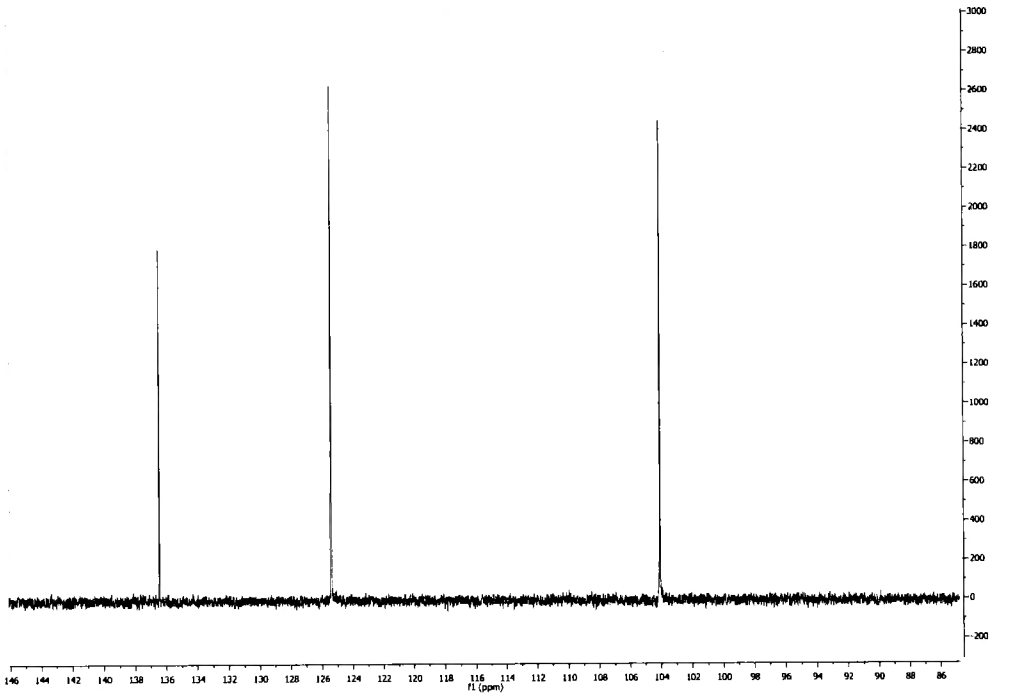

Figure 2.5: Partial ^{13}C NMR of 2-(β-D-galactosyloxy)ethyl methacrylate. The anomeric resonance is clearly seen at ~104 ppm (β-anomer), no resonance is seen at ~99 ppm (α-anomer).

ing to need to filter the reaction before quenching any residual boron trifluoride. Another interesting feature of this synthesis compared to common carbohydrate chemistry is the use of an excess of the glycosyl donor. It is usually protocol to use either a 1:1 stoichiometry of glycosyl acceptor:donor or an excess of the acceptor in glycosylation reactions. This is understandable considering that the glycosyl donor being used is often synthetically challenging and/or expensive to produce. For the monomers used here it has previously been shown that when an excess of the acceptor is used its removal from the glycosylated product can be problematic, requiring acetylation by pyridine/acetic anhydride followed by flash chromatography before deprotection of the sugar moiety can be performed. [118] As the glycosyl

donors used in this study are readily available and relatively cheap – at the time of writing β-D-glucose pentaacetate and its galactose analogue were available for approximately £25 and £80 per 100 g respectively – approximately 10 mol % excess was used compared to the acceptor. In conjunction with sonication of the reaction mixture, this resulted in no detectable HEMA being present in the crude monomer by both TLC and ES^+ mass spectrometry. Consequently, except when samples were required for analysis, crude peracetylated monomers were used directly for synthesis of their deprotected analogues, thus reducing the synthetic time required further by removing the superfluous acetylation and purification steps. An excess of the glycosyl donor also appears to reduce the formation of byproducts of the glycosylation. Glycosylations with 2-*O*-acetyl protected sugars have previously been reported to yield products of esterification of the alcohol acceptor, in the case of HEMA leading to 2-(acetoxy)ethyl methacrylate. [118] Such products are thought to derive from the reaction between the the nucleophilic alcohol and the orthoester intermediate formed by neighbouring-group participation resulting in transfer of the acyl moiety and regio-selective deacetylation at the 2-*O* position; [147, 148] no such products have been observed when acceptor and donor were used in 1:1 stoichiometry. [149] Here no such side products were observed and it is fair to assume that the increased reaction rate and excess glycosyl donor resulted in complete conversion of HEMA to the desired product without the opportunity for side reactions to occur.

Removal of the acetyl protecting groups was achieved with either NaOMe or K_2CO_3 in MeOH. Despite previous reports, [150] little difference in the reaction yield or level of methacrylate cleavage was seen between these methods. Overall,

the K_2CO_3 method was considered to be advantageous as it removes the need for dry solvents, in fact reacting more rapidly in damp MeOH due to the increased level of dissolved K_2CO_3. Its use also removes the precautions required in the use of elemental sodium for the production of fresh NaOMe. As has been noted before, cleavage of the methacrylate ester occurs at a significant level and thus reaction progress was monitored by TLC (9:1 MeCN:H_2O). [118, 150] Here the deprotection was not quenched as soon as the cleavage product ($R_f \sim 0.15$) was detected as this usually resulted in a significant quantity of partially deprotected material remaining. As well as reducing potential yield this complicates purification as the multiple isomers of mono-acetylated material and fully deprotected material run very close together on a silica gel chromatography column. In order to remove this complication the reaction was allowed to proceed until no partially deprotected material was detectable ($R_f > 0.5$) before quenching. At this time undissolved potassium carbonate was removed by filtration and any dissolved base quenched by addition of strongly acidic ion exchange resin (Amberjet 1200H or equivalent). To minimise cleavage of the methacrylate ester the apparatus required for quenching was assembled prior to the deprotection allowing its immediate use when required. Purification was achieved by flash column chromatography, initially manually using an isocratic eluent of 8:2 $CHCl_3$:MeOH and later automatically on a Biotage® SP1 Flash Purification system running a $CHCl_3$:MeOH gradient elution. Both methods yielded pure product but the latter required shorter preparation and running times which, when combined with the shortened glycosylation reaction, reduced the overall synthesis time from 3–4 days to a day. Another advantage of the Biotage® system was its use of pre-

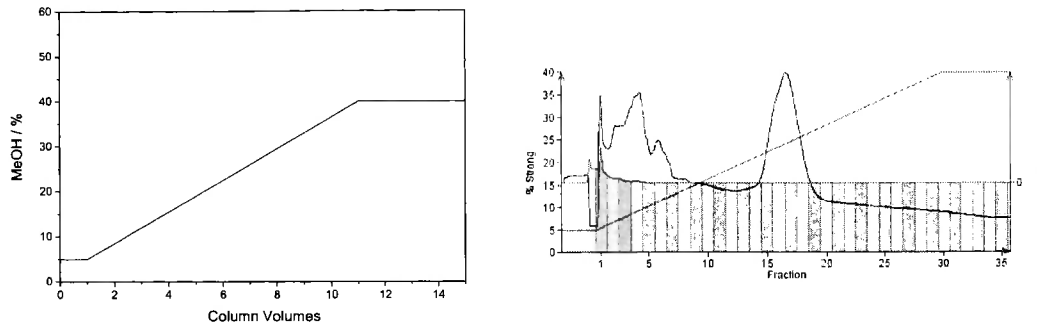

(a) (b)

Figure 2.6: Elution gradient and example UV spectrum for the purification of GalEMA. (a) Elution profile; (b) Time-resolved UV spectrum for the purification of GalEMA

packed Si columns making the purification highly repeatable as their was little or no variation between packing density reducing the possibility of inadequate separation from an inconsistently packed column. The Biotage system is also equipped with a dual wavelength UV detector system that allows facile determination of the fractions that are most likely to contain the desired product. 2-(β-D-galactosyloxy)-ethyl methacrylate (GalEMA, **2.14a**) and 2-(β-D-glucosyloxy)ethyl methacrylate (GlcEMA, **2.14b**) were isolated as colourless oils that became amorphous solids upon lyophilising, although this was generally avoided as some polymerisation often occured even in the presence of an organic free radical inhibitor. Instead they were dried under high vacuum and dissolved in D_2O as 0.5 mol dm^{-3} stock solutions. An inhibitor was not added to the solutions as its removal prior to polymerisation was found to be problematic, instead the solutions were stored frozen at -18 °C to prevent any unwanted polymerisation. GalEMA and GlcEMA were characterised

by ^{1}H and ^{13}C NMR spectroscopy, mass spectrometry, IR spectroscopy and elemental analysis, all of which agree with literature values. [118, 128] Yields were found to be heavily dependent on the deprotection reaction, but were typically 40–50 %, based on moles of HEMA used, over the two steps. Although these yields were not as high as some previous syntheses of glycosyl methacrylates the reduced reaction time, cheap substrates and ease of preparation more than compensateds for this reduction.

2.2.2 Synthesis of (4-cyanopentanoic acid)-4-dithiobenzoate

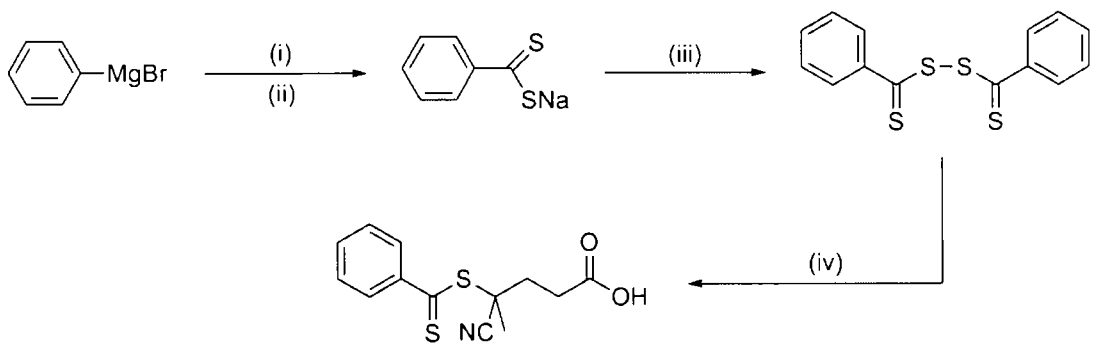

Figure 2.7: Synthesis of (4-cyanopentanoic acid)-4-dithiobenzoate: i. Carbon disulfide, THF, 0 °C; ii. aqueous NaOH; iii. aqueous $K_3Fe(CN)_6$; iv. 4,4'-azobis(4-cyanopentanoic acid), EtOAc, reflux.

(4-Cyanopentanoic acid)-4-dithiobenzoate (CPADB, **2.1**) was synthesised according to a literature procedure. [99] Briefly, sodium dithiobenzoate was synthesised by the Grignard reaction between phenylmagnesium bromide and carbon disulfide to give dithiobenzoic acid, followed by acidic, basic and organic washes. The resulting aqueous solution of sodium dithiobenzoate was then oxidised by excess potassium

ferricyanide to give the di(thiobenzoyl) disulfide as a red-purple precipitate. After recrystallisation from EtOH, the disulfide was refluxed in the presence of excess 4,4'-azobis(4-cyanopentanoic acid) to yield the desired product which was purified by flash column chromatography and recrystallisation from toluene. NMR (^{1}H and ^{13}C) and IR spectroscopies, mass spectrometry and elemental analyses were found to be in good agreement with the literature values.

2.2.3 Polymer Synthesis

2-(β-D-galactosyloxy)ethyl methacrylate and 2-(β-D-glucosyloxy)ethyl methacrylate were polymerised using a RAFT system modified from that of Albertin et al. [132] Solutions of RAFT agent (4-cyanopentanoic acid)-4-dithiobenzoate and initiator 4,4'-azobis(4-cyanopentanoic acid) in EtOH were added to stock 0.5 M monomer solution; polymerisations were thoroughly deoxygenated by repeated freeze-pump-thaw cycles and performed under N_2 atmosphere. At the end of the polymerisation samples (100 μl) were removed for aqueous SEC and ^{1}H NMR analyses. The remaining reaction solution was dialysed (Pierce Snakeskin, 3.5 kDa MWCO) against UHQ water ($\geq$ 18.2 MΩ·cm^{-1}) to remove any low molecular weight impurities such as residual monomer and initiator. Molecular weights of the polymers were determined by both aqueous SEC (see section 2.2.4.1) and end group analysis of the purified polymer by ^{1}H NMR. Monomer conversion was determined from the ratio of the vinyl and anomeric protons in the ^{1}H NMR spectrum of the crude reaction mixture. Polymers were also characterised by ^{1}H and ^{13}C NMR spectroscopy.

The mechanism of free radical polymerisation was outlined in section 1.3.1. One

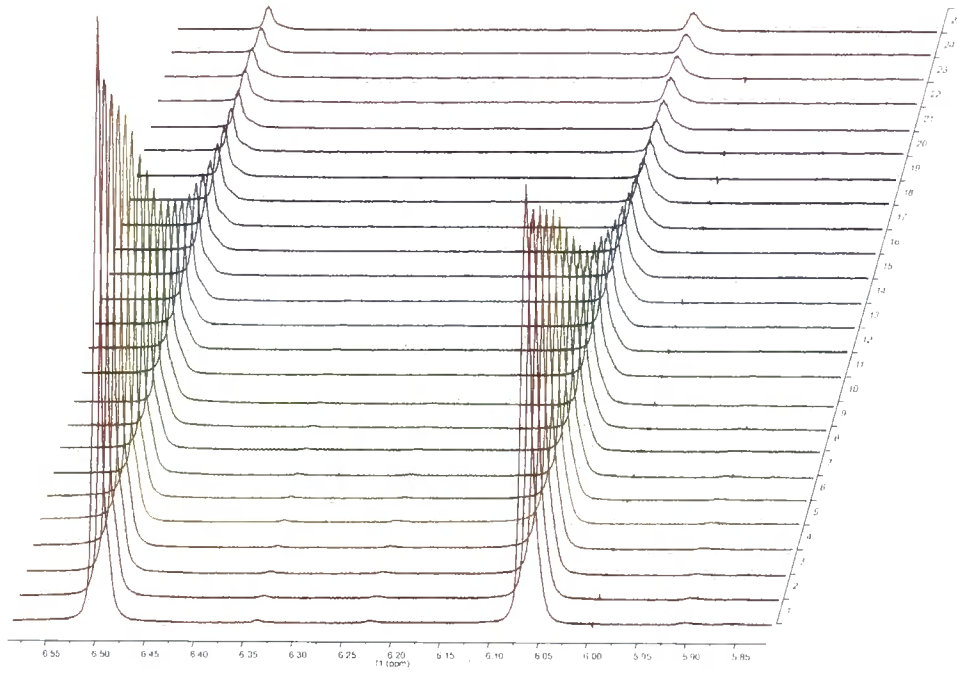

Figure 2.8: Stack plot of the vinyl region of the ^{1}H NMR for the polymerisation of GalEMA. Spectra were recorded at 5 minute intervals.

consequence of this mechanism is that radical concentration is, to a large extent, self-regulatory – an influx of radicals into the system due to initiator decomposition will quickly result in an increased rate of termination and subsequent reduction in radical concentration. This results in steady-state conditions and so polymerisations display pseudo-first order kinetics with respect to monomer. Although the mechanism of RAFT polymerisation is more complex that than of conventional free radical polymerisation, pseudo-first order kinetics are still expected; albeit at an overall decreased rate of polymerisation. The kinetics of GalEMA polymerisation were determined for three different monomer to RAFT agents ratios by monitoring the disappearance of the vinyl protons in the ^{1}H NMR spectrum: monomer concentration and RAFT:initiator ratio were kept constant. Spectra were recorded at

5 minute intervals and the integrals of the vinyl and anomeric protons used to determine the conversion, and thus kinetics, for the polymerisation. As can be seen in figure 2.9, polymerisations at all ratios proceed almost identically. In RAFT polymerisations it is usual to see a retardation in polymerisation rate with increasing CTA concentration, here it appears that the lowest polymerisation rate was observed in the sample with the lowest concentration of CTA (fig. 2.9d, targeted DP_n 97). Observed rate constants (k_{obs}), calculated by linear regression of the plots for $t \geq 20$ min., are given in table 2.2. These, indeed, show this to be the case (DP_n 97, $k_{obs} = 0.485 \times 10^{-3}$ s^{-1}), with the two higher CTA concentrations having very similar polymerisation rates ($k_{obs} \sim 0.6 \times 10^{-3}$ s^{-1}). Here, though, the concentration of initiator has been scaled with that of the CTA and consequently the picture is not necessarily that simple. The decomposition rate of ACPA in D_2O has been studied previously and values for activation energy ($E_a = 132.9$ kJ mol^{-1}) and the pre-exponential factor ($A = 6.43 \times 10^{15}$ s^{-1}) have been determined. Decomposition rates of azo-initiators have also been shown to vary little between solvents so, [151, 152] assuming this to be true for the addition of EtOH, an estimate of the number of radicals produced by initiator decomposition may be calculated by use of the Arrhenius and first order rate equations. As:

$$k = Ae^{-E_a/RT} \tag{2.1}$$

thus, using values of 6.21×10^{15} s^{-1}, [152] 132.9 kJ mol^{-1}, 8.314 J K^{-1} mol^{-1} and 343 K for A, E_a, R and T respectively, a value of k_d at 70 °C can be estimated to be 3.58×10^{-5} s^{-1}.

Also, as

$$k_d \cdot t = ln\left(\frac{[ACPA]_0}{[ACPA]_t}\right) \tag{2.2}$$

thus,

$$[ACPA]_t = \frac{[ACPA]_0}{e^{k_d \cdot t}} \tag{2.3}$$

and, as each decomposition produces two radicals,

$$[ACPA]_0 - [ACPA]_t = \frac{radicals}{2} \tag{2.4}$$

The values derived from equations 2.1 to 2.4 are summarised in table 2.2. It must be noted that the concentration of radicals given is not the overall radical concentration at $t = 120$, nor the concentration of initiator derived radicals at this time. Instead it is the cumulative concentration of initiator-derived radicals at $t = 120$ or the concentration of radicals the initiator has injected into the polymerisation. From these values it is evident that, within the timescale of the reaction, approximately 25 % of ACPA decomposes to produce a pair of radicals. Initiator efficency for ACPA is approximately 0.7, [153] although this will vary with monomer structure and concentration, so the number of radicals that may actually initiate polymerisation will be approximately 30 % lower than these values. Despite this, it is clear that the number of initiator derived radicals will be far higher in polymerisations where lower values of DP_n are targeted. The retardation of propagation rate that is expected to increase with increasing CTA concentration does just that; the similar values of k_{obs} for the two higher CTA concentrations, despite the vastly different initiating radical concentrations, testifies as such.

The differing concentrations of ACPA will have particular effect in the early stages of polymerisation where monomer concentration, and thus initiator efficiency,

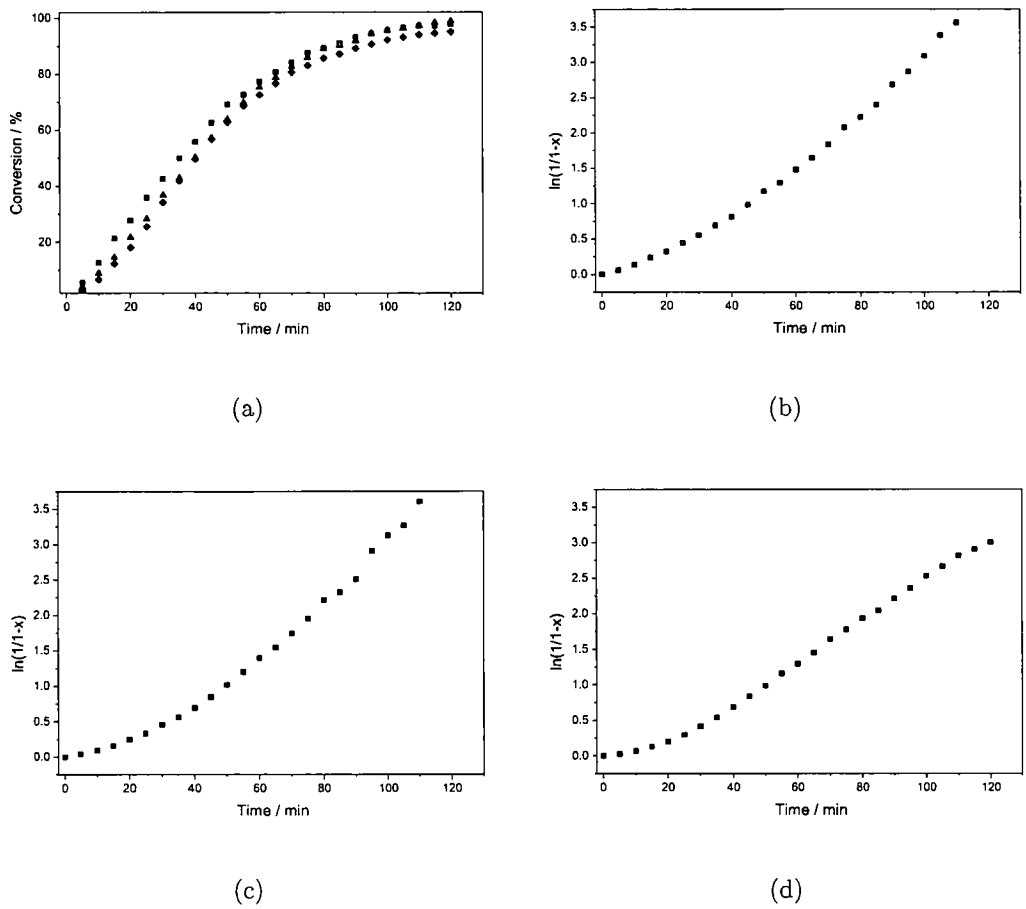

Figure 2.9: (a) Conversion and (b – d) Kinetic plots for the polymerisation of 2-(β-D-galactosyloxy)ethyl methacrylate at various [Monomer]/[RAFT] ratios: (b)= 25, (c) 51, (d) 97.

is highest. It is common to see a period of induction at the start of RAFT polymerisations, the cause of which is still open to debate, before steady-state conditions are reached. [154] Here it is seen to last for approximately 30 minutes (figures 2.9c (DP_n 51) and 2.9d (DP_n 97)) and increases with decreasing target DP_n. At the highest CTA concentration the induction period is interesting. At first glance it appears to be shorter than the lower CTA concentrations with no obvious change of

reaction rate during the polymerisation. Upon closer inspection it is arguable as to whether a steady-state is ever achieved with the plot never reaching true linearity. Similar results have been reported previously in the synthesis of glycopolymers via RAFT and it is thought that the length of the non-steady-state period is that time required for the CTA to be transformed into a polymeric macroCTA; [155] recent literature in other RAFT systems appears to support this idea. [156]

Table 2.2: Data for polymerisation kinetics of GalEMA an aqueous RAFT polymerisation system

DP_n	$[GalEMA]_0$ (mM)	$[CPADB]_0$ (mM)	$[ACPA]_0$ (mM)	k_{obs} ($s^{-1} \times 10^6$)	$[ACPA]_t$[a] (mM)	$[radicals]_t$[a,b] (mM)
25	397	15.6	7.8	594	6.03	3.54
51	397	7.8	3.9	661	3.01	1.77
97	397	4.1	2.0	485	1.55	0.91

[a] t = 120 minutes, calculated as described in text; [b] cumulative concentration of initiator derived radicals.

In all cases polymerisations proceeded to high conversion ($\geq$ 95 %) in approximately 2 hours when conducted under the conditions used for kinetic analysis, that is the reaction being undertaken was performed in an NMR tube fitted with a Young's tap within the probe of the spectrometer. When routine polymerisations were performed a Schlenk tube was used and similar levels of conversion were only observed after 3 hours. This discrepancy in reaction time is likely to be a product of heating and mixing efficiency. In both vessels no agitation was applied, and when polymerisations were conducted in an NMR spectrometer only the base of the tube is heated directly and thus thermal gradients within the system are larger; conse-

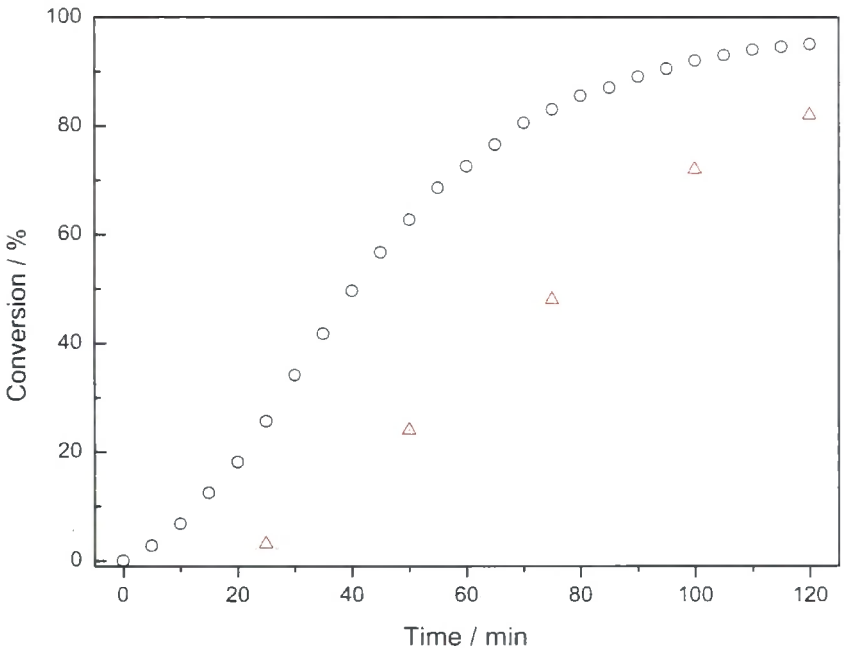

Figure 2.10: Comparison of conversion in different polymerisation vessels: Young's NMR tube (○); Schlenk tube (△).

quently convection currents will aid in the mixing. When the polymerisations were conducted in a Schlenk tube the reaction mixture was fully submerged in a water bath, reducing any anisotropy in the heating and mixing by convection. Further, the increased thickness of glass used in the vessel would increase the time required to get the solution to temperature resulting in an increased induction period. From fig. 2.10 the difference in induction period between the two reaction vessels is clear, for the NMR tube reaction little, if any, induction period is seen; in the case of the Schlenk tube reaction no conversion is detectable until 30 min. into the reaction.

One of the requirements of a controlled polymerisation is that the molecular weight must be predetermined by the ratio of the amount of reacted monomer and

the initiating species, thus as a polymerisation proceeds molecular weight should increase linearly with conversion. Similarly, final molecular weight should be predictable from the mole ratio of monomer to CTA in the feed. To determine if this was true in this system a series of experiments targeting varying molecular weights were carried out as well as experiments where M_n was determined at different levels of monomer conversion. In order to conduct these experiments methods for the accurate determination of polymer molecular weight were required, namely size exclusion chromatography (SEC) and NMR spectroscopy.

2.2.4 Polymerisation control

2.2.4.1 Determination of polymer molecular weight via TriSEC

Molecular weight determination of glycopolymers via SEC is not entirely straightforward: the use of DMF SEC with conventional calibration (PS standards) having been reported to give artificially low values of M_n on several occasions. [136,157,158] Here aqueous SEC with triple detection (TriSEC) using refractive index (RI), right-angle light-scattering (RALS) and viscometry detectors was used to remove the inaccuracy of inadequate polymer standards. One of the main advantages of the TriSEC system is the removal of the need to calibrate with multiple standards, requiring a single calibrant, the nature of which is unimportant, to determine detector responses. Using Viscotek's OmniSEC® software it is possible to calculate M_n, M_w (and thus M_w/M_n) as well as several other parameters; the theory of TriSEC has been described in detail previously, [159–161] but is briefly summarised below.

When light is passed through a solution it interacts with the solvent and solute

resulting in scattering. By measuring the intensity of scattered light from both a solution of the molecules of interest and pure solvent it is possible to determine the excess scattering due to solute by simple subtraction. [N.B. For the purposes of this explanation the term *solute* refers to the macromolecules undergoing analysis and the term *solvent* refers to the eluent used for said analysis. Consequently the *solvent* may also contain dissolved salts such as buffers.] The intensity of excess scattering is proportional to the concentration and molecular weight (MW) of the solute as seen in eqn. 2.5 where C is the solute concentration, K is an optical constant, A_2 is the second virial coefficient, R_θ is the excess Rayleigh ratio and P_θ is the particle scattering function, which allows for angular dependence of scattering intensity. [160]

$$\frac{KC}{R_\theta} = \frac{1}{MWP_\theta} + 2A_2C \tag{2.5}$$

At experimental concentrations, A_2 may be approximated to zero and P_θ is determined by iteration within the software. R_θ is measured during the experiment by the RALS detector and thus sample concentration is the only variable required to obtain accurate values of molecular weight. At each time point measured by the detectors a value of MW is determined and consequently, if the concentration of the solute at each point is known, then values of M_n, M_w and M_w/M_n may be determined.

Obviously it is possible to prepare accurate solutions of known concentrations of each and every polymer that requires analysis, but it is a laborious task requiring high purity polymers, making rapid reaction sampling and analysis difficult. Fortu-

nately there is an alternative method, using the online RI detector, which is essentially a concentration detector, along with the refractive index increment (dn/dc) of the sample being analysed to determine concentration, at each chromatogram slice, online. For common polymers, dn/dc values are readily available in literature. Unfortunately, very few reports on glycopolymers have utilised TriSEC and dn/dc is also specific to solute, solvent, temperature and wavelength; consequently values of dn/dc have to be determined prior to analysis.

Within the OmniSEC® software it is possible to calculate dn/dc values from a single sample of known concentration, unfortunately there is no way of gauging the accuracy of the value obtained. To determine values of dn/dc for GalEMA and GlcEMA, solutions of varying, but known, concentrations were analysed by SEC. By plotting the RI detector response area against concentration dn/dc values may be calculated using equations 2.6 to 2.8 and the plot provides a visual gauge as to the accuracy of the value obtained.

The RI_{Area} is described by:

$$RI_{Area} = \frac{RI_{Cal}}{n_0} \cdot \frac{dn}{dc} \cdot V_{inj} \cdot C \tag{2.6}$$

where RI_{Cal}, n_0 and V_{inj} are the RI detector calibration factor, determined during calibration of the system with a standard of known molecular weight and dn/dc, the refractive index of the solvent and the injection volume respectively. The first differential with respect to concentration is:

$$\frac{\Delta RI_{Area}}{\Delta C} = \frac{RI_{Cal}}{n_0} \cdot \frac{dn}{dc} \cdot V_{inj} = gradient \tag{2.7}$$

As RI_{Cal}, V_{inj} and n_0 are all known parameters, dn/dc may be calculated simply

from the gradient by:

$$\frac{dn}{dc} = \frac{gradient \cdot n_0}{RI_{cal} \cdot V_{inj}} \tag{2.8}$$

In order to obtain accurate, and thus meaningful, values of dn/dc high purity polymers must be used in their determination. Consequently, when values of dn/dc were determined the polymers were dialysed thoroughly against high purity water and lyophilised prior to SEC analysis. Solutions of known, accurate concentrations were then prepared. Figure 2.11 shows an example plot of RI_{Area} against c for

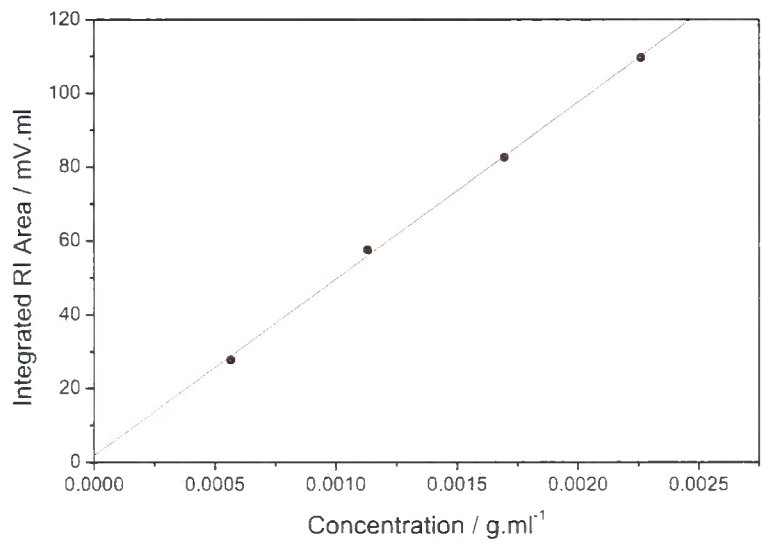

Figure 2.11: Plot for the determination of dn/dc for pGlcEMA. (—) Linear fit, R^2 = 0.999.

poly[GlcEMA]. It is clear that a good linear fit was obtained (R^2 = 0.999). Unfortunately, when extrapolated to zero concentration the fit does not pass exactly through the origin as would be expected from theory. This small discrepancy can be easily explained by slight inaccuracies in the preparation of the polymer solutions.

Table 2.3: Specific refractive index increments (dn/dc) of synthesised polymers as determined by RI method.

Polymer	dn/dc $ml \cdot g^{-1}$
poly[2-(β-D-galactosyloxy)ethyl methacrylate]	0.153[a,b]
poly[2-(β-D-glucosyloxy)ethyl methacrylate]	0.146[a,b]
poly[GalEMA$_{50}$-*stat*-HEMA$_{50}$]	0.114[a,c]
poly[GalEMA$_{64}$-*stat*-HEMA$_{36}$]	0.113[a,c]
poly[GalEMA$_{50}$-*block*-DMAEMA$_{25}$]	0.106[c,d]

[a] Eluent: 0.2 M $NaNO_3$ and 0.1M NaH_2PO_4 in UHQ water; [b] calculated by multiple injections of differing, known concentrations; [c] calculated from a single injection of known concentration; [d] eluent: 80% HPLC-grade water, 20% methanol, 0.05 M $NaNO_3$ and 2.5 $ml \cdot l^{-1}$ 1.0 M NaOH.

Due to their nature glycopolymers are very hygroscopic, ergo the preparation of solutions with accurate polymer and buffer concentrations can prove problematic as, despite thorough drying, samples absorb water quickly upon exposure to air. In the case of block and statistical copolymers values of dn/dc were calculated from a single injection of known concentration; values are summarised in table 2.3.

2.2.4.2 Control of M_n during polymerisation

The evolution of molecular weight during polymerisation was monitored by removal of 100 μl samples of the reaction mixture at regular intervals. Upon their removal the samples were split in two and quenched by dilution in D_2O or the SEC eluent ready for analysis. As before, ^1H NMR spectroscopy was used to determine monomer conversion and M_n and M_w/M_n were determined by aqueous TriSEC. As SEC of very

low molecular weight species was found to be at least non-trivial, if not impossible, a DP_n of 200 was targeted as this gave analysable polymers even at low conversions. Figures 2.12a and 2.13a contain the SEC RI detector chromatographs for the polymerisation of GalEMA and GlcEMA respectively. It is clear that, as conversion increases, there is a shift towards lower retention time and thus higher molecular weight; the peaks are also seen to narrow characteristically. There is no evidence of any high molecular weight polymer formation, that would manifest as a shoulder on the front of the peak, with all peaks being unimodal and near symmetrical. Figures 2.12b and 2.13b are plots of M_n and M_w/M_n vs monomer conversion for the same pair of polymerisations; theoretical M_n determined by equation 1.2 is shown for clarity. For both monomers the evolution of M_n is seen to be linear with conversion ($R^2 \geq 0.99$) but the linear fits do not match the theoretical values precisely. Similar results have been reported before for the synthesis of glycopolymers via RAFT polymerisation. In those cases the discrepancies between measured and theoretical values were very large and were attributed to the use of polystyrene standards resulting in inadequate SEC calibration. [132, 162] Here the values measured are not nearly as far from the theoretical, at most being ± 10 %, and are probably due to small quantities of termination that cannot be detected in the chromatographs or slight inaccuracies in their determination. The latter is a distinct possibility as these samples were not purified prior to analysis instead being removed from the reaction, diluted in the eluent and injected into the SEC. Consequently the analytes contained additional, albeit very small, quantities of solutes other than polymer. Such impurities should be separated on the column but may remain associated with the polymer

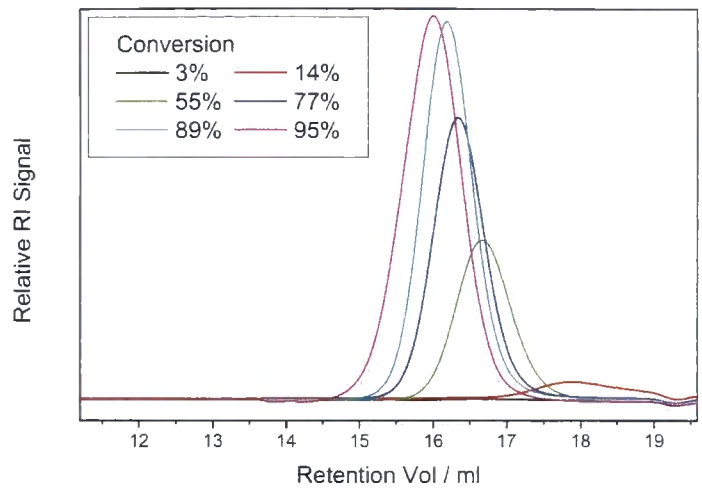

(a)

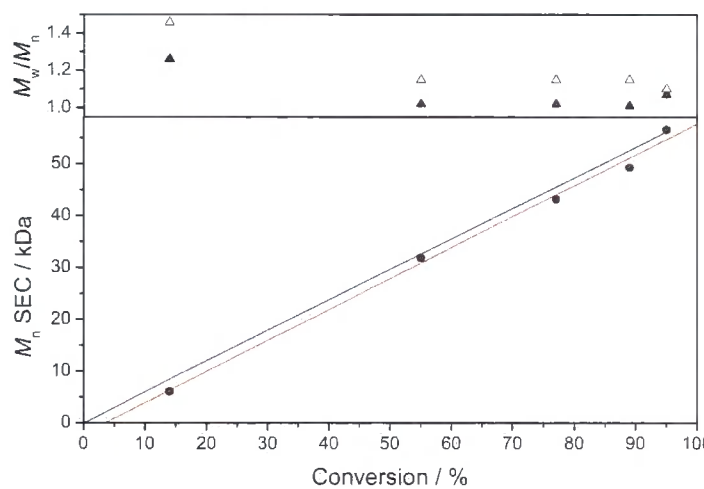

(b)

Figure 2.12: Data for molecular weight control during the polymerisation of GalEMA: (a) Evolution of aqueous SEC RI signal with increasing conversion: (b) M_n and M_w/M_n vs. conversion. (•) M_n (SEC). (—) linear fit of M_n (SEC) (R^2 = 0.997). (—) M_n (Thr), (▲) M_w/M_n (RALS), (△) M_w/M_n (Conv.).

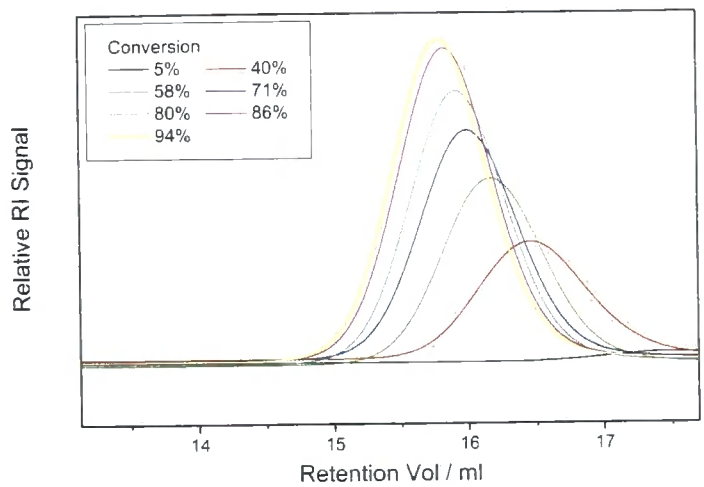

(a)

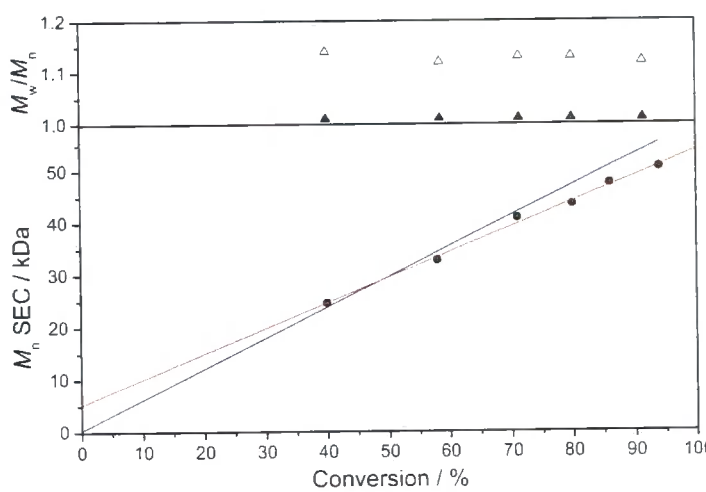

(b)

Figure 2.13: Data for molecular weight control during the polymerisation of GlcEMA: (a) Evolution of aqueous SEC RI signal with increasing conversion; (b) M_n and M_w/M_n vs. conversion. (•) M_n (SEC), (—) linear fit of M_n (SEC) (R^2 = 0.997), (—) M_n (Thr), (▲) M_w/M_n (RALS); (△) M_w/M_n (Conv.).

if the interaction is strong enough. Consequently there will be a small change in the solution behaviour and thus the values of M_n determined. The polydispersity of the polymers was seen to be consistently low throughout the polymerisation ($\leq$1.2).

2.2.4.3 Synthesis of polymers of predetermined molecular weight

In order to determine if polymers of varying, pre-determined, molecular weights could be achieved a series of polymers of different targeted degrees of polymerisation were synthesised as detailed in table 2.4 After completion of the reaction samples were analysed by aqueous TriSEC and ^{1}H NMR spectroscopy as before. Figures 2.14 and 2.15 contain SEC data for these series of polymers. Figures 2.14a and 2.15a are normalised RI response traces from aqueous SEC of a series of polymers of different targeted degrees of polymerisation (Table 2.4). In all cases the polymers formed have narrow unimodal molecular weight distributions and no high molecular weight shoulders are evident, suggesting no bimolecular termination products; similarly, no low molecular weight termination products are seen. Molecular weights as determined by aq. TriSEC agree well with those calculated by eqn. 1.2, typically within 10 %, although some deviation is seen (figures 2.14b and 2.15b). Molecular weights calculated by ^{1}H NMR spectroscopy agree closely with those measured by SEC at low DP_n but can only be described as erratic when longer chain lengths are targeted. This is to be expected as the longer the polymer the weaker the end group signals are relative to the rest of the polymer. Even with extended aquisition times, acquiring accurate integrals for the aromatic end group of the polymers is challenging as the signal to noise ratios are too low. At high molecular weights, where end groups only constitute a fraction of a percent of the overall molecular

mass, such errors are exaggerated. Polydispersities were calculated using TriSEC

Table 2.4: Data for the polymerisation of 2-(D-glycosyloxy)ethyl methacrylates

#	Monomer	DP_{thr}[a]	Conv.[b] (%)	M_n (kDa)			M_w/M_n	
				Theory[c]	NMR[d]	SEC[e]	Conv[f]	RALS[g]
1	GalEMA	25	92	7.0	8.2	8.2	1.26	1.03
2	GalEMA	50	98	14.7	13.4	11.0	1.19	1.19
3	GalEMA	97	95	27.2	20.3	21.8	1.13	1.01
4	GalEMA	145	97	41.5	44.7	42.4	1.16	1.11
5	GalEMA	201	95	56.2	39.4	56.6	1.17	1.10
6	GlcEMA	25	96	7.3	7.0	6.2	1.17	1.12
7	GlcEMA	50	98	14.7	12.3	12.7	1.14	1.02
8	GlcEMA	101	97	28.8	35.1	27.8	1.22	1.08
9	GlcEMA	151	91	40.4	37.7	34.2	1.21	1.02
10	GlcEMA	201	94	55.6	25.1	50.6	1.12	1.01

[a] Ratio of [M]:[RAFT], [RAFT]:[I] = 2. [b] Calculated by ^{1}H NMR spectroscopy using the ratio of the integrals of the vinyl and anomeric protons. [c] Calculated using equation 1.2 on page 36. [d] Calculated by ^{1}H NMR spectroscopy using the ratio of the integrals of the aromatic and backbone protons. [e] Using dn/dc values of 0.153 ml g^{-1} and 0.146 ml g^{-1} for GalEMA and GlcEMA respectively; dn/dc values calculated using eqns. 2.7 and 2.8. [f] Determined using conventional calibration. [g] from TriSEC.

triple detection (M_w/M_n (RALS)) and using conventional calibration with PEO standards (M_w/M_n (Conv.)). The two sets of values vary greatly, those determined via TriSEC are lower than would be expected for polymers synthesised by CRP, often below 1.05, and consistently lower than the values determined by conventional calibration. In order to determine which of set of values is more realistic a PEO

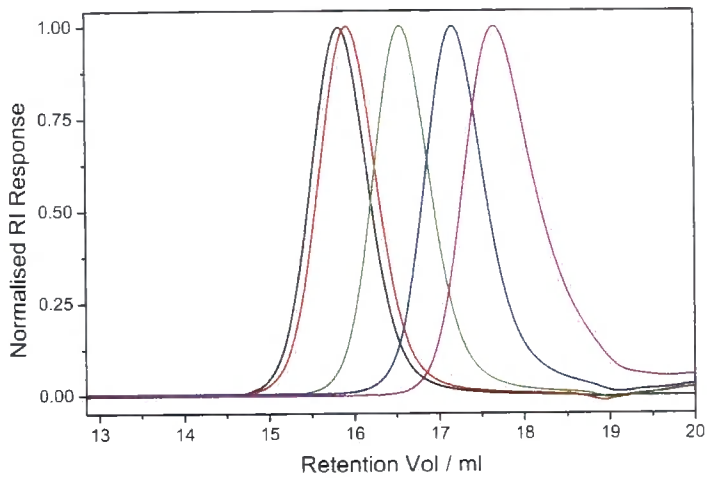

(a)

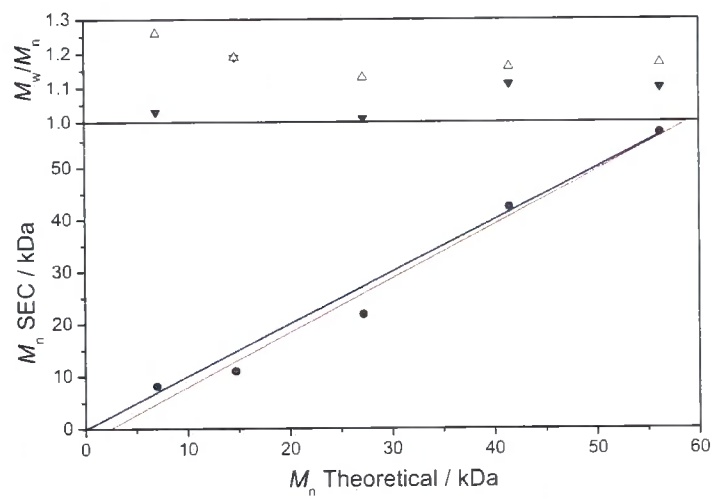

(b)

Figure 2.14: Data for the synthesis of poly[GalEMA] of varying targeted M_n: (a) Normalised RI traces of varying targeted M_n: (b) Plot of M_n (SEC) and M_w/M_n vs. M_n (Thr). (•) M_n (SEC), (—) linear fit of M_n (SEC) ($R^2 = 0.99$). (—) M_n (Thr), (▲) M_w/M_n (RALS), (△) M_w/M_n (Conv.).

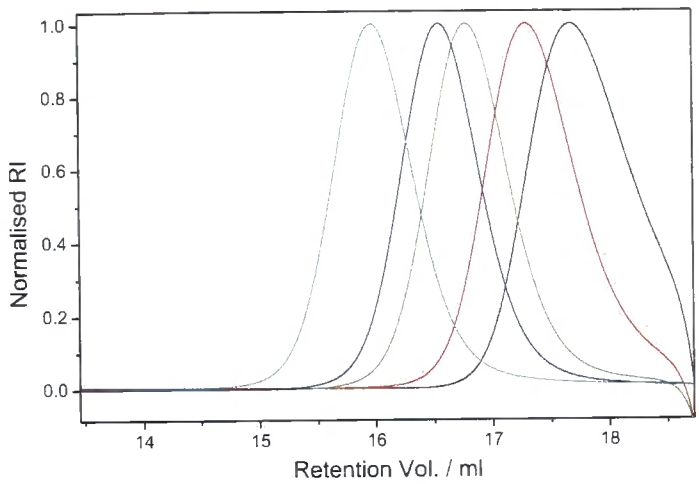

(a)

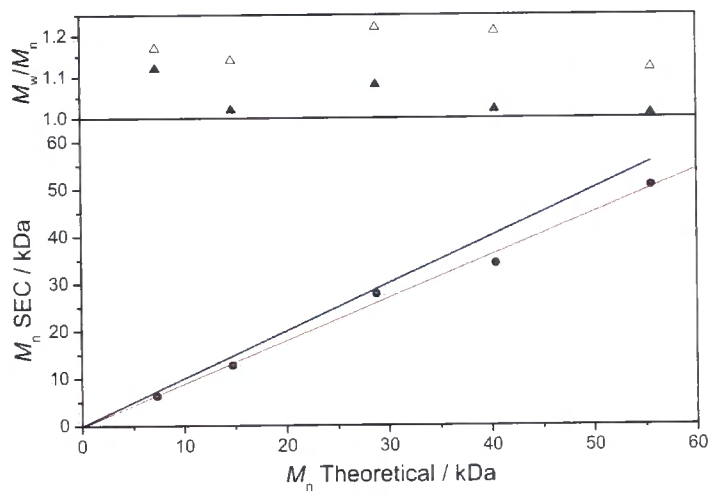

(b)

Figure 2.15: Data for the synthesis of poly[GlcEMA] of varying targeted M_n: (a) Normalised RI traces of varying targeted M_n: (b) Plot of M_n (SEC) and M_w/M_n vs. M_n (Thr). (•) M_n (SEC), (—) linear fit of M_n (SEC) ($R^2 = 0.99$), (—) M_n (Thr)., (▲) M_w/M_n (RALS), (△) M_w/M_n (Conv.).

standard (Polymer Labs, M_n = 28.7 kDa, M_w/M_n = 1.04, dn/dc = 0.133 ml g^{-1}) was analysed under the same conditions. Here values of M_w/M_n were calculated as 1.02 and 1.19 for TriSEC and conventional calibration methodologies respectively, compared with the manufacturers quoted value of 1.04. Thus, although the values of M_w/M_n from TriSEC appear to be lower than the real values they also appear to be far more realistic than those calculated by conventional calibration. The cause of the artificially low values currently remains unknown.

2.2.4.4 Chain extension and block copolymer synthesis

To confirm the presence of the dithioester polymer end groups, p[GalEMA] was chain extended with GalEMA and 2-(dimethylamino)ethyl methacrylate (DMAEMA). A poly[GalEMA] macroRAFT agent ($DP_n \sim 50$) was synthesised as before and purified by dialysis. The macro-RAFT agent was then used in the polymerisation of the appropriate monomer in a similar manner.

Table 2.5: Data for block copolymer synthesis with poly[2-(β-D-galactosyloxy)ethyl methacrylate]

Polymer	Initial M_n (kDa)	Initial M_w/M_n	$M_{n,thr}$ (kDa)	$M_{n,SEC}$ (kDa)	M_w/M_n
p[GalEMA-*b*-GalEMA]	13.2	1.01[a]	24.9	21.1	1.13[a]
p[GalEMA-*b*-DMAEMA]	15.0	1.03[a]	19.1	18.4	1.01[a]

[a] M_w/M_n values as determined by triple detection SEC.

Figure 2.16 contains the SEC chromatographs for a poly[GalEMA] macroRAFT, its chain extension by 2-(β-D-galactosyloxy)ethyl methacrylate (fig. 2.16a) and block

copolymer with 2-(dimethylamino)ethyl methacrylate (fig. 2.16b). In both cases it is clear that the copolymers elute at lower retention volume and thus have increased in molecular weight compared to the initial block and the copolymers have narrow, unimodal molecular weight distributions. Neither displays either a high molecular weight shoulder, the result of bimolecular termination, or obvious residual homopolymer, suggesting that reinitiation of the polymerisation is quantitative and still controlled. Chain extension of p[GalEMA] with GalEMA results in an increase in polydisperity as is commonly seen with block copolymer synthesis (table 2.5). With DMAEMA the polydispersity decreases although, rather than being a true value of M_w/M_n, this is more likely caused by an inaccurate value of dn/dc which was calculated from a single injection SEC experiment.

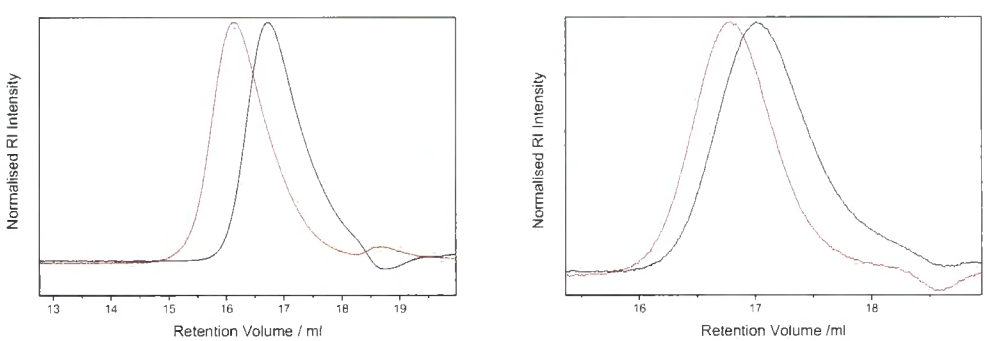

(a) (b)

Figure 2.16: SEC chromatographs for poly[2-(β-D-galactosyloxy)ethyl methacrylate] block copolymers: (a) chain extension with GalEMA; (b) block copolymer with 2-(dimethylamino)ethyl methacrylate.

2.2.5 Synthesis of statistical copolymers with HEMA

In order to produce polymers of reduced carbohydrate density, statistical copolymers with 2-hydroxyethyl methacrylate were synthesised at varying GalEMA/HEMA feed ratios (table 2.6). Polymerisations were conducted as before but the reaction time was increased to 16 h and an increased [CTA]:[Initiator] ratio to increase control over the extended reaction time. After this time the reaction solution was diluted with UHQ water and dialysed as before. Except for the HEMA homopolymer (entry 4, table 2.6), which precipitated upon dilution, all polymers were found to be water soluble. Overall monomer conversion was determined by ^{1}H NMR spectroscopy of the crude reaction mixture using the ratio of vinyl and backbone/methyl protons. As the vinyl peaks of GalEMA and HEMA overlap closely the conversion of the individual monomers was not determined although it is expected that, considering its usual reactivity, the conversion of GalEMA will approximate to 100 %. Composition of the polymers was determined by integration of the anomeric and backbone/methyl protons in the ^{1}H NMR spectra of the purified polymers.

For feed ratios of up to 50 % HEMA the conversions were high ($\geq$ 95 %) but were limited when the feed ratio reacheds 75 % HEMA. Polymer compositions agreed well with the monomer feed ratios when 25 and 50 % GalEMA were used but were somewhat reduced where 75 % GalEMA was used with a glycomonomer content of 69 mole %. The reduced incorporation of GalEMA was unexpected as it was thought to be the more reactive monomer under the polymerisation conditions, requiring an increased reaction time to reach similar conversion. Although the reason for this remains unknown one explanation lies in the solubility of HEMA. HEMA is water

Table 2.6: Data for the statistical copolymerisation of 2-hydroxyethyl methacrylate and 2-(β-D-galactosyloxy)ethyl methacrylate

Run	[GalEMA][a] (mM)	[HEMA][a] (mM)	f GalEMA[b] Thr	NMR	χ[c] (%)	M_n/kDa Theory[d]	SEC	M_w/M_n
1	296	99	75	69	98	12.2	18.3	1.05
2	197	197	50	50	95	10.3	18.3	1.07
3	99	296	25	26	80	6.9	—[e]	—[e]
4	0	395	0	0	—[f]		—[f]	—[f]

[a] Added as 0.5 M solutions; [b]Thr, monomer fraction from feed ratio; NMR, feed ratio as calculated from ^{1}H NMR spectroscopy of purified polymer; [c] monomer conversion as calculated from ^{1}H NMR spectrum of crude polymerisation solution; [d] calculated using eqn. 1.2 on page 36 with allowance for the differing monomer compositions; [e] sample too small to analyse accurately by SEC; [f] polymer insoluble in D_2O.

soluble but the solubility of its homopolymers is highly dependent on chain length and temperature with relatively short polymers displaying a lower critical solution temperature. [163] Thus, at polymerisation temperatures, a propagating polymer chain containing a large amount of HEMA will have a reduced rate of propagation as it will be less hydrated and accessible to monomer, particularly bulky monomers such as GalEMA. This reduced reactivity is evident in the comparatively low conversion seen in the 75–25 HEMA-GalEMA polymer even after 16 h of reaction. When lower feed ratios of HEMA are used the propagating chains will have a solubility nearer that of a GalEMA homopolymer and chain terminus should be more accessible to monomer. Also, the lower rate of HEMA polymerisation is probably not due to it being inherently less reactive, in fact its smaller size and less hindered nature would

suggest a higher reactivity than GalEMA. Consequently its slower propagation rate is probably due to reduced polymer solubility whereas when the polymer chain is solubilised by the presence of saccharides the true reactivity of HEMA may be seen.

2.3 Conclusions

Synthesis of anomerically pure 2-(D-glycosyloxy)ethyl methacrylates has been demonstrated by modification of literature procedures. Although such monomers have been synthesised on multiple occasions reaction conditions have often been laborious and materials expensive. The combination of sonication and an excess of the glycosyl acetate allowed multi-gram quantities of peracetylated glycomonomers to be synthesised in hours, rather than days, and at a level of purity that was high enough to use in further synthetic steps without the need for chromatography. Post-deprotection, the use of automated flash column chromatography increases the repeatability of producing high purity glycomonomers whilst further reducing the synthetic time.

Reversible addition-fragmentation chain transfer polymerisation has been demonstrated to polymerise these monomers, under aqueous conditions, to yield polymers of defined molecular weight and narrow polydispersity, two aspects that may be required for good manufacturing practice were such polymers to be used in pharmaceuticals. Equally, the 'living' nature of the these polymerisations has been demonstrated by chain extension and block copolymer synthesis allowing the construction of more complex polymer architectures without needing to resort to more challenging polymerisation techniques or protecting group chemistry.

2.4 Experimental

2.4.1 General

2.4.1.1 Materials

β-D-Galactose pentaacetate (98 %), β-D-glucose pentaacetate (98 %), phenylmagnesium bromide (1M in THF), carbon disulfide (98 %), potassium ferricyanide (98 %), 2-hydroxyethyl methacrylate (98 %, HEMA) and potassium carbonate (99 %) were purchased from Aldrich. Boron trifluoride diethyl etherate (purum, dist.), 4,4'-azobis(4-cyanopentanoic acid) (98 %) and 2-(dimethylamino)ethyl methacrylate (98 %) were purchased from Fluka. Amberjet 1200H strong acid cation exchange resin was purchased from Fisher. All solvents were Fisher HPLC grade, when anhydrous solvents were required they were passed through alumina columns prior to use. 2-Hydroxyethyl methacrylate and 2-(dimethylamino)ethyl methacrylate were chromatographed on basic alumina to remove inhibitors prior to polymerisation. All other chemicals were used without further purification. Flash column chromatography was performed using a Biotage SP1 automated purification system using pre-packed silica columns.

2.4.1.2 Analysis

NMR spectra were recorded using a Varian Inova 500 spectrometer at 499.87 (^{1}H) and 125.67 MHz (^{13}C, ^{1}H decoupled at 500 MHz) or using a Bruker Avance 400 spectrometer at 400.13 MHz (^{1}H) or 100.26 MHz (^{13}C, ^{1}H decoupled at 400 MHz). NMR spectra were analyzed using the Varian VNMR 6.1C or MestRe Nova 5.2 soft-

ware. IR spectra were recorded on a Perkin-Elmer 1600 Series FT-IR spectrometer by casting a film on NaCl plates from either DCM or MeOH. Mass spectra were acquired using a Micromass LCT spectrometer using ES+ and ES- modes of ionization. Elemental analyses were obtained using an Exeter Analytical Inc. E-440 Elemental Analyzer. Aqueous SEC was performed using a triple detection method (with angular correction) and measurements were performed on a Viscotek TDA 301 triple detection SEC fitted with two (300 × 7.5 mm) GMPWxl methacrylate-based mixed bed columns with an exclusion limit of 5×10^7 g mol^{-1}, having refractive index, viscometer and RALLS detectors. The eluent was 0.2 M $NaNO_3$ and 0.1M NaH_2PO_4 in UHQ water, unless otherwise stated, at a flow rate of 1.0 ml/minute and a constant temperature of 30 °C. Calibration (for detector response) was achieved using a single narrow PEO standard (Polymer Labs) of 82,500 g mol^{-1} and a dn/dc value of 0.133 ml g^{-1}. Conventional calibration was achieved using a selection of narrow PEO standards (Polymer Labs, M_p = 400–126500 Da). Molecular weights were determined using the Omnisec 4.0 for Windows software with dn/dc values as given in table 2.3.

2.4.2 Synthesis of 2-(2',3',4',6'-tetra-*O*-acetyl-β-D-galactosyloxy)ethyl methacrylate

β-D-Galactose pentaacetate (5.0 g, 12.8 mmol) and 2-hydroxyethyl methacrylate (1.4 ml, 1.5 g, 11.5 mmol) were dissolved in anhydrous dichloromethane (20 ml) and sonicated under a blanket of anhydrous N_2 for 5 minutes; subsequently, $BF_3.Et_2O$ (5.0 ml, 5.75 g, 40.5 mmol) was added via syringe and the solution was sonicated for

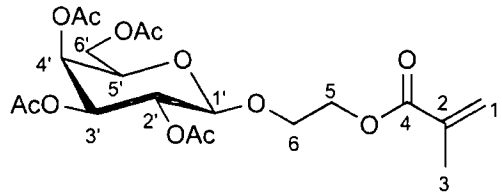

Figure 2.17: 2-(2',3',4',6'-tetra-*O*-acetyl-β-D-galactosyloxy)ethyl methacrylate.

a further 45 min. The reaction mixture was washed with brine (30 ml), the organic layer dried over $MgSO_4$ and butylhydroxytoluene was added as an inhibitor. The solvent was removed under reduced pressure, yielding crude AcGalEMA as a yellow oil; this was used directly for the synthesis of 2-(β-D-galactosyloxy)ethyl methacrylate (GalEMA). A sample for analysis was purified by flash column chromatography (7:3, hexane:ethyl acetate).

Found C, 51.88; H, 6.18; $C_{20}H_{28}O_{12}$ requires C, 52.17; H, 6.13. FT-IR ν/cm^{-1}: 1751 (C=O of acetate groups) 1719 (C=O of methacrylate ester) 1637, 1320, 1298 (C=C). δ_H: (400 MHz, $CDCl_3$) 1.98 (3H, s, 3 × H-3), 2.01, 2.04, 2.05, 2.15, (3H × 4, 4s, Ac × 4), 3.84 (1H, ddd, $J_{6a,6b}$ 11.5 Hz, $J_{5a,6a}$ 7.5 Hz, $J_{5b,6a}$ 4.0 Hz, H-6a), 3.92 (1H, td, $J_t = J_{5',6a'} = J_{5',6b'}$ 6.6 Hz, $J_d = J_{4',5'}$ 1.1 Hz, H-5'), 4.06 (1H, ddd, $J_{6a,6b}$ 11.6 Hz, $J_{5b,6b}$ 5.9 Hz, $J_{5a,6b}$ 3.7 Hz, H-6b), 4.10 (1H, dd, $J_{6'a,6'b}$ 10.3 Hz, $J_{5',6'a}$ 6.7 Hz, H-6'a), 4.18 (1H, dd, $J_{6'a,6'b}$ 10.9 Hz, $J_{5',6'b}$ 6.5 Hz, H-6'b), 4.29 (2H, m, H-5a,b), 4.55 (1H, d, $J_{1',2'}$ 8.05 Hz, H-1'), 5.01 (1H, dd, $J_{2',3'}$ 10.4 Hz, $J_{3',4'}$ 3.6 Hz, H-3'), 5.23 (1H, dd, $J_{2',3'}$ 10.4 Hz, $J_{1',2'}$ 8.0 Hz, H-2'), 5.39 (1H, dd, $J_{3',4'}$ 4.5 Hz, $J_{4',5'}$ 1.2 Hz H-4'), 5.59–5.61 (1H, m, H-1 Z to Me-C=C), 6.13–6.14 (1H, m, H-1 E to Me-C=C). δ_C: (100.26 MHz, decoupled, ^1H 400 MHz; $CDCl_3$) 18.25 (C-3), 20.6, 20.8, 21.0 (4 × H_3CCO_2, 2 resonances overlap), 61.3 (C-6'), 63.5 (C-5), 66.8 (C-4'), 67.4 (C-6),

68.7 (C-2'), 70.7 (C-3'), 70.9 (C-5'), 101.3 (C-1'), 125.9 (C-1), 136.1 (C-2), 167.1 (C-4), 169.4, 170.2, 170.3 ($MeCO_2$). LR-MS (ES^+) m/z requires 483.4, found 483.2 ($M + Na^+$).

2.4.3 Synthesis of 2-(β-D-galactosyloxy)ethyl methacrylate

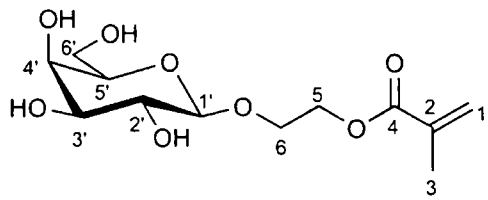

Figure 2.18: 2-(β-D-galactosyloxy)ethyl methacrylate.

Typically, crude AcGalEMA (2.5 g, 5.5 mmol) was stirred in damp MeOH (20 ml). K_2CO_3 (1.0 g, 7.2 mmol) was added and the reaction was monitored by TLC (9:1, MeCN:H_2O). When the product of methacrylate ester cleavage was seen in the TLC (R_f = 0.15) the reaction was neutralized by filtering into a flask containing Amberjet 1200H (H^+) cation exchange resin and the mixture was stirred for 15 minutes. [NB: The deprotection reaction can proceed very rapidly; to prevent loss of the product because of methacrylate cleavage, ensure that the apparatus for filtration and neutralization are set up and ready for use before addition of K_2CO_3]. The resin was removed by filtration and the solvent was removed under reduced pressure. The resulting oil was purified by column chromatography ($CHCl_3$:MeOH, gradient elution) to yield a colorless oil which became a white amorphous solid upon lyophilising. The resulting GalEMA was dissolved in D_2O to give a 0.50 M solution that was stored at -18 °C.

Found C, 49.12; H, 6.94; $C_{12}H_{20}O_8$ requires C, 49.31; H, 6.90. FT-IR (NaCl Plates) ν/cm^{-1}: 3360 (br, OH), 1708 (C=O of methacrylate ester) 1636, 1320, 1298 (C=C). δ_H: (500 MHz; D_2O) 1.94 (3H, m, 3 × H-3), 3.48 (1H, dd, $J_{2',3'}$ 9.7 Hz, $J_{3',4'}$ 3.3 Hz, H-3'), 3.53 (2H, dt, J_t 5.09 Hz, J_d 5.7 Hz, H-5'), 3.74 (2H, m, H-6') 3.84 (1H, m, H-4') 3.86 (1H, ddd, $J_{6a,6b}$ 11.8, $J_{5b,6b}$ 6.0, $J_{5b,6a}$ 3.8 Hz, H-6a) 4.12 (1H, ddd,$J_{6a,6b}$ 11.6, $J_{5b,6b}$ 5.9, $J_{5a,6b}$ 3.7 Hz, H-6b) 4.29 (1H, d, 7.5, H-1') 4.35 (2H, m, H-5) 5.64 (1H, m, H-1 Z to Me-C=C) 6.14 (1H, m, H-1 E to Me-C=C); δ_C: (100.62 MHz; decoupled ^1H 500 MHz; D_2O) 18.4 (C-3), 62.5 (C-6'), 65.3 (C-5), 68.5 (C-6), 70.3 (C-4'), 72.4 (C-2'), 74.9 (C-3'), 76.7 (C-5'), 103.2 (C-1'), 126.4 (C-1), 137.7 (C-2), 168.8 (C-4). LR-MS (ES^+) m/z requires 315.3, found 315.1 ($M + Na^+$).

2.4.4 Synthesis of 2-(2',3',4',6'-tetra-*O*-acetyl-β-D-glucosyloxy)ethyl methacrylate

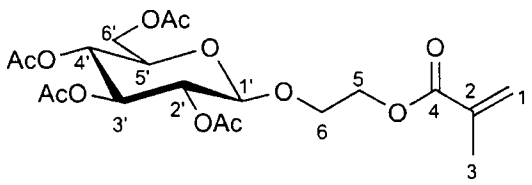

Figure 2.19: 2-(2',3',4',6'-tetra-*O*-acetyl-β-D-glucosyloxy)ethyl methacrylate.

AcGlcEMA was synthesised using an identical procedure to AcGalEMA from glucose pentaacetate and HEMA. Crude AcGlcEMA was isolated as a yellow oil and used directly in the synthesis of GlcEMA.

Found C, 51.79; H, 6.75; $C_{20}H_{28}O_{12}$ requires C, 52.17; H, 6.13. FT-IR ν/cm^{-1}: 1756 (C=O of acetate groups), 1716 (C=O of methacrylate ester), 1637, 1320, 1298

(C=C). δ_H: (400 MHz, $CDCl_3$) 1.98 (3H, s, 3 × H-3), 2.00, 2.02, 2.04, 2.12, (3H × 4, 4s, Ac × 4), 3.65 (1H, td, $J_{4',5'}$ 10.4 Hz,J_t = $J_{5',6a'}$ 2.4 Hz, $J_{5',6b'}$ 4.6 Hz, H-5'), 3.84 (1H, ddd, $J_{6a,6b}$ 11.5 Hz, $J_{5a,6a}$ 7.2 Hz, $J_{5b,6a}$ 3.6 Hz, H-6a), 4.08 (2H, m, H-6) 4.24 (1H, dd, $J_{6'a,6'b}$ 12.4 Hz, $J_{5',6'b}$ 4.6 Hz, H-6'b), 4.26-4.32 (2H, m, H-5a,b), 4.55 (1H, d, $J_{1',2'}$ 8.05 Hz, H-1'), 5.02 (1H, dd, $J_{1',2'}$ 8.0 Hz, $J_{2',3'}$ 9.8 Hz, H-2'), 5.10 (1H, dd, $J_{3',4'}$ 1.1 Hz, $J_{4',5'}$ 10.4 Hz H-4') 5.21 (1H, dd, $J_{2',3'}$ 9.8 Hz, $J_{3',4'}$ 1.1 Hz, H-3'), 5.60-5.63 (1H, m, H-1 Z to Me-C=C), 6.11-6.13 (1H, m, H-1 E to Me-C=C). δ_C: (100.26 MHz, decoupled, ^1H 400 MHz; $CDCl_3$) 18.3 (C-3), 20.6, 20.9, 21.1 (4 × H_3CCO_2, 2 resonances overlap), 61.6 (C-6'), 63.4 (C-5), 67.6 (C-6), 68.1 (C-4'), 68.9 (C-2'), 71.7 (C-5'), 72.8 (C-3'), 100.7 (C-1'), 127.4 (C-1), 136.3 (C-2), 168.1 (C-4), 169.4, 170.2, 170.3 ($MeCO_2$). LR-MS (ES^+) m/z requires 483.4, found 483.3 ($M + Na^+$).

2.4.5 Synthesis of 2-(β-D-glucosyloxy)ethyl methacrylate

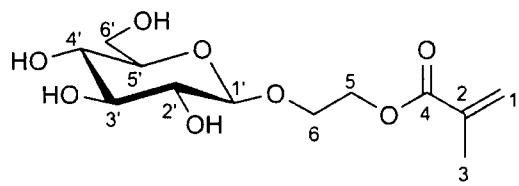

Figure 2.20: 2-(β-D-glucosyloxy)ethyl methacrylate.

2-(β-D-glucosyloxy)ethyl methacrylate was synthesised using an indentical procedure to GalEMA from AcGlcEMA and was isolated as a colorless oil which became a white amorphous solid upon lyophilising. The resulting GlcEMA was dissolved in D_2O to give a 0.50 M solution and stored in a freezer. Found C, 49.12; H, 6.94;

$C_{12}H_{20}O_8$ requires C, 49.31; H, 6.90. FT-IR (NaCl plates) ν/cm^{-1}: 3360 (br, OH), 1708 (C=O of methacrylate ester) 1636, 1320, 1298 (C=C); δ_H: (500 MHz; D_2O) 1.90 (3H, m, 3 × H-3), 3.16 (1H, dd, $J_{1',2'}$ 7.81 Hz, $J_{2',3'}$ 9.27 Hz, H-2'), 3.32–3.47 (3H, m, H-3', H-4', H-5'), 3.68 (1H, dd, $J_{6'a,6'b}$ 11,96 Hz, $J_{5',6'a}$ 5.37 Hz, H-6'a), 3.74 (1H, dd, $J_{6'a,6'b}$ 11.96 Hz, $J_{5',6'b}$ 7.0 Hz, H-6'b), 3.79–3.86 (2H, m, H-4', H-6a), 4.07 (1H, ddd, $J_{6a,6b}$ 11.65 Hz, $J_{5b,6b}$ 5.80 Hz, $J_{5a,6b}$ 3.78 Hz, H-6b), 4.26-4.35 (2H, m, H-5a, H-5b), 4.29 (1H, d, $J_{1',2'}$ 7.81 Hz, H-1'), 5.61–5.71 (1H, m, H-1 Z to Me-C=C), 6.04–6.14 (1H, m, H-1 E to Me-C=C); δ_C: (100.62 MHz; decoupled ^1H 500 MHz; D_2O) 18.4 (C-3), 62.5 (C-6'), 65.3 (C-5), 68.5 (C-6), 70.3 (C-4'), 72.4 (C-2'), 74.9 (C-3'), 76.7 (C-5'), 103.2 (C-1'), 126.4 (C-1), 137.7 (C-2), 168.8 (C-4). LR MS (ES^+) m/z requires 315.3, found 315.1 ($M + Na^+$).

2.4.6 Synthesis of (4-cyanopentanoic acid)-4-dithiobenzoate

(4-Cyanopentanoic acid)-4-dithiobenzoate was synthesised according to a literature procedure. [99]

2.4.6.1 Synthesis of di(thiobenzoyl) disulfide

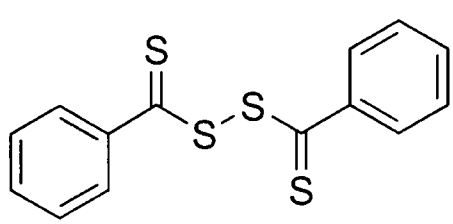

Figure 2.21: Structure of di(thiobenzoyl) disulfide

Typically, a solution of phenylmagnesium bromide in THF (300 ml, 1.0 M,

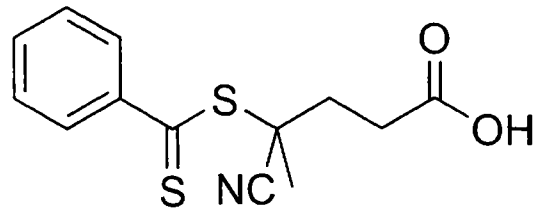

Figure 2.22: Structure of (4-cyanopentanoic acid)-4-dithiobenzoate

0.30 mol) was stirred under nitrogen at 0 °C. Carbon disulfide (25.65 g, 0.34 mol) was added dropwise and the mixture was stirred for a further hour. After this time the reaction was allowed to warm to room temperature and stirred for a further 30 min.; diethyl ether (500 ml) was then added. Hydrochloric acid (0.1 M) was added until the aqueous phase changed from red/brown to colourless. The purple organic phase was washed twice with distilled water, then NaOH (1 l, 0.1 M). The aqueous phase was then washed with diethyl ether, resulting in an aqueous solution of sodium dithiobenzoate. To this solution, potassium ferricyanide (99 g, 0.3 mol) in distilled water (1 l) was added over the course of 1 h. with stirring. The resulting red precipitate was filtered and washed with water until the washings were colourless. The precipitate was dried overnight and used for the synthesis of (4-cyanopentanoic acid)-4-dithiobenzoate without further purification.

2.4.6.2 Synthesis of (4-cyanopentanoic acid)-4-dithiobenzoate

Di(thiobenzoyl) disulfide (26 g, 85 mmol) and dry 4,4'-azobis(4-cyanopentanoic acid) (36 g, 126 mmol) in ethyl acetate (500 ml) were refluxed under nitrogen overnight, after cooling the solvent was removed under reduced pressure. TLC showed three spots (2:3 ethyl acetate:hexane) with the product spot being the middle one, $R_f = 0.3$.

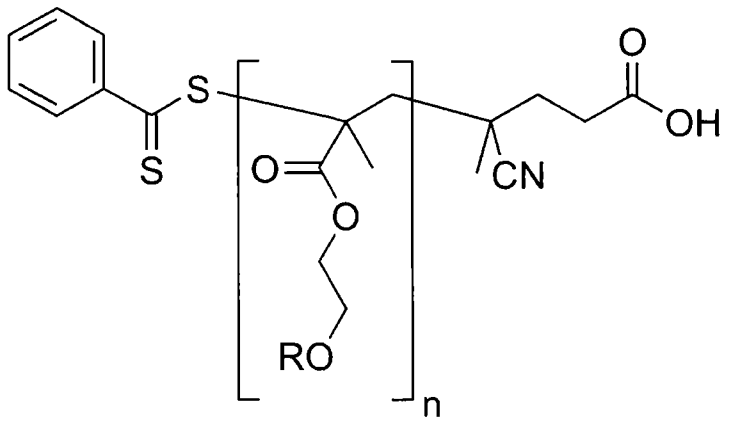

R = galactoside or glucoside

Figure 2.23: Structure of poly[2-(β-D-glycosyloxy)ethyl methacrylate]

The product was purified by flash column chromatography in the same solvent system, fractions which were red in colour were combined. Removal of the solvent left a red, viscous, oily residue which crystallised overnight in the freezer. The target compound was then recrystallised from toluene at 80 °C (14.9 g, 31%).

Found: C, 55.68; H 4.57; N, 4.78; S, 22.98; $C_{13}H_{13}NO_2S_2$ requires C, 55.89; H, 4.69; N, 5.01; S, 22.95. FT-IR (NaCl plates) ν / cm^{-1}: 3350-2600 (broad, COO-*H*); 2234 (CN); 1710 (C=O); 1048 (C=S). δ_H (500 MHz, $CDCl_3$): 1.93 (s, 3H, Me), 2.35-2.78 (m, 4H, 2 × CH_2), 7.38 (m, 2H, $H_{meta,arom.}$), 7.55 (m, 1H, $H_{para,arom.}$), 7.83 (m, 2H, $H_{ortho,arom.}$).

2.4.7 Polymerisation of 2-(β-D-galactosyloxy)ethyl methacrylate

For a typical polymerisation, a GalEMA solution (1.0 ml, 0.5 M, 0.5 mmol) was introduced to a small Schlenk tube and ethanol solutions of (4-cyanopentanoic acid)-

4-dithiobenzoate (175 μl, 0.015 M, 5.0 μmol) and 4,4'-azobis(4-cyanopentanoic acid) (83 μl, 0.015 M, 2.5 μmol) were added. The flask was sealed and the solution was degassed by 3 freeze-pump-thaw cycles, back-filled with N_2 and placed in an oil bath at 70 °C. Aliquots (100 μl) of the polymerisation solution were removed at regular intervals under N_2 flow, split in two and quenched by freezing in liquid nitrogen; the pairs of samples were analysed by ^{1}H NMR and aqueous SEC to determine conversion and molecular weight respectively. The remainder of the solution was dialysed against high purity water (Pierce Snakeskin dialysis tubing; MWCO 3.5 kDa) and the purified polymer solution was lyophilized to yield a pink hygroscopic solid.

δ_H (500 MHz, D_2O) 0.61-1.50 (3H, br, m CH_3-C), 1.53-2.41 (2H, br, backbone CH_2), 3.37-3.62, 3.62-3.72, 3.72-3.86, 3.86-4.02, 4.02-4.16, 4.16-4.36 (10H, protons of carbohydrate and methylene side chain), 4.44 (1H, br, anomeric proton), 7.52 ($H_{meta,arom.}$), 7.70 ($H_{para,arom.}$), 7.99 ($H_{ortho,arom}$). *Aromatic resonances from terminal dithiobenzoate moiety..*

2.4.8 Polymerisation of 2-(β-D-glucosyloxy)ethyl methacrylate

GlcEMA was polymerised using a protocol identical to that used in the polymerisation of GalEMA.

δ_H (500 MHz, D_2O) 0.61-1.50 (3H, br, m CH_3-C), 1.53-2.41 (2H, br, backbone CH_2), 3.37-3.62, 3.62-3.72, 3.72-3.86, 3.86-4.02, 4.02-4.16, 4.16-4.36 (10H, protons of carbohydrate and methylene side chain), 4.44 (1H, br, anomeric proton), 7.52

($H_{meta,arom.}$), 7.70 ($H_{para,arom.}$), 7.99 ($H_{ortho,arom}$). *Aromatic resonances from terminal dithiobenzoate moiety.*.

2.4.8.1 Kinetics of polymerisation

Experiments for the determination of polymerisation kinetics were prepared as described in section 2.4.7 but in an NMR tube fitted with a Young's valve. After degassing and backfilling with N_2, the tube was placed in an NMR spectrometer at 70 °C and ^{1}H NMR spectra were acquired at 5 minute intervals. The resulting spectra were analysed and conversion levels were calculated from the ratio of the integrals for the vinyl protons and the carbohydrate protons.

2.4.9 Chain extension of 2-(β-D-galactosyloxy)ethyl methacrylate

Typically, a macroRAFT agent of poly[GalEMA] was synthesised by polymerisation of GalEMA as described in section 2.4.7. Upon completion of the polymerisation the reaction vessel was opened to air and an equivalent quantity of the second monomer added as a solution in D_2O; an additional quantity of ACPA (2.5 μmol) was added as an EtOH solution. The reaction vessel was then resealed and degassed by three freeze-evacuate-thaw cycles before back-filling with N_2. The flask was then placed in a water bath at 70 °C for 4 h. After this time samples were removed for analysis by ^{1}H NMR and SEC and the remaining solution was dialysed against UHQ water.

2.4.10 Statistical copolymers of 2-hydroxyethyl methacrylate and 2-(β-D-galactosyloxy)ethyl methacrylate

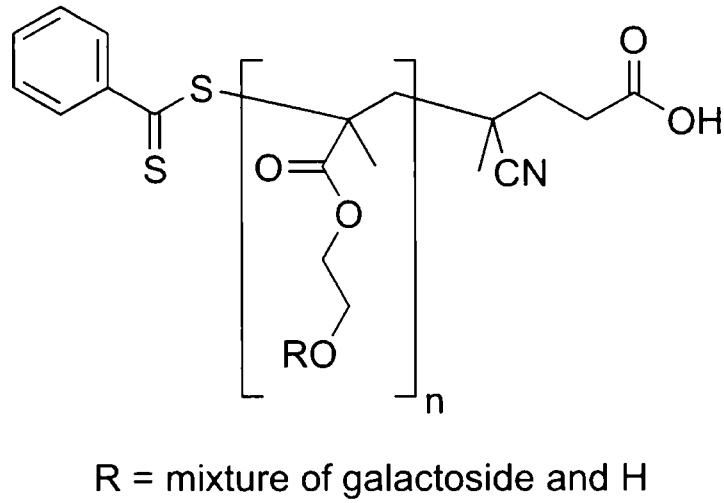

Figure 2.24: Structure of statistical copolymer of GalEMA and HEMA]

Table 2.7: Quantities used in the synthesis of statistical copolymers of 2-(β-D-galactosyloxy)ethyl methacrylate and 2-hydroxyethyl methacrylate

Run	[GalEMA][a] (mM)	[HEMA][a] (mM)	[CPADB][b] (mM)	[ACPA][b] (mM)	[M]/[CTA][c]	[CTA]/[Init]
1	296	99	7.9	3.1	50	2.6
2	197	197	7.9	3.1	50	2.6
3	99	296	7.9	3.1	50	2.6
4	0	395	7.9	3.1	50	2.6

[a] As 0.5 M solutions in D_2O; [b] as solutions in EtOH; [c] based upon total monomer concentration.

Statistical copolymers were synthesised as detailed in Table 2.7. Typically (entry 2 in Table 2.7), GalEMA (500 μl, 0.50 M, 0.25 mmol) and HEMA (500 μl,

0.50 M, 0.25 mmol) were added to a small Schlenk tube. CPADB (175 μl, 0.058 M, 10.0 μmol) and ACPA (90 μl, 0.043 M, 3.8 μmol) were added as solutions in EtOH and the mixture was degassed by three freeze-evacuate-thaw cycles and backfilling with N_2. The flask was then placed in an oil bath preheated to 70 °C overnight (approximately 16 h). A sample of the solution was removed and the conversion level was calculated by ^{1}H NMR spectroscopy and the remainder of the solution was diluted and dialysed against high purity water (Pierce Snakeskin dialysis tubing; MWCO 3.5 kDa) and lyophilised.

It is disconcerting to reflect on the number of students we have flunked in chemistry for not knowing what we later found to be untrue.

Robert L. Weber (1913–1997)

3

Binding of RAFTed glycopolymers to lectins

3.1 Introduction

The importance of multivalency in carbohydrate binding events was discussed briefly in section 1.1.2 and methods for the synthesis of glycopolymers of varying valency have been described in Chapter 2. Several reports investigating multivalent interactions in both carbohydrate and non-carbohydrate systems have been published previously (prominent examples include [17, 164]) and the area has been recently reviewed. Despite the considerable quantity of research in the area, the mechanisms behind the cluster glycoside/multivalency effect are still not completely determined. [15] In order to probe what parameters affect avidity, quantitative methods for its measurement are required. Two methods are commonly used to investigate binding interactions quantitatively; isothermal titration calorimetry (ITC) and surface plasmon resonance (SPR) and these have been used here in order to understand further the interaction of glycopolymers with lectins.

3.1.1 Isothermal titration calorimetry

Isothermal titration calorimetry is a technique that can be used to determine binding energies through classical thermodynamics. During any binding event heat is either released or absorbed. ITC measures the heat change in a system allowing for the determination of the binding constant (K_a), reaction stoichiometry (n), enthalpy change (ΔH), entropy change (ΔS) and Gibbs energy change (ΔG).

An ITC calorimeter consists of a pair of cells in an adiabatic enclosure (fig. 3.1). The first of these cells is the reference and contains only the solvent in which the binding event is to be measured; the second contains a solution of the macromolecule,

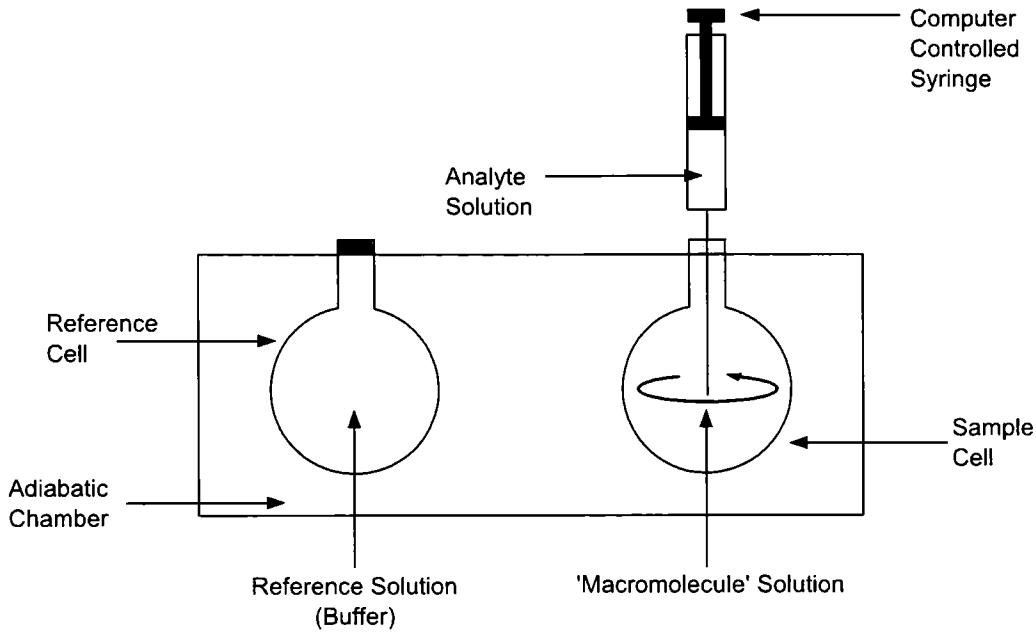

Figure 3.1: Schematic of an isothermal titration calorimeter

usually a protein, whose binding properties are under investigation. The ligand under investigation is injected into the cell by a computer controlled syringe allowing repeat injections, of accurate volumes, at specific time intervals. To maintain the cells at constant temperature, a small heater is attached to each and controlled by a power feedback system. In the case of an exothermic event, heat is released when the ligand and macromolecule bind resulting in increased temperature in the sample cell. If the cells are to remain at the same temperature, less heating must be applied to the sample cell compared to the reference. When endothermic events are investigated the situation is reversed. The difference in the power applied to the cells as a function of time is what is measured by an ITC experiment. Integration with respect to time provides the heat generated by each successive injection of

ligand solution. Early additions result in the formation of a large number of ligand-macromolecule complexes and similarly large heat changes. As the macromolecule binding sites start to become saturated the heat produced at each injection is reduced until complexation is not the main contributor to the signal and ligand dilution and mixing effects dominate. ΔH, K_a and n can be calculated by means of a non-linear least squares curve-fitting using an appropriate model; ΔS and ΔG may be calculated from these.

In order to calculate accurate values the curve needs to be reasonably sigmoidal, but the curve shape is affected by K_a, n and the concentration of binding sites ($[M]$). To aid the design of ITC experiments the so-called *Wiseman parameter*, c, is used (eqn. 3.1).

$$c = n.[M].K_a \tag{3.1}$$

Figure 3.2 contains simulated isotherms in the range $0.1 \leq c \leq 500$, such isotherms can only be deconvoluted to produce accurate values for the range ca. $1 \leq c \leq 1000$. [165]

3.1.2 Surface plasmon resonance for the study of binding events

Surface plasmon resonance is a phenomenon that is observed when light is reflected from thin metal surfaces or interacts with metal nanoparticles. In the latter case, the electromagnetic field causes a resonating polarisation of the conduction band electrons of the particle, yielding the intense colours seen in the solutions of such particles. For planar surfaces, at a particular angle, dependent on the refractive

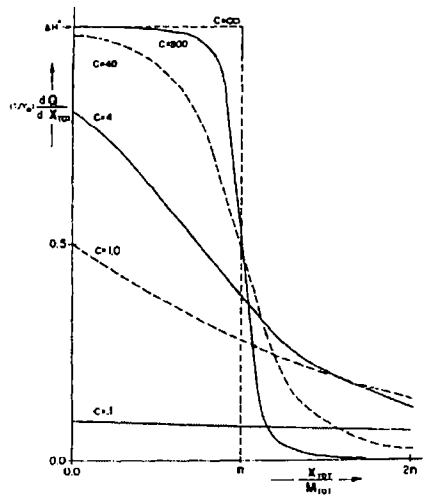

Figure 3.2: Simulated isotherms with varying parameter c. Reprinted from ref. [165] with permission from Elsevier.

index of the reverse side of the film, a fraction of the light energy interacts with the conduction band electrons resulting in a decrease in reflected intensity. Binding events can be probed by functionalising the backside of the film with a molecule to be investigated and incorporating the film into a flow cell, as seen in the BIAcore® systems. When an analyte solution is flowed through the cell then a shift in the refractive index occurs if the analyte binds. This results in a shift in the resonance angle which may be quantified to give the strength of binding. For a schematic of the experimental setup see Fig. 3.3.

Typically, the flow cell has four channels on the chip allowing different substrates, or varying levels of a single substrate, to be tested with a ligand within an individual experiment. It is also common to make allowances for non-specific binding by allocating one channel as a "blank" where, at the stage where a substrate would usually be attached, instead a simple molecule, such as ethanolamine, is used.

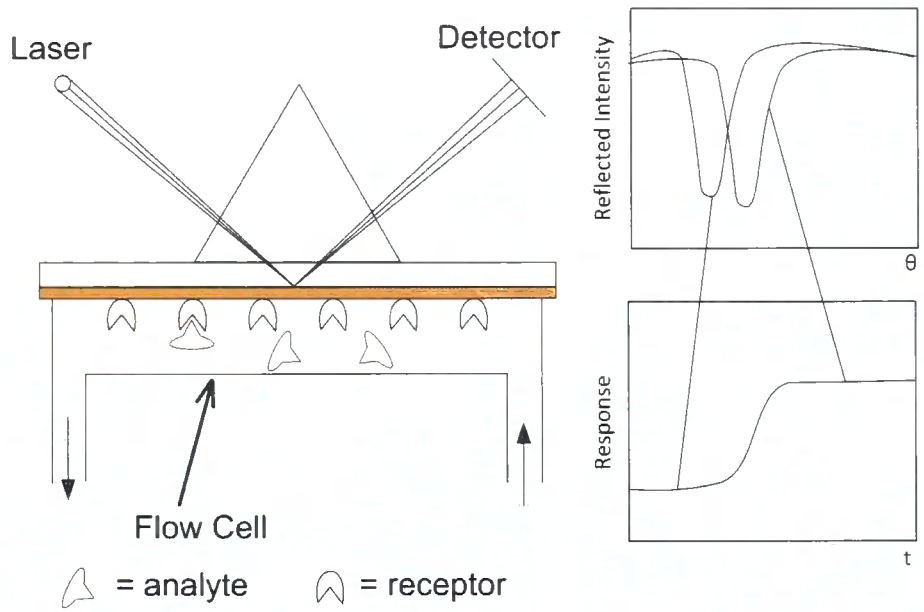

Figure 3.3: Schematic of a surface plasmon resonance experiment.

3.1.3 *Ricinus communis* agglutinins

Ricin and *Ricinus communis* agglutinin 120 (RCA_{120}) are lectin containing glycoproteins found in the seeds of the castor bean plant *Ricinus communis*. Ricin is a 60 kDa heterodimeric protein consisting of a pair of chains, 'A' and 'B' ~30 kDa each, linked by a disulfide bridge. Ricin is a Type II ribosome-inactivating protein (RIP): it is able to enter cells and, in turn, ribosomes. The B chain is the lectin component of the protein and binds terminal β-D-galactosyl or *N*-acetyl-β-D-galactosamino residues, allowing ricin to enter the cell via endocytosis. Once inside the cell, the A chain is released via reduction of the disulfide bridge.

The A chain is *N*-glycosidase that, once within the ribosome, depurinates an adenosine residue from ribosomal RNA resulting in inactivation of the ribosome and subsequent cell death through inhibition of protein synthesis. The target of

depurination is within the sarcin-ricin loop, an area that is highly conserved in eukaryotic cells; consequently ricin is a potent toxin. Due to its high toxicity and relatively easy availability (a large quantity of contaminated material is a byproduct of castor oil production) ricin is classified as a Schedule 1 agent under the Chemical Weapons Convention. [166]

RCA_{120} is a 120 kDa tetrameric protein formed by the non-covalent association of two identical 60 kDa heterodimeric subunits. Like ricin, these are comprised of 'A' and 'B' chains and are closely related to those of the ricin heterodimer (93 % and 84 % amino acid homology respectively). [167] Despite this close relationship the toxicity of RCA_{120} is considerably lower than that of ricin ($\sim$ 2000 fold [168]) but displays increased agglutination activity. [169] The reduced toxicity is not due to low *N*-glycosidase activity of the A chain as, in cell free assays, protein synthesis inhibition is only one order of magnitude lower than that of the ricin A chain and when the RCA_{120} A chain is combined with the ricin B chain the resulting heterodimer has a cytotoxicity nearing that of native ricin. Instead its reduced toxicity appears to be due to the differing quaternary structure resulting in a diminished ability to enter cells. [170]

3.2 Results and Discussion

The binding between RCA_{120} and a series of β-D-galactose bearing ligands was subjected to two forms of analysis: surface plasmon resonance and isothermal titration calorimetry. Although these techniques provide similar information regarding binding events, they are complementary, allowing investigation of different aspects of the

event occuring. ITC allows the determination of the thermodynamics of a binding event and can thus provide an insight into its mechanism, for example entropically driven events are likely to involve the displacement of water or other small ligands from the protein binding site. [171] SPR is more comparable to how the binding event may occur in vivo, where it is likely that lectins will be clustered on a cell surface with the ligand flowing past transiently. *Ricinus communis* agglutinin 120 (RCA_{120}) was chosen because initial SPR studies using *Peanut agglutinin* (PNA) found the binding to be so weak as to be undetectable by this method. This is unlikely to be due to genuinely weak interaction with the polymers as their binding to PNA has previously been demonstrated by ITC. [164] Instead, it is likely to be due to the lectin binding preferentially to the carboxylated methylcellulose coating on the SPR chip to which the lectin is attached covalently. Similar effects have been reported before by Kamerling et al. [172]

3.2.1 ITC studies on the binding between glycopolymers and RCA_{120}

Isothermal titration calorimety has previously been used to investigate the binding of p[GalEMA] to the PNA. The polymers investigated were synthesised by standard free radical polymerisation, consequently molecular weight was uncontrolled and those investigated were disparate: one low ($M_n \sim 3$ kDa, $M_w/M_n = 2.15$), the other high ($M_n \sim 461$ kDa, $M_w/M_n = 2.21$). [164] Here a set of polymers of intermediate molecular weights ($20 \leq M_n \leq 60$ kDa), in addition to the monomeric species, were compared with respect to their binding to RCA_{120}. Experiments were conducted by

a standard protocol and heats of dilution/mixing were determined by titration of the carbohydrate ligands into buffer alone and subtracted from the values for ligand–lectin binding. In all cases the Wiseman parameter, c, was in the range 1–100. Calorimetry data was analysed using Origin Labs Origin 7.0. Due to its potential toxicity, RCA_{120} is not available as a lyophilised powder, only as a buffered solution. The high sensivity of ITC requires that both ligand and macromolecule be dissolved in the same buffer to minimise the effect of solute dilution. As the accuracy of the buffer in which RCA_{120} was supplied could not be guaranteed it was buffer exchanged using gel filtration prior to use. The concentration of the resulting solution was determined by UV spectroscopy using a value of $A^{1\%}$ of 15.7 at 280 nm. [173] Some RCA_{120} precipitation was observed upon storage, consequently concentrations were redetermined prior to each experiment.

The previous study on poly[2-(β-D-galactosyloxy)ethyl methacrylate] binding to PNA utilised a complex model to fit the data, noting that the "single set of sites" model within the ITC software did not produce adequate fitting to derive thermodynamic parameters; a problem attributed to precipitation of polymer:protein aggregates formed upon binding. [164] Brewer et al. have reported successful derivation of thermodynamic parameters with multivalent ligands using the single sites model when the concentrations of ligand and macromolecule were such that no precipitation was observed. [174, 175] Here, although a small quantity of precipitation was observed when the largest ligand was used, a single site model was found to fit adequately. Figure 3.4 contains example raw calorimetry data, binding isotherm and curve of best fit for the binding between $p[GalEMA]_{144}$ and RCA_{120}. Despite the

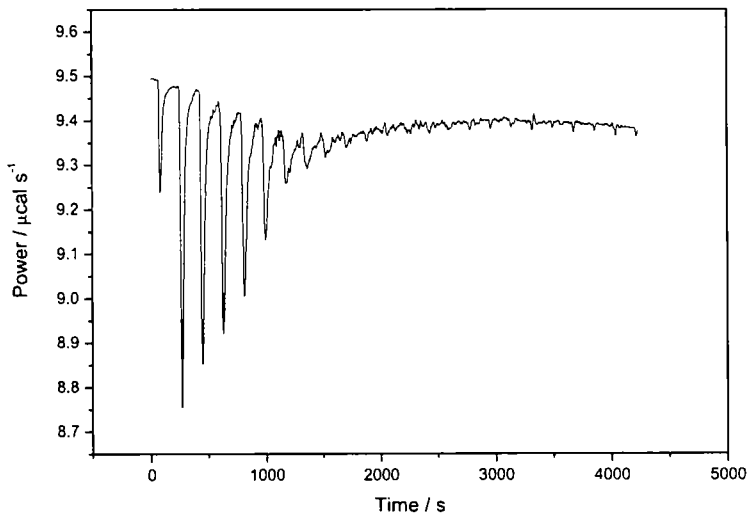

(a)

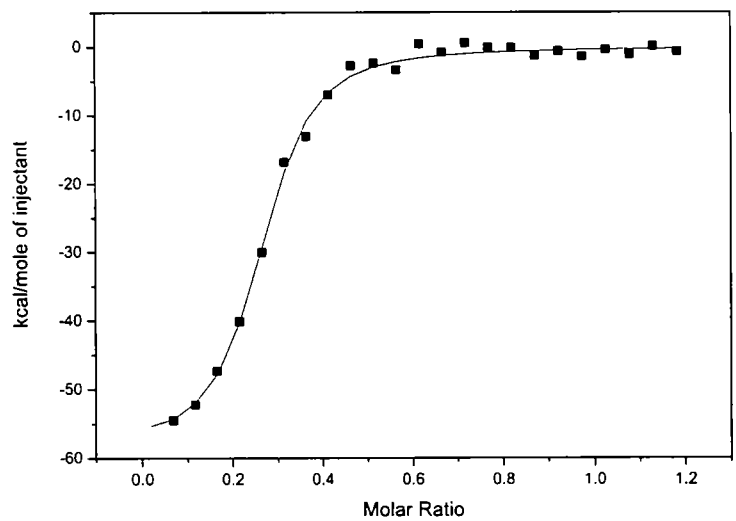

(b)

Figure 3.4: Isothermal titration calorimetry data for the binding of p[GalEMA]$_{144}$ to RCA$_{120}$

relatively poor quality of the raw data (fig. 3.4a), baseline correction and processing within the software resulted in an isotherm with the expected sigmoidal shape and fitting with the single set of identical sites model resulted in a curve in close agreement to the data. As the RCA_{120} tetramer is known to have two identical binding sites [173] n was fixed at 2 for monomeric GalEMA to simplify fitting. Ideally, each ligand:lectin binding event would have been measured in triplicate and mean values calculated. Here only a single experiment has been performed for each ligand due to the cost and availability of RCA_{120}. Although this means the values determined may not be considered completely accurate they certainly allow for the determination of general trends. An estimate of the accuracy of these values may be taken when the value of K_a for the monomeric species is compared to that of its binding to PNA as well as other monomeric galactose-ligands to RCA_{120}. Ambrosi et al. determined K_a for GalEMA:PNA binding to be 5.65×10^3 M^{-1} at 25 °C [164] and Sharma et al. determined K_a for methyl β-galactoside and galactose binding to RCA_{120} as 7.7×10^3 and 2.2×10^3 M^{-1} respectively at 15 °C. [173] An earlier report found similar values for the binding between RCA_{120} and galactose. [176] Here GalEMA was found to have a binding constant of 8.7×10^3 M^{-1} at 25 °C, within the expected range for a monovalent galactoside ligand binding to RCA_{120}.

3.2.1.1 Avidity

Values of K_a determined by various methods are given in table table 3.1. From these data it is clear that binding avidity to RCA_{120} is greatly enhanced through multivalency with K_a rising rapidly with molecular weight. The largest polymer here (DP_n 193) has an overall avidity over 4000-fold greater than the monomeric ligand.

On a per sugar basis this 22-fold increase is no less striking (fig. 3.5a). The non-linear behaviour observed is similar to that demonstrated by Kiessling et al. [177] with mannosylated polymers, who found a limiting molecular weight, after which avidity no longer increased. This may also be the case here but would require larger polymers to be synthesised. Kiessling et al. attributed the large increase on the longer polymers' ability to bridge binding sites on a single lectin. This is possible here as there is a particularly prominent increase in avidity between DP_n 144 and 193. The fully extended chain lengths for these polymers are ~36 and 47 nm respectively; assuming a C–C bond length of 1.54 Å and a dihedral angle of 109.5°. These are maximum lengths and solution conformations are likely to be considerably smaller with hydrodynamic diameters of ~8 and 11 nm respectively. The binding sites of RCA_{120} are approximately 11 nm apart (measured with Jmol [178,179] using the Protein Data Bank file from reference [180]) so, in solution, it seems likely that the 144 unit polymer is unlikely to be able to bridge both binding sites whereas the longer polymer would be able to do so, albeit with some loss of degrees of freedom.

Figure 3.5b plots 1/n, the number of lectins bound per ligand molecule (assuming both sites to be bound, the number of sites per ligand is equal to 2/n), against ligand valency. As is expected the number of bound lectins increases with valency of the ligand, although it appears that there is a slight decrease between the DP_n 68 and 144 polymers. It is unlikely that this is a real effect and is likely to be due to an inaccuracy in the model fitting in one case as values of n were easily affected with little change to other parameters. Considering the experimental error on these values it may be assumed that there is no increase in the number of ligands/sites

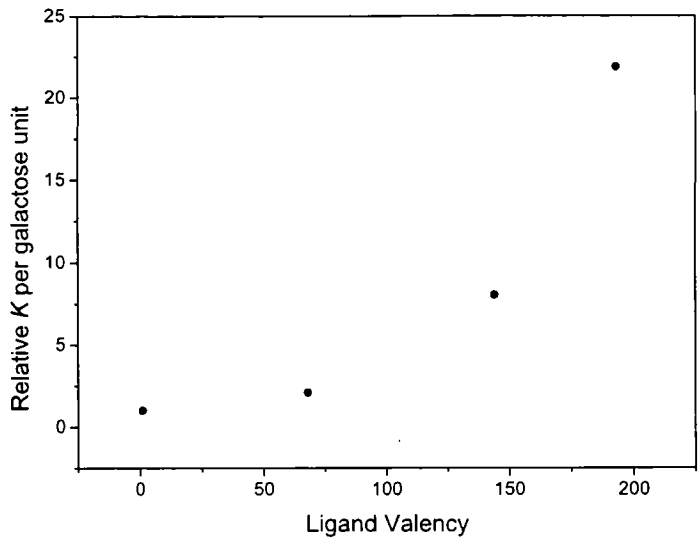

(a)

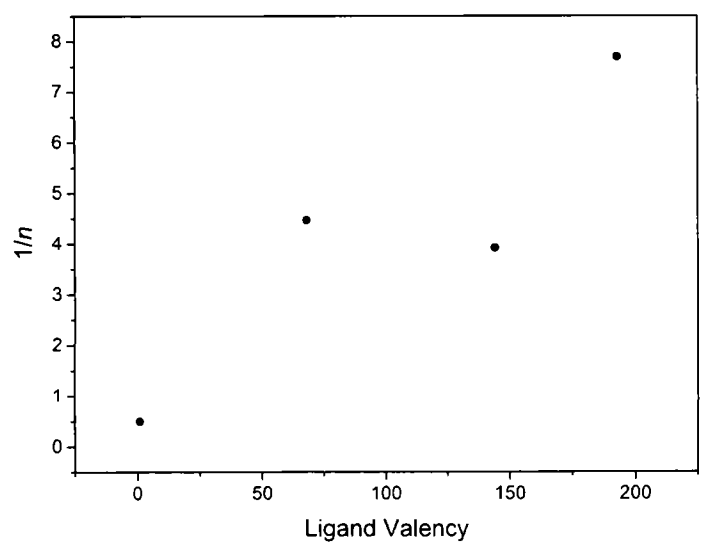

(b)

Figure 3.5: Dependence of K_a and 1/n on the valency of carbohydrate ligands

Table 3.1: Binding affinities and polymer sizes from different analyses.

Ligand	K_N^{poly} / M^{-1}			K_{ave}^{poly} / M^{-1}		l^a	$D_h{}^b$
	ITC	(rel)	Scatchard	ITC	(rel)	(nm)	(nm)
GalEMA	8.74×10^3	(1)	7.19×10^3	8.74×10^3	(1)	—	—
$pGalEMA_{68}$	1.24×10^6	(142)	1.06×10^6	1.82×10^4	(2)	17.2	6.2
$pGalEMA_{144}$	1.01×10^7	(1156)	9.87×10^6	7.01×10^4	(8)	36.2	8.3
$pGalEMA_{193}$	3.69×10^7	(4222)	3.58×10^7	1.91×10^5	(22)	46.6	11.4

[a] Approximate fully extended chain length assuming C–C bond length of 1.54 Å and a dihedral angle of 109.5°; [b] Hydrodynamic diameter as measured by TriSEC.

bound between these polymers but there is still a 4-fold difference in K_a per sugar. If the number of simultaneous binding events is not responsible for increased avidity then another factor must be. It is proposed that the increase in affinity is due to the increased probability of rebinding: i.e. if a lectin–carbohydrate interaction is broken there is a higher probability of a second interaction occuring in the longer polymer as there is larger local concentration of sugars available to bind.

3.2.1.2 Cooperativity?

Cooperativity in binding events is of great importance in biological systems. Binding cooperativity falls into three categories: positively cooperative, or synergistic, where one binding makes a latter more energetically favourable; non-cooperative where binding has no effect on subsequent binding(s); and negatively cooperative where binding makes a latter binding event less favoured. The most famous and well-studied case of cooperativity is the binding of oxygen to hemoglobin which displays positive cooperativity with each of the oxygen molecules binding having a greater

affinity than the previous.

Whitesides et al. have suggested that, in a polyvalent system, free energies may be considered thus: [181]

$$\Delta G_{\text{ave}}^{\text{poly}} = \alpha \Delta G^{\text{mono}} \tag{3.2}$$

$$N\Delta G_{\text{ave}}^{\text{poly}} = \Delta G_{N}^{\text{poly}} = \alpha N \Delta G^{\text{mono}} \tag{3.3}$$

where $\Delta G_{\text{ave}}^{\text{poly}}$ is the average free energy of each interaction in a polyvalent interaction, ΔG^{mono} is the free energy of the monovalent interaction, $\Delta G_{N}^{\text{poly}}$ is the overall free energy of a polyvalent interaction, N is the valency and α is the degree of cooperativity. Similarly, affinities may be considered thus:

$$K_{N}^{\text{poly}} = (K_{\text{ave}}^{\text{poly}})^{N} = (K^{\text{mono}})^{\alpha N} \tag{3.4}$$

where K_{N}^{poly} is the overall affinity of a polyvalent interaction, $K_{\text{ave}}^{\text{poly}}$ is the average affinity and K^{mono} is the affinity of the monovalent interaction. [181] In a positively cooperative system, one where $\alpha > 1$, it would be expected that a doubling of valency would result in at least a squaring of affinity. Values of K_{N}^{poly} are given in table 3.2 and these data make it clear that, although binding is increased greatly through polyvalency, $K_{N}^{\text{poly}} \ll (K^{\text{mono}})^{N}$ and thus binding is negatively cooperative. This result is expected because, to date, no multivalent system has been shown to be positively cooperative and a linear polymeric system is likely to be highly negatively cooperative due to steric crowding of the binding moieties.

3.2.1.3 Scatchard analysis

Modified Scatchard plots, based upon the method of Brewer et al. (see section 3.4.1.1 for details), [174, 175] are shown in figure 3.6. This methodology introduces

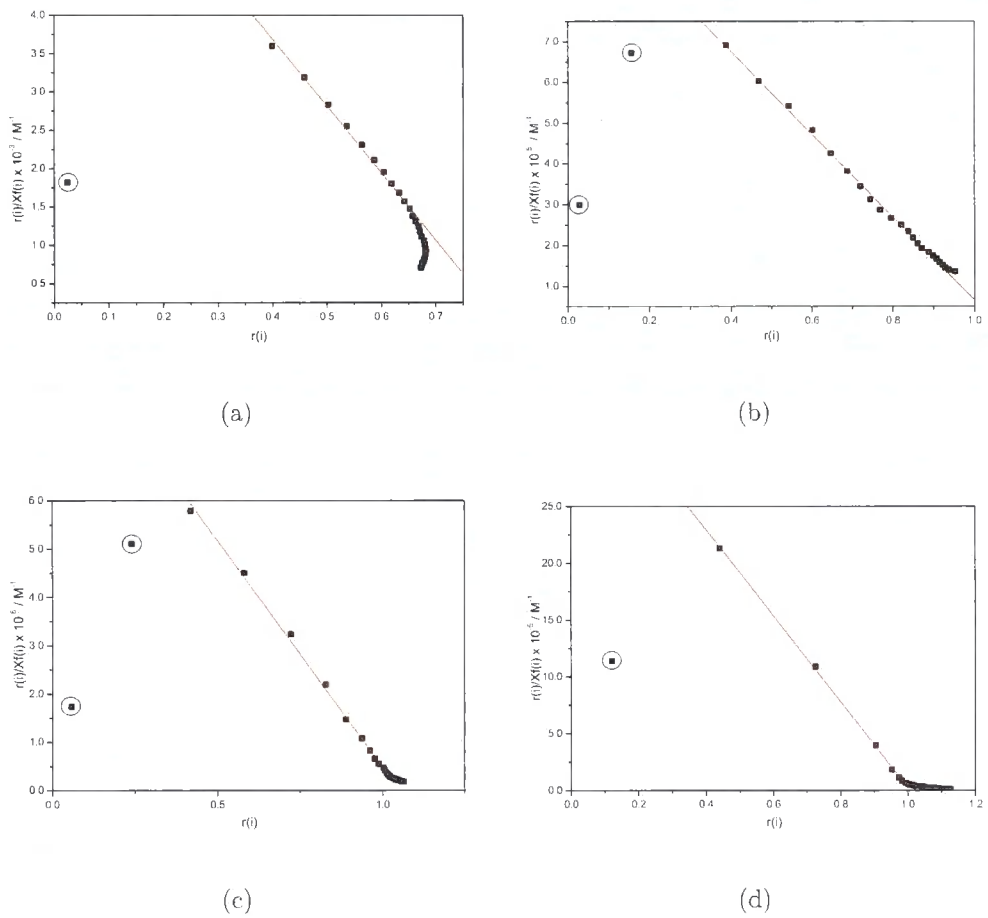

Figure 3.6: Scatchard plots for binding of GalEMA based ligands to RCA_{120}. (a) monomeric GalEMA; (b) $pGalEMA_{68}$; (c) $pGalEMA_{144}$; (d) $pGalEMA_{193}$. Circled points were discounted from analyses; (—) linear regression of linear segment of plot, $R^2 \geq 0.99$.

an additional term to allow for multivalent ligands and thus:

$$r(i) = \frac{X_b(i)[\text{average functional valency of ligand}]}{M_t(i)} \tag{3.5}$$

where the average functionality of ligand is the value $1/n$ given in table 3.2, $r(i)$ is the ligand occupancy after the ith injection, $X_b(i)$ concentration of bound ligand after the ith injection and $M_t(i)$ is the total concentration of lectin . Scatchard plots may then be constructed by plotting $r(i)/X_f(i)$ versus $r(i)$. To confirm the applicability of the method to this system values of K_N^{poly} were calculated by regression analysis of the linear section in each plot. These values may be found in table 3.1 and are in good agreement with those directly calculated using the Origin software. The Scatchard plots for all ligands studied are given in figure 3.6. All plots feature a maximum at the second or third point with a downward trend at low ligand occupancy ($r(i)$). Normally this would be indicative of positively cooperative binding but it has been noted before that, at low occupancies, Scatchard plots of calorimetry data are extremely sensitive to measurement errors. It has been estimated that an error of just 0.4 % in the initial heat measurements can result in such behaviour. [182] Consequently, these initial points (circled in the plots) were discounted from the analyses. Ignoring these points allows us to see that all plots are fundamentally linear with some deviation at high levels of occupancy. In the case of the polymer ligands there is a decrease in gradient at high occupancy, suggesting again that the binding is negatively cooperative. [183] In the case of the monomeric species there is an increase in gradient at high occupancy. This is unlikely to be a real effect and is probably due to the poor quality of data in the latter injections of such a weakly binding ligand.

3.2.1.4 Thermodynamic basis of binding

Table 3.2: Thermodynamic parameters for the binding between RCA_{120} and β-D-galactose bearing ligands

Ligand	ΔH_{obs}[a] kJ mol^{-1}	ΔG_{obs}[a] kJ mol^{-1}	$T\Delta S_{obs}$[a] kJ mol^{-1}	K_N^{poly}[b] M^{-1}	(rel.)	n[c]	$1/n$
GalEMA	-42.4	-22.5	-19.9	8.74×10^3	(1)	2[d]	0.5
$pGalEMA_{68}$	-159	-34.8	-124	1.24×10^6	(140)	0.224	4.46
$pGalEMA_{144}$	-245	-40.7	-204	1.01×10^7	(1155)	0.255	3.92
$pGalEMA_{193}$	-391	-43.7	-347	3.69×10^7	(4222)	0.130	7.69
$pGalEMA^e_{144}$	-242	-40.1	-202	1.07×10^7	(1224)	0.260	3.85

[a] As molarities rather than activities were used the values are reported as observed; [b] values relative to monomer are shown in brackets; [c] stoichiometry with respect to lectin, i.e. number of ligands per RCA_{120} tetramer; [d] n was fixed during curve fitting to allow calculation of the K and ΔH; [e] Calculated from isotherm without subtraction of heats of dilution.

The full thermodynamic parameters, as measured by ITC, are given in table 3.2. From these it is clear that for all ligands binding is enthalpically favoured yet entropically opposed. This is in contrast to both modelled behaviour of multivalent binding [184] and the binding of p[GalEMA] to PNA, which showed enthalpically and entropically driven multivalent binding. [164] The difference in thermodynamics between to the two lectin bindings is probably due to a combination of effects. Ambrosi et al. partly attributed the entropic factor to displacement of water from the protein surface through aggregation. As aggregation was only observed to a slight degree here less of an entropic factor is likely. Similar behaviour has been reported

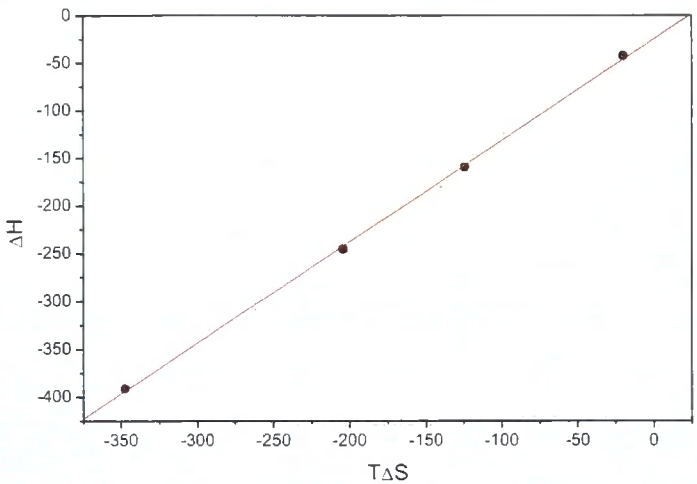

Figure 3.7: Compensation plot (ΔH vs. TΔS) for the binding of galactosyl ligands to RCA_{120}. (—) Linear fit. $R^2 = 0.999$, slope = 1.06.

by Brewer et al. for lectin binding of dendritic multivalent carbohydrates when aggregation was absent. [174, 175, 182] The enthalpic driving force is confirmed by the compensation plot (fig. 3.7) which is linear with a slope near unity (1.06 ± 0.02; $R^2 = 0.999$). As the value is greater than unity it suggests that the free energy is marginally more sensitive to changes in enthalpy, conversely a value less than unity would suggest a greater sensitivity to changes in entropy. Ambrosi et al. also noted that thermodynamic parameters were heavily influenced by ionic strength of the buffer used in the titration. Higher concentrations of salts resulted in an increased enthalpic contribution and a reduced entropic contribution: K_a was also reduced dramatically. This was particularly prominent when tris buffer was used, instead of citrate, with the binding becoming entropically disfavoured. It should also be noted that, due to the high heat of ionisation of tris ($\Delta H_{ion} \sim 46$ kJ mol^{-1} [185]),

values may not have been completely accurate. Here phosphate-buffered saline was used for all experiments due to the high solubility of RCA_{120} in this solution and heats of ionisation are relatively low ($-1 \leq \Delta H_{ion} \leq 4$ kJ mol^{-1} depending on ionic strength [185]). The minimal effect of buffer ionisation is confirmed by comparison of the thermodynamic parameters calculated with and without correction for heats of dilution/mixing (entries 3 and 5 in table 3.2) confirming that the lack of entropic contribution is not due to buffer choice. Entropic favourability would be likely if lectin binding leads to dispersion of polymer aggregates via increased degrees of freedom of the polymer chains. Glycopolymers have already been shown to self-associate in aqueous solution [186] with association attributed to intermolecular hydrogen bonding and hydrophobic interactions by the polymer backbone. No polymer aggregates have been detected, via SEC, for the polymers here so it can assumed that their disaggregation is not of concern. Overall binding would be expected to be entropically disfavoured as a bound polymer will have fewer possible solution conformations and thus a reduced number of degrees of freedom.

Interestingly, as molecular weight increases, the ratio $\Delta H/-T\Delta S$ decreases and tends towards 1 (black squares in figure 3.8). Similar behaviour has been noted in dendritic systems where ΔH was seen to scale approximately with valency, i.e. for a tetravalent system ΔH was approximately 4-fold that of the monovalent, but $-T\Delta S$ became more positive disproportionately. [187] This behaviour was attributed to the inability of a relatively rigid ligand to fill both binding sites on an individual lectin, instead binding one lectin for each ligand presented, resulting in a greater entropic cost. The same explanation is possible here as, although it appears that the longest

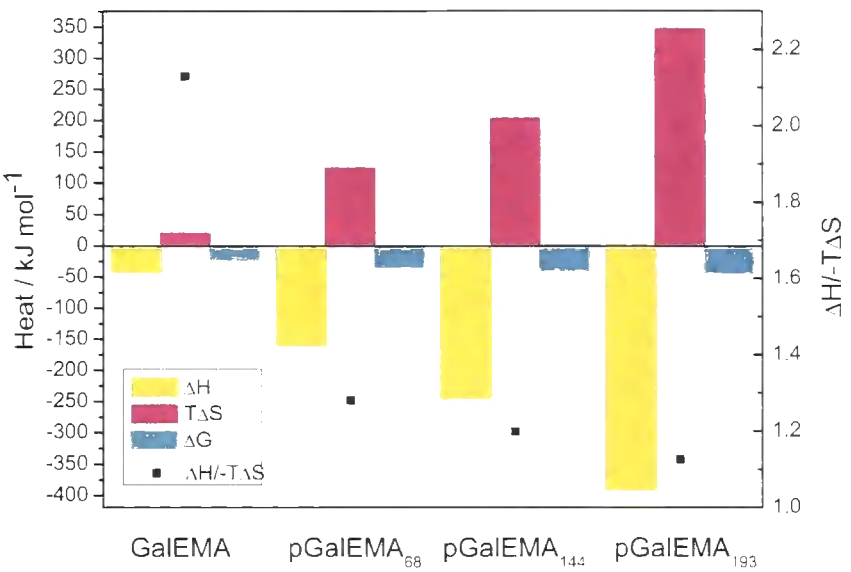

Figure 3.8: Thermodynamic parameters of binding of GalEMA based ligands to RCA_{120}

two polymers may be able to bind both sites of RCA_{120} simultaneously, to do so would restrict the degrees of freedom of the chain considerably, particularly for the DP_n 144 polymer which would be very extended. For the DP_n 196 this restriction would be reduced but it also binds a greater number of lectins resulting in a net loss of entropy. The decreasing ratio also suggests that, as reported by Kiessling et al., there may be a limiting chain length at which no further increase in avidity is seen as the increased enthalpic favourability can only match the entropic loss.

3.2.2 SPR studies on glycopolymers

Several reports of SPR studies on glycopolymers have been published previously. Unfortunately, all but one of these studies immobilised the polymer on the surface, only allowing determination of the multivalent to monovalent interaction. [188–190] Kiessling et al. have utilised polymer solutions in competitive assays by measuring Con A binding to mannosylated surfaces in the presence or absence of other mannosylated ligands. [177] Again, this does not allow elucidation of multivalent–multivalent interactions that are likely to occur between a multivalent polymer and a biological surface where receptors are clustered and not discrete. For the experiments RCA_{120} was attached to the surface of a sensor chip at various levels of functionalisation (ca. 200, 2000 and 5000 response units) using a standard amine coupling protocol. The final channel was modified with ethanolamine and used as a blank. Initially, a series of poly[2-(β-D-galactosyloxy)ethyl methacrylate] polymers of varying molecular weights and compositions as synthesised in Chapter 2 was assessed to determine whether binding was detectable and if there was any difference within the group. It was found that, of all the polymers tested, two general groups were found; one polymer in each group was selected for full analysis ($p[GalEMA]_{37}$, M_n 11.0 kDa, M_w/M_n 1.10 and $p[GalEMA]_{144}$, M_n 42.4 kDa, M_w/M_n 1.11). Solutions of each polymer, ranging from 500 pM to 10 μM, were prepared and analysed for the binding to each channel. Initial test runs found the binding too tight, with very long off times. To reduce this time, allowing rapid acquisition of another sample, a 30 s injection of methyl β-D-galactoside solution was performed. The blank was substracted from the functionalised channels to allow for non-specific binding.

Table 3.3: Kinetic and thermodynamic parameters of binding between RCA_{120} and poly[GalEMA] as calculated by surface plasmon resonance

Ligand	k_{on}	k_{off}	K_a	ΔG_{obs}[a]	Param.	Ratio[b]
	1/Ms	1/s	M^{-1}	kJ mol^{-1}	k_{on}	1.6
$p[GalEMA]_{37}$	9.54×10^{5}	5.28×10^{-3}	1.81×10^{8}	-47.1	k_{off}	0.2
$p[GalEMA]_{144}$	1.56×10^{6}	1.12×10^{-3}	1.39×10^{9}	-52.2	K_a	7.7

[a] Calculated from K_a; [b] $p[GalEMA]_{144}/p[GalEMA]_{37}$.

The channels with the lowest and highest levels of RCA_{120} modification were found to give too weak or too strong binding respectively. Sensorgrams were thus acquired on channel 2 (ca. 2000 RU RCA_{120}) by a 180 s injection of the ligand and a 240 s off period. Between acquisitions a 30 s injection of methyl β-D-galactoside and 60 s off period were performed to return the surface to its background level.

Sensorgrams for the two polymers at various concentrations are shown in figure 3.9. The data from these was fitted within the BIAcore software using a single sites model. For each polymer five consecutive concentrations were chosen from those analysed; 5 nM–1 μM for the DP_n 37 polymer and 500 pM–50 nM for $DP_n\tilde{1}44$ polymer. The highest concentrations were removed as the binding was too rapid to enable accurate fitting. In the case of the shorter polymer, the lowest two concentrations were removed as the response was too weak to allow accurate fitting. Thermodynamic and kinetic parameters for these polymers are shown in table 3.3. As was seen with the ITC experiment, there is a large increase in K_a with increased molecular weight, here a 4-fold increase in M_n/DP_n leads to a near 8-fold increase

in avidity. The larger polymer also displays more than a 130-fold increase in K_a compared to the value measured by ITC (1.39×10^9 M^{-1} c.f. 1.01×10^7 M^{-1}). This increase is due to a multivalent ligand interacting with a multivalent receptor (the surface of the sensor chip) and supports the hypothesis that increased avidity is a product of both multipile binding events and the increased probability of increased rebinding if an interaction is lost. In the ITC experiment, this relied on rebinding of a sugar to the same receptor as, at experimental concentrations, few proteins would be in close proximity. Here, the immobilisation of the receptor on a surface results in a high local concentration and more opportunity for a rebinding event to occur. Although an increased number of simultaneous bindings per polymer is also likely in this system they will still be limited by the polymer dimensions. For poly[GalEMA]$_{144}$ the fully extended chain length is $\sim$ 36 nm and its hydrodynamic diameter is 8.3 nm, although it is likely to be more extended in the shear present in the flow cell. Despite this, the lectins are not presented here at particularly high density, the surface modification may be at least 2.5-fold higher (5000 versus 2000 RU), so it seems unlikely that binding of multiple sites will be possible.

More interesting are the kinetic parameters for the two ligands. Despite the large difference in K_a there is less than a 2-fold difference in k_{on}, the rate of binding. Looking at this value alone it would be expected that these ligands would have similar avidities. However, the smaller ligand has a value of k_{off} 5-fold higher than that of the larger ligand and, consequently, has a far lower avidity ($K_a = k_{on}/k_{off}$). The smaller polymer has a fully extended chain length of $\sim$ 9 nm and a hydrodynamic diameter of 4.4 nm, from SEC, and is simply too small to bind multiple RCA$_{120}$ moi-

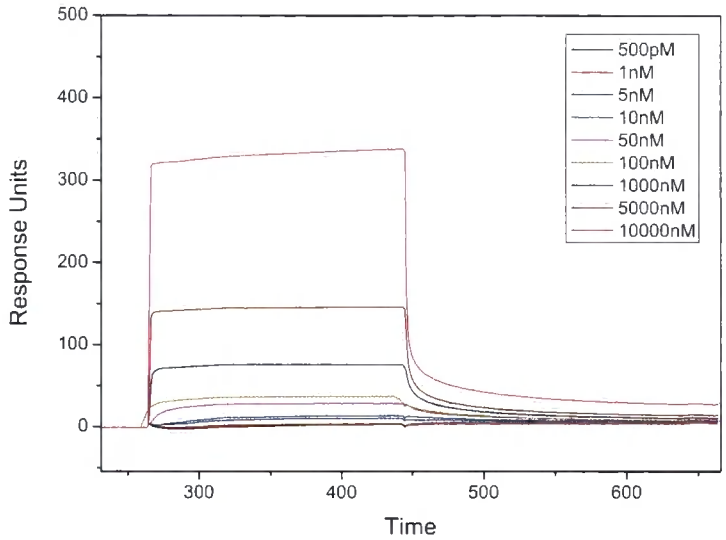

(a)

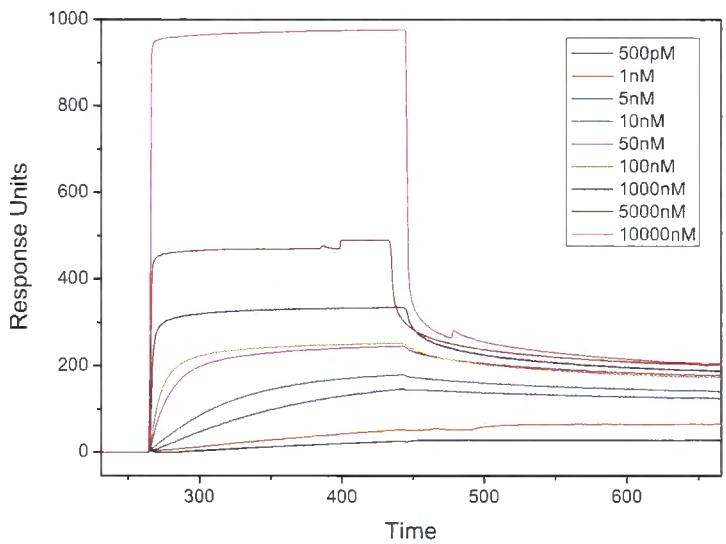

(b)

Figure 3.9: SPR sensorgrams for poly[GalEMA] binding to a RCA_{120}-modified sensor chip. (a) $p[GalEMA]_{37}$; (b) $p[GalEMA]_{144}$.

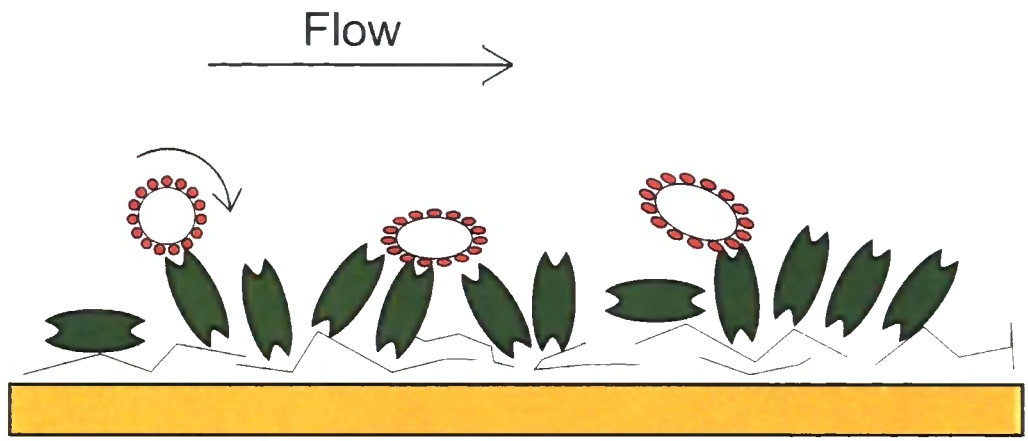

Figure 3.10: Schematic representation of polymer 'rolling' across lectin modified SPR sensor chip.

eties unless they are in very close proximity. Its small size also means it cannot bind both sites of a single RCA_{120} dimer either, as the distance between them is too great. As the polymer is too short to bind to several sites, it supports the assertion that one factor affecting increased avidity is the increased probability of binding. The longer polymer may be able to bind both sites simultaneously, but to do so would be highly entropically disfavoured due to the restriction on its degrees of freedom. The reduced dissociation rate of the larger polymer, and hence its greater avidity, must be due to the increased probability of rebinding. If the polymers are approximated to being a deformable sphere then they can be considered to have a footprint that will be proportional to their radius. In the same manner, a tyre of a larger diameter will maintain a larger contact area with the road than a smaller one; assuming all other factors to be the same. Deformable spheres have been modelled to roll along 'sticky', i.e. interacting, surfaces. [191, 192] a phenomenon that has also been modelled and observed experimentally in leukocytes. [193, 194] An increased contact

area during rolling will result in a greater probability of secondary binding events occuring, resulting in increased retention on the surface. Thus smaller polymers, with their reduced footprints will be shed more readily, increasing k_{off} valuess.

3.3 Conclusions

In order to investigate further the binding of multivalent glycoconjugates to lectins, isothermal titration calorimetry and surface plasmon resonance were used in combination. ITC experiments found, as has been demonstrated previously, that poly[GalEMA] does bind strongly to an appropriate lectin. Additionally, binding strength was shown to be highly dependent on molecular weight and, although not determined, a limiting value of valency is likely based on the increasing entropic cost of increasing avidity. Together with surface plasmon resonance data it appears that increased affinity is not due solely to an increased number of simultaneous lectin–carbohydrate interactions but through the increased probability of a multivalent ligand to form a secondary binding interaction if the initial binding interaction is broken. To confirm this hypothesis and determine whether there is a limiting avidity gain through increased valency, additional experiments comparing a wider range of polymer molecular weights by both ITC and SPR are required.

3.4 Experimental

3.4.1 Isothermal titration calorimetry

Isothermal titration calorimetry was conducted using a MicroCal VP-ITC calorimeter equilibrated at 298 K. Ligands for analysis were prepared in aqueous buffer (10 mM phosophate buffer, 137 mM NaCl, 2.7 mM KCl) and allowed to equilibrate for 24 h and degassed at 297 K. RCA_{120} (Vector Labs, supplied as 5 mg/ml solution in PBS) was buffer exchanged by use of centrifugal size exclusion columns (Pierce Zeba Desalting Columns) prewashed with the required buffer. After buffer exchange RCA_{120} was further diluted in buffer and its concentration measured by UV absorption using an $A^{1\%}$ value of 15.7 at 280 nm. RCA_{120} showed some solution instability and subsequently, prior to each experiment, the stock solution was centrifuged to remove aggregated protein and the concentration redetermined. The lectin solution was added to the sample cell ensuring no trapped air bubbles and the mixture was equilibrated to 298 K. Ligand solutions were added to RCA_{120} as a series of injections (25 aliquots of 5 μl) at 3 min. intervals by means of a computer controlled syringe with constant stirring at 307 rpm. The resulting data was analysed using Origin 7.0 Pro (OriginLabs) and fitted using the single site model incorporated into the software.

3.4.1.1 Modified Scatchard analysis

Scatchard analysis was performed by the modified methodology of Brewer et al. [174] Briefly, the total concentrations of ligand ($X_t(i)$) and lectin ($M_t(i)$) after the ith injection and the heat evolved in that injection ($Q(i)$) were extracted directly from

the raw ITC file. The concentration of bound ligand is given by:

$$X_b(i) = [Q(i)/\Delta H \cdot V] + X_b(i-1) \tag{3.6}$$

where is ΔH is the enthalphy of binding (in J mol^{-1}) and V is the volume of the sample cell (in ml). This allows the calculation of the concentration of free ligand after the ith injection ($X_f(i)$) from:

$$X_f(i) = X_t(i) - X_b(i) \tag{3.7}$$

In a normal Scatchard analysis, the average number of ligands bound per lectin ($r(i)$) is the ratio $X_b(i)/M_t(i)$. The modified Scatchard analysis introduces an additional term to allow for multivalent ligands and thus:

$$r(i) = \frac{X_b(i)[\text{average functional valency of ligand}]}{M_t(i)} \tag{3.8}$$

where the average functionality of ligand is the value $1/n$ given in table 3.2. Scatchard plots may then be constructed by plotting $r(i)/X_f(i)$ versus $r(i)$.

3.4.2 SPR studies on glycopolymers

All SPR measurements were performed on a BIAcore 3000 system. A CM5 sensor chip was equilibrated with HEPES buffer (10 mM HEPES pH 7.4, 150 mM NaCl, 0.005 % P20 surfactant) then activated by a flowing a mixture of 0.1 M *N*-hydroxysuccinimide and 0.1 M *N*-ethyl-*N*'-(dimethylaminopropyl)carbodiimide over the chip for 5 minutes at 25 °C at a flow rate of 5 μl min^{-1}. RCA_{120} was immobilised on channels 1, 2 and 3 via injection of a solution (67 μl of 5 mg·ml^{-1} solution diluted in 1ml 10 mM acetate buffer pH 4); contact times of 7, 3 and 1

min. respectively resulted in functionalisation of the surface at 5000, 2000 and 200 response units (RU). All channels were then modified by a solution of ethanolamine to produce a blank on channel 4 and remove remaining reactive groups on channels 1–3.

Solutions of polymers were prepared in the same HEPES buffer. Sensorgrams for each polymer concentration were recorded with a 180 s injection of polymer solution (on period) followed by 240 s of buffer alone (off period). After this time the chip was regenerated by a 30 s injection of methyl β-D-galactoside (1 mg·ml^{-1}) and 60 s of buffer alone. After regeneration was complete the next sample was injected. For each polymer 5 consequetive concentrations were used for kinetic analysis using a single set of sites model in the BIAevalulation software.

Not to be absolutely certain is, I think, one of the essential things in rationality.

Bertrand Russell (1872–1970)

4

Synthesis and properties of glycopolymer functionalised gold nanoparticles.

4.1 Introduction

Colloidal gold has been used since ancient Roman times, but was not truly studied until Faraday's work in the 1850s. In 1857 Faraday described the "Experimental Relations of Gold (and other Metals) to Light" in a Royal Society lecture; within this he described a multitude of results in the area that has more recently become known as solid state nanotechnology. One aspect of Faraday's lecture, under the subtitle "Diffused particles of gold–production–proportionate size–colour–aggregation and other changes", he described what is now regarded to be the first scientific synthesis of gold nanoparticles (AuNPs) from aqueous gold solutions, phosphorous and carbon disulfide (figure 4.1a). Despite, by today's standards, the primitive nature of Faraday's equipment he, as his chosen title implies, knew that the resulting ruby-red solutions were not truly solutions but very fine suspensions. [195]

> [Referring to his gold sols] The latter, when in their finest state, often remain unchanged for many months, and have all the appearance of solutions. But they never are such, containing in fact no dissolved, but only diffused gold.

Since Faraday, the nanosciences have progressed hugely and in 2006 more than 2000 academic articles were published on the synthesis of gold colloids/nanoparticles (figure 4.1b). [197] Despite this huge quantity of literature, the vast majority fall into one of two categories: those synthesised by the method of Turkevich, [198–201] later refined by Frens, [202] or those synthesised by the method of Brust. [203] Both of these methodologies have previously been applied to the synthesis of glycosylated AuNPs, *glycoNPs*, and are briefly described below.

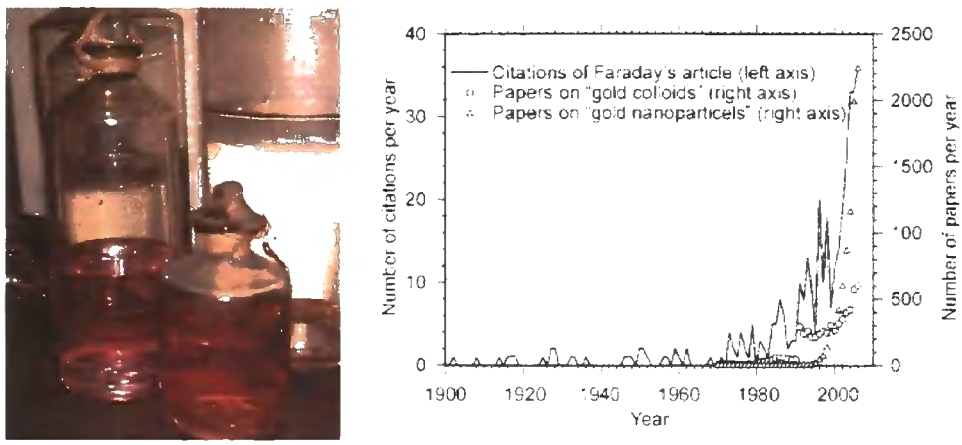

(a) (b)

Figure 4.1: (a) Photograph of Faraday's colloidal gold, reproduced from ref. [196]; (b) Citation and publication data for papers on gold colloids/nanoparticles. Copyright Wiley-VCH Verlag GmbH & Co. KGaA. Reproduced with permission from reference [197].

4.1.1 Synthesis of gold nanoparticles

4.1.1.1 Turkevich/Frens method

In the early 1950s Turkevich developed a procedure for the synthesis of gold nanoparticles by the reduction of an aqueous solution of a gold salt, usually hydrogen tetrachloroaurate ($HAuCl_4$), by a reducing agent/stabilising ligand, typically a carboxylic acid or carboxylate such as sodium citrate, acrylate or ascorbic acid. [198–201] Later, Frens improved upon this method allowing the synthesis of particles with controlled diameter (10 - 200 nm) by varying the [Au]:[citrate] ratio, unfortunately polydispersity also tends to increase with particle size. [202] As the particles are only charge stabilised by the reducing group, they are susceptible to precipitation by changes

in pH or addition of salts. This feature also means they can be easily functionalised by ligand transfer with appropriate molecules, usually thiols due to their high aurophilicity.

4.1.1.2 Brust method

In the early 1990s Brust et al. developed an alternate method for the synthesis of gold nanoparticles using a biphasic system of toluene and water. $AuCl_4^-$ was transferred into toluene by use of tetraoctylammonium bromide as phase-transfer catalyst and then a mercaptoalkane was added to the same phase; addition of excess $NaBH_4$ resulted in rapid formation of a dark brown solution of alkyl capped nanoparticles. [203] Although originally applied to the synthesis of organically soluble AuNPs this method may also be applied to the synthesis of hydrophilic AuNPs in a single phase system using a water soluble thiol as a stabilising ligand.

4.1.2 Application of Frens and Brust methods to the synthesis of glycoNPs

A large part of AuNP, and other metal or semiconductor particle, research has been fuelled by the interesting catalytic, electronic and optical properties many display. At the biological end of the spectrum, research has been more concerned with the use of nanoparticles as nanoscale scaffolds to which biological functionality could be added. If the intrinsic properties of the particles could, in addition, be exploited then that was an additional advantage. The area has recently been reviewed [204] and here only a few examples will be highlighted. GlycoAuNPs were

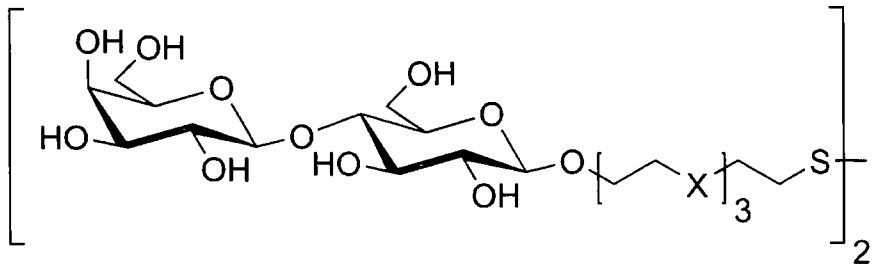

4.1 X= O, CH_2

Figure 4.2: Lactosyl disulfide as synthesised by Penadés et al. [205]

first reported by Penadés et al. in 2001, who utilised a Brust-type methodology to produce gold nanoparticles decorated with the saccharides lactose and Lewis^x. These were synthesised by in situ reduction of the correspondingly glycosylated disulfide (see **4.1** in figure 4.2 for the lactosyl disulfide) in the presence of $HAuCl_4$ in aqueous methanol by $NaBH_4$. The resulting suspension was dried under vacuum before dissolution in water and purification by centrifugal filtration. Particles functionalised with Lewis^x were found to aggregate in the presence of calcium ions and show potential as models of cell–cell interactions. [205,206] Penadés et al. have also used the same methodology for the synthesis of bifunctional nanoparticles where additional functionality, such as a fluorophore, has been incorporated by performing the reduction in the presence of a small quantity of the appropriately functionalised disulfide. [207] Gervay-Hague et al. have attempted to probe the binding of the HIV-associated glycoprotein gp120 to glycosylated cellular receptors by synthesis of galactosyl-functionalised nanoparticles using the same methodology. [208]

Penadés et al. have also proposed the use of glycosylated particles as therapeutic agents for the treatment and prevention of cancer. Glyconanoparticles presenting

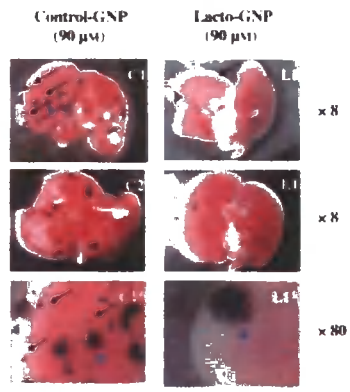

Figure 4.3: Image of lung metastases after treatment with lactosyl and glucosyl nanoparticles. In the lactosyl group (right) far fewer metastases (dark areas) are seen. Copyright Wiley-VCH Verlag GmbH & Co. KGaA. Reproduced with permission from reference [209]

glucose or lactose were investigated as anti-adhesive cancer therapies in a mouse model. Mice were administred an intravenous injection of murine melanoma cells, B16F10 line, or the same cells that had been pre-incubated with glycoNPs. It was found that, when the cells were pretreated with lactose-bearing nanoparticles, the mice produced siginificantly fewer lung metastases than those treated with glucosyl particles or the control group (figure 4.3). [209] A cancer vaccine system has been proposed by synthesising particles that present two carbohydrate cancer antigens, sialyl-Tn and Lewis^y, and a peptide designed to promote immune response. [210] Currently no report on the efficacy of such a vaccine has been reported. Barchi et al. have reported the synthesis of nanoparticles displaying the Thomson-Friedenreich antigen (TF_{ag}), another tumour-associated carbohydrate antigen, using the same methodology as Penadés et al. [211] Recently they have also synthesised particles

presenting a glycopeptide featuring TF_{ag}. [212]

Field and Russell have utilised the Frens method to produce near monodisperse AuNPs which were then functionalised with carbohydrates. AuNPs were synthesised from $HAuCl_4$ and trisodium citrate at such a ratio as to produce particles of 16 nm average diameter. These were then functionalised, via ligand transfer, by addition of a carbohydrate ligand with a thiol, or disulfide, terminated linker. Particles of this type were found to still display the brilliance of colour seen in the original gold sols but had the benefit of increased stability and functionality. The applicability of such particles as colorimetric sensors was first demonstrated by addition of the lectin Concanavalin A (Con A) to a solution of mannosylated particles. After addition the particles were seen to aggregate resulting in a shift in the plasmon band and a colour change. [213] After this proof of principle they demonstrated that cholera toxin [214] and RCA_{120}, as a surrogate for ricin, [215] could be detected in a similar manner by adjusting the carbohydrate used.

4.1.3 Application of RAFTed polymers in the synthesis of metal nanoparticles

Considering the nature of one terminus of RAFTed polymers it is unsurprising that they have been utilised in the synthesis of gold, and other noble metal, nanoparticles. Lowe et al. first reported the synthesis of metal nanoparticles with RAFT polymers in 2002, although their methodology is less than clear. Polymer coated gold nanoparticles were synthesised not from a solution of the gold salt, but instead by the reduction of dithioester terminated polymers in the presence of a commeri-

cally obtained gold sol. Particles of Ag, Pt and Rh were synthesised by simultaneous reduction of the corresponding metal salt and polymer. [216]

Tenhu et al. investigated several methods for the synthesis of polymer-AuNP conjugates from thiol and dithioester terminated polymers. Poly[*N*-isopropylacrylamide] (p[NIPAM]) was synthesised using either cumyl dithiobenzoate (CDB) or CPADB as the RAFT agent. Thiol-terminated p[NIPAM] was synthesised by hydrazinolysis of the dithioester terminated p[NIPAM] or conventional free radical polymerisation initiated of NIPAM by ACPA and modification of the carboxylic acid end group by coupling to cysteamine. The thiol and dithioester terminated polymers were then used in the synthesis of AuNPs by lithium triethylborohydride (Super-Hydride®) reduction of $HAuCl_4$ in their presence. Overall it was found that direct synthesis of AuNPs from $HAuCl_4$ and dithioester terminated polymers was not only synthetically less challenging than either the prior end group reduction or cysteamine functionalisation methods, but also resulted in the greatest level of control over the size of gold core synthesised. [217] AuNPs featuring a mixture of pNIPAM and poly[styrene] chains were synthesised by the same methodology. [218]

Narain et al. recently synthesised glycosylated AuNPs from RAFTed glycopolymers (for polymer details see section 2.1.2). Particles were synthesised by reduction of polymer and $HAuCl_4$ by $NaBH_4$, in the presence or absence of biotin-PEG-SH. The particles were then purified by dialysis with a 3500 MWCO membrane, which appears inadequate considering the polymers used were reported as having $M_n >$ 20 kDa; thus if any free polymer remained in solution it would not have been removed. [141] The same group also synthesised glyconanoparticles by a pho-

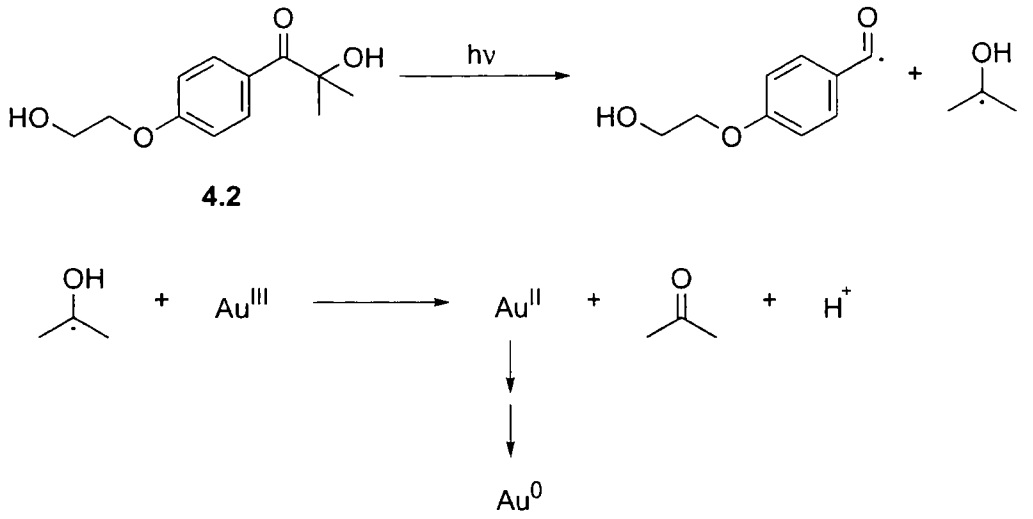

Figure 4.4: Photochemical reduction of Au^{III} as demonstrated by Scaiano et al. [219]

tochemical method first introduced by Scaiano et al. (figure 4.4). Irgacure® 2959 (1-[4-(2-hydroxyethoxy)phenyl]-2-hydroxy-2-methyl-1-propane-1-one, **4.2**), a photochemical initiator, decomposes homolytically under UV irradiation to produce ketyl radicals. Subsequently these reduce Au^{III} to Au^0 resulting in stable aqueous gold nanoparticles even in the absence of a capping ligand; functionalisation may be achieved by addition of such a ligand. [219] Narain et al. used a combination of RAFTed pNIPAM, thiol-terminated PEG and the glycosylated block copolymer described earlier (section 2.1.2) in the presence of the photoinitiator and $HAuCl_4$.

4.2 Results and discussion

4.2.1 Synthesis of gold particles stabilised by glycopolymers

Gold nanoparticles were synthesised as previously demonstrated by Lowe et al. and Tenhu et al. [216–218] In initial experiments, $HAuCl_4$ was reduced by $NaBH_4$ in the presence of poly[2-(β-D-galactosyloxy)ethyl methacrylate] (M_n = 24.1 kDa, M_w/M_n = 1.09) at a mole ratio of 1:2 ([Au]:[dithioester end groups]). Upon addition of the reducing agent a rapid colour change from orange–yellow to golden brown was observed (see fig. 4.5a). Typically gold nanoparticle solutions have a characteristic instense red-violet hue, dependent on particle diameter, due to plasmon resonance. However, gold sols of very small diameter (below $\sim$ 3.5 nm) typically display a yellow-brown colouration dependent on concentration. [220] If was found that, 24 h after reduction, a small quantity of macroscopic aggregates had formed and these were removed by filtration (0.2 μm PTFE membrane). The absence of free polymer was confirmed by SEC. The synthesised particles were analysed in solution by dynamic light-scattering (DLS) and transmission electron microscopy (TEM). DLS gave a peak diameter of 11.5 nm and TEM gave a diameter of the gold core as 1-3 nm (figures 4.5c and 4.5b respectively). Extremely small particles such as these have been synthesised previously by Brust et al. from sulfide-terminated poly(methacrylic acid) using a similar protocol. [221] DLS produces a larger diameter than TEM as the former measures the hydrodynamic radius and therefore includes the polymer corona whereas the TEM method only measures the gold core.

(a)

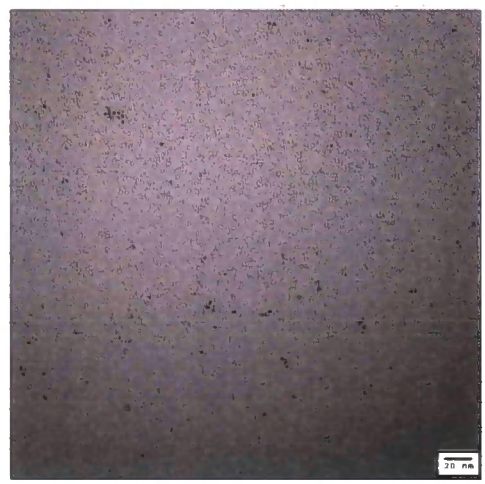

(b)

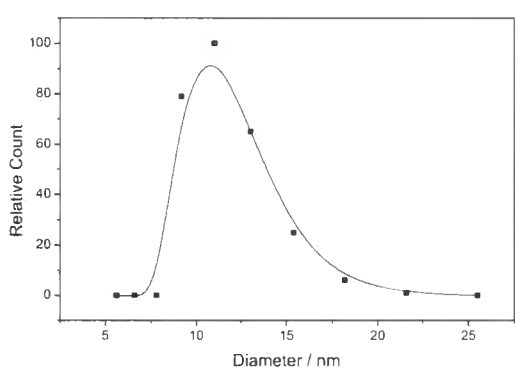

(c)

Figure 4.5: Photograph (a), TEM (b) and DLS (c) of gold nanoparticles initially synthesised by modified Brust procedure from poly[GalEMA]

Table 4.1: Data for the synthesis of pGalEMA-coated gold nanoparticles of varying size

Run	[polymer] (mM)	[Au]:[polymer]	Diameter / nm[a]	
			TEM	DLS
1	0.161	1.25	1.98±0.03	559 ±7
2	0.081	2.50	3.11±0.03	34.0±3.1
3	0.040	5.0	3.26±0.05	34.0±3.8
4	0.020	10.0	3.29±0.06	41.9±0.9
5	0.010	20.0	3.36±0.06	48.3±0.7

[a] ± one SEM, values determined after filtration through 0.2 μm membrane but prior to purification by centrifugal filtration.

4.2.2 Particle size control and functionality

Some control over the size of particles formed by the Brust-type synthesis has been demonstrated previously by varying the ratio of thiols to gold. [221] To determine if such control could be achieved in this system a series of experiments were performed with varying gold:polymer ratio (table 4.1). $HAuCl_4$ solutions of the same concentration were stirred vigorously in the presence of varying concentrations of poly[GalEMA] ($M_n \sim 9.8$ kDa). Upon reduction with $NaBH_4$ the solutions were seen to change colour rapidly from pale yellow to colours ranging from yellow–brown to violet (see fig. 4.6a). UV-visible absorbance spectra for the particle samples are shown in figure 4.6b and it is clear from these that, as the ratio of gold to polymer increases, a peak absorbance appears in the region of 525–540 nm, characterisitic of gold colloids and suggesting an increasing core diameter. Particle diameters were measured by both TEM and DLS, giving the core and hydrodynamic diameters

respectively. Core diameters were determined by image analysis of multiple TEM micrographs using ImageJ software. [222,223] ImageJ does not measure particle diameter directly unless each individual particle is measured manually. Instead, core areas were measured using a circularity range of 0.70–1.00, where a value of 1 indicates a perfect circle, and core diameters determined using equation 4.1. In all cases at least 200 particles were measured.

$$diameter = 2 \cdot \sqrt{\frac{area}{\pi}} \tag{4.1}$$

The mean particle diameters, and appropriate error bars, are plotted against Au:polymer ratio in figure 4.7a. At all ratios there is quite a large range of particle sizes in the samples as is clearly seen by the size of the standard deviation (bars), although, as the standard errors (boxes) are small, the mean values are representative of the populations being investigated. A sharp increase in particle diameter is seen between the two lowest ratios (highest polymer concentrations) and then a slight increase across the remaining range although statistical analysis (Student t-test) implies that the differences between the higher polymer concentrations is insignificant. Overall it appears that, although some control of particle size is achievable, it is not possible to produce particles larger than ~3.5 nm via this methodology. DLS analysis gave an anomalous result for the the diameter of the particles with the lowest ratio with a diameter of ~ 560 nm despite samples being filtered through a 0.2 μm telfon membrane prior to analysis. Such a large value is likely to be due to weakly associated aggregates that may be deaggregated by filtration but rapidly reaggregate as is seen with high molecular weight glycopolymers. [186] The other diameters are equally curious showing no significant difference between the 2.5 and

5 Au:polymer ratio but a significant difference between these and the higher ratios.

To ensure no free polymer was remaining in the samples they were purified by repeated centrifugal filtration through a membrane with a MWCO of 30 kDa. In the cases of the two highest gold:polymer ratios considerable precipitation was seen on the polyethersulfone filtration membrane and these samples were discarded. The remaining three samples were analysed by thermal gravimetic analysis to determine their mass percentage of gold and this was used to determine the average number of polymer chains per particle. Hostetler et al. have previously calculated the number of gold atoms in a particle of a given core diameter (n_{Au}). [224] These figures were used to determine the number of ligands per particle as follows:

$$M_{Au} = n_{Au} \cdot 196.96 \tag{4.2}$$

$$M_{total} = \frac{M_{Au}}{\%Au} \cdot 100 \tag{4.3}$$

$$M_{poly} = M_{total} - M_{Au} \tag{4.4}$$

$$n_{poly} = \frac{M_{poly}}{M_n} \tag{4.5}$$

Where M_{total}, M_{Au} and M_{poly} are the total mass, mass of gold and mass of polymer per particle; %Au is the weight percentage gold from TGA; n_{Au} is the number of gold atoms per particle core and n_{poly} is the number of polymer chains per particle.

The number of ligands per particle calculated in this manner (table 4.2) is surprisingly low when compared to polymer modified clusters of a similar size. Brust et al. reported 60–70 capping ligands for 2 nm diameter particles and 200–500 for those 3–4 nm in diameter when calculated using the Hostetler data and the Au:S ratio from atomic emission spectroscopy. [221] The poly[methacrylic acid] used as the capping

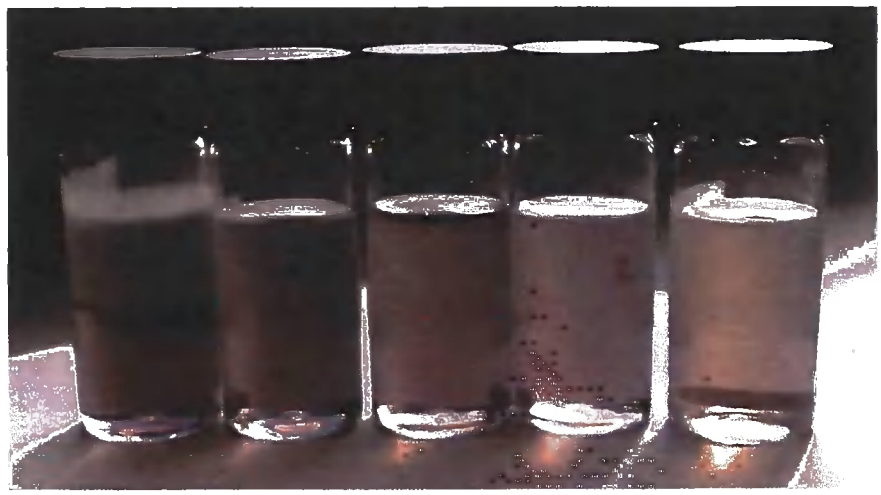

(a)

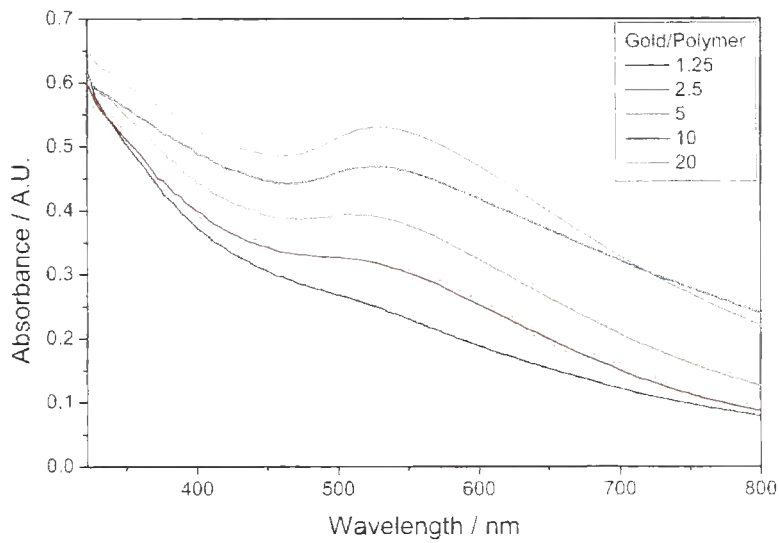

(b)

Figure 4.6: Photograph (a) and UV-Vis spectra (b) of gold nanoparticle solutions synthesised at different gold to polymer ratios. (a) L-R: 20, 10, 5, 2.5, 1.25.

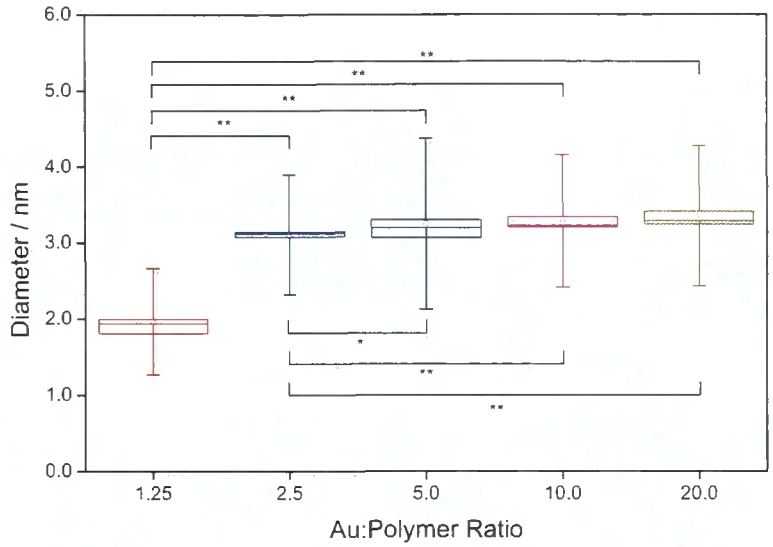

(a)

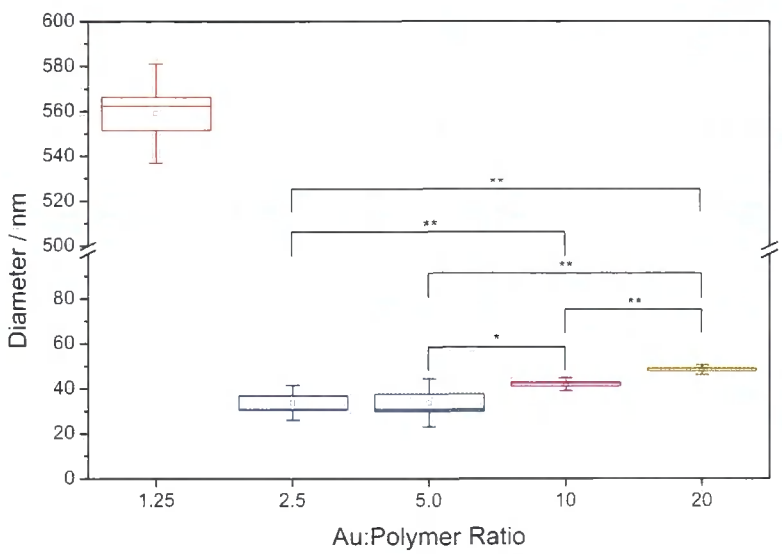

(b)

Figure 4.7: Particle diameters as measured by (a) transmission electron microscopy and (b) dynamic light scattering. Small squares represent mean values; boxes, standard error of the mean; and bars, standard deviation. $*$ $p \leq 0.05$. $**$ $p \leq 0.01$.

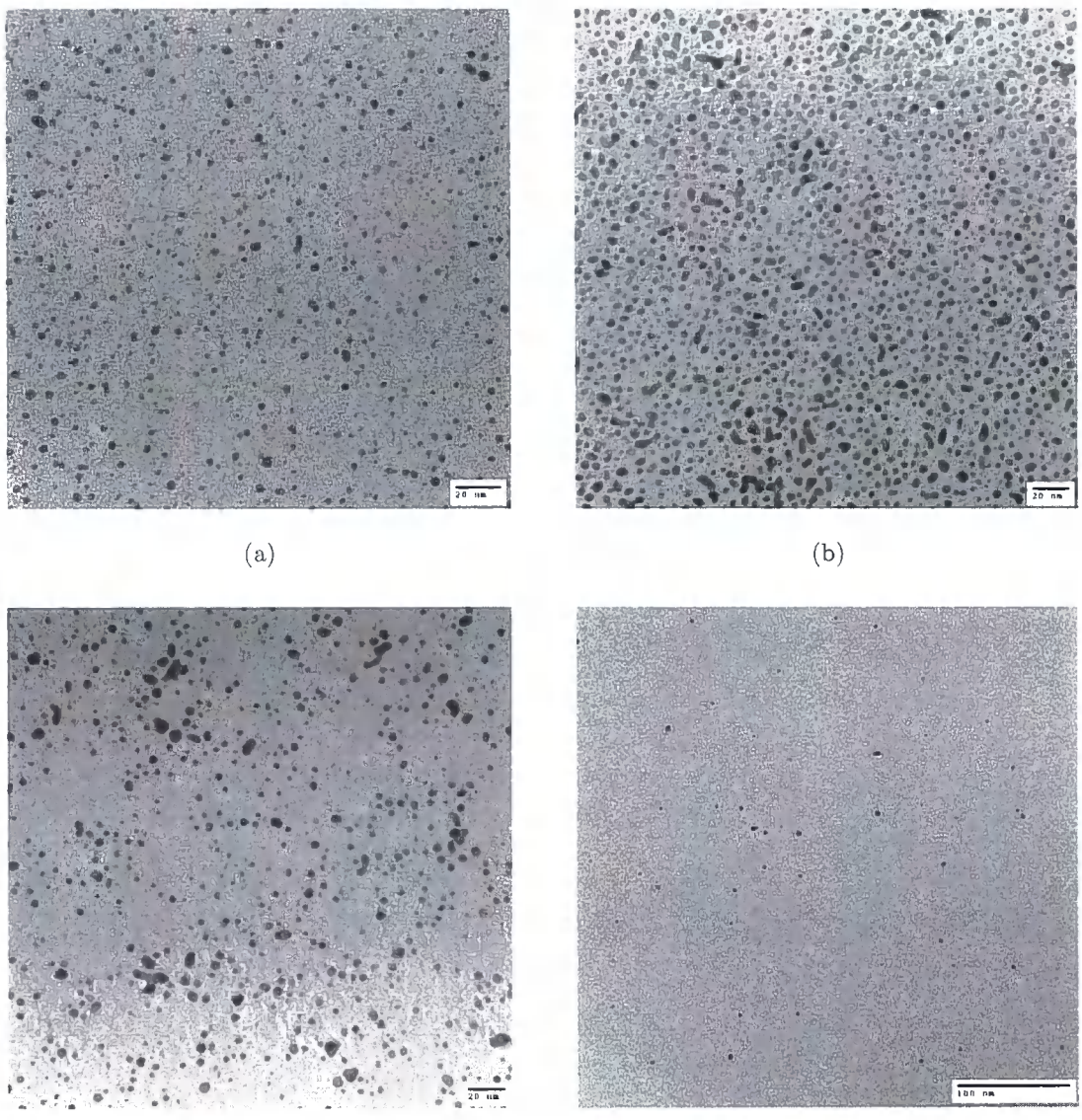

(a) (b)

(c) (d)

Figure 4.8: TEM micrographs of gold nanoparticles synthesised at varying gold:polymer ratios

agent was of a similar molecular weight and DP_n to the polymer used here (M_n 5 kDa, DP_n 50 c.f. M_n 9.7 kDa, DP_n 32) but the nature of the polymers is significantly different. Poly[GalEMA] is far more sterically bulky than poly[methacrylic acid] and likely to shield a greater surface area for a single point of attachment; it has a greater *steric footprint*. Additionally polyanions, such as poly[methacrylic acid], are known to form relatively extended structures at high pH and ionic strength, particularly when tethered to a surface. Consequently, during the particle synthesis the steric footprint of such polymers on the surface should be minimal. Poly[GalEMA] has no inherent charge and is thus less affected by pH and ionic strength and is likely to be a random coil, almost globular, in solution. Once attached to a surface p[GalEMA] will act like an umbrella, shielding a relatively large surface area for a single point of attachment. This does not, however, explain why the larger particles with a greater surface area have fewer tethered polymers than the smaller particles. The answer may lie in the difference in the radii of curvature of the different sizes. The smaller a particle the smaller its radius of curvature and thus the more curved its surface. Figure 4.9 is a schematic of the packing of polymers on the surface of particles of radii 1 and 3. As can be seen the reduced curvature at the surface of a large particle will reduce the density of packing, the number of ligands per unit area, as steric hinderance is increased in the corona. This phenomenom is documented in the calculations of Hostetler et al. who found that surface coverage decreased with increasing particle radius; [224] however, the number of ligands still increased greatly with increasing particle size.

Although the above factors do not explain completely the low level of function-

Table 4.2: Thermal gravimetric analysis and ligand density data for the poly[GalEMA] functionalised gold nanoparticles

Sample	% Au[a]	n_{Au}[b]	Surface area / nm^2 [b]	n_{poly}	Area per ligand / nm^2
1	40	225	15.19	6.9	2.2
2	82	976	40.02	4.4	9.1
3	87	1289	47.22	3.7	12.8

[a] From thermal gravimetric analysis; [b] from Hostetler et al. ref. [224].

alisation of larger particle surfaces, they may provide some insight, in combination with Ostwald ripening, into the apparent limiting core size of ~3.5 nm and the instability of the larger particles during purification by centrifugal filtration. Ostwald ripening is a process by which large larger particles in an emulsion grow at the expense of smaller ones, resulting in an increased mean size of particles within the system. This competitive growth is due the Gibbs-Thomson effect whereby the higher the curvature of a surface, the higher its chemical potential. [225] For the particles synthesised at the lowest Au:polymer ratio, the high surface energy of the particles is stabilised by the relatively high concentration of bound polymer; there is a polymer for every 2.2 nm^2 of surface. For lower polymer concentrations stabilisation of smaller particles is not possible and larger ones form at their expense. If the levels of polymer adsorption measured are correct, it would suggest the low polymer concentrations result in particles that are vulnerable to agglomeration; each polymer has to protect 12.9 nm^2 of surface. In the two highest Au:polymer ratio examples, where the particles were seen to agglomerate on centrifugal filtration, the area each chain would be required to protect would increase further if this trend continued. Consequently, it is likely that these particles are only metastable, kept discrete due

to the high dilution of the solution only to aggregate upon concentration.

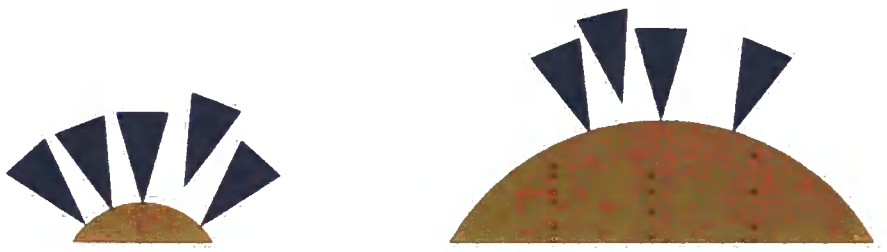

Figure 4.9: Schematic of polymeric ligand packing on the surface of particles of radii 1 and 3. On larger particles, ligands (triangles) pack less densely as the lower curvature of the surface results in increased steric hinderance in the corona.

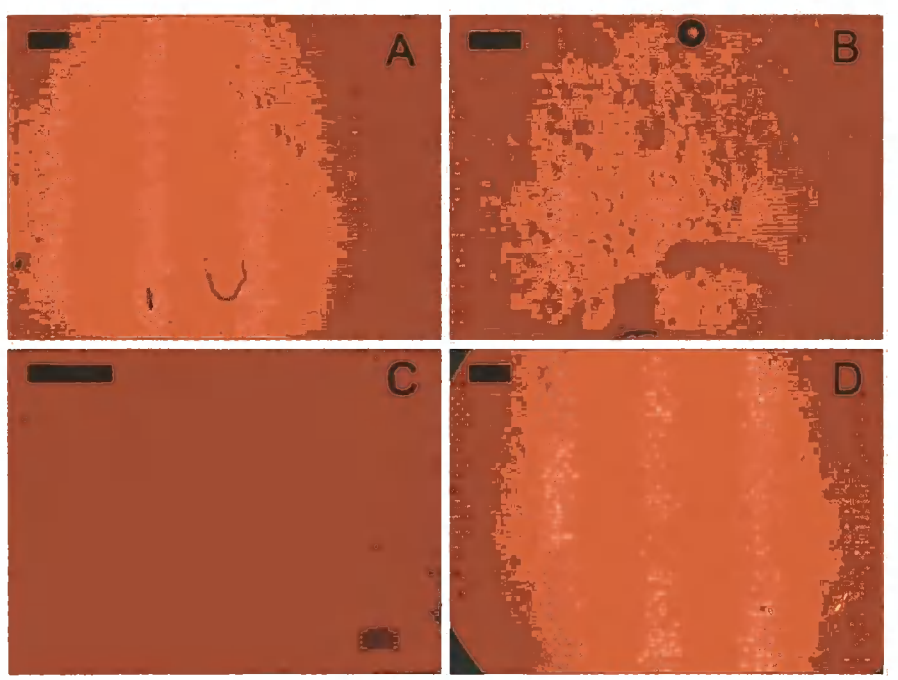

Figure 4.10: Agglutination of lectin functionalised beads by p[GalEMA]-modified gold nanoparticles. A. PNA-modified agarose beads; B. 5 minutes after addition of glycoNPs; C. 30 minutes after addition of glycoNPs; D. redispersion of particles after addition of free methyl β-D-galactoside. All scale bars represent 500 μm.

4.2.3 Are glycosylated particles still ligands for lectins?

To determine whether particles still retain lectin affinity and confirm that the synthesis did not inadvertantly cleave the carbohydrate moieties, a simple agglutination assay was performed. A suspension of agarose beads functionalised with the lectin *Peanut agglutinin* was added to a microscope slide (fig. 4.10 A) and a solution of poly[GalEMA]-modified particles added. The slide was monitored over a period of 30 minutes via optical microscopy and the agarose beads were seen to aggregate (fig. 4.10 B and C). To determine if the agglutination was carbohydrate specific a solution of methyl β-D-galactoside or methyl β-D-glucoside was added to the aggregates. In the former case the beads were seen to redisperse (fig. 4.10 D) whereas in the latter no change was seen. This specificity was confirmed by repeating the experiment using nanoparticles coated with poly(methyl 6-*O*-methacryloyl-α-D-glucoside) synthesised in an identical manner. Methyl α-D-glucoside is not a ligand for PNA and additionally the 6-*O* linkage presents the sugar in a unnatural conformation. In this case the particles were not seen to agglutinate confirming that binding is galactose-specific and was not a result of binding to a polyol.

4.2.4 In vitro cell studies of glycosylated nanoparticles

Nanoparticles modified with biological moieties have many potential applications as pharmaceuticals, models and visualising agents. The last of these is already used widely in the form of immunogold labelling where gold particles are modified with antibodies and used to determine the localation of the complementary antigen.

To investigate the cytotoxicity and labelling ability of poly[GalEMA]-modified

nanoparticles, in vitro studies were performed on HepG2 cells. HepG2 cells are a human hepatic carcinoma cell line and consequently carry the galactoside-binding asialoglycoprotein receptor (ASGPR). Confluent cultures were trypsinised, washed and resuspended, counted on a hæmocytometer and plated at equal densities into standard 6-well plates in the presence or absence of nanoparticle solutions as detailed in 4.11. Nanoparticle solutions were prepared by repeated centrifugal filtration and resuspension in deionised water. After the third filtration they were resuspended in DMEM buffer and filter sterilised. Three independent replicates were performed.

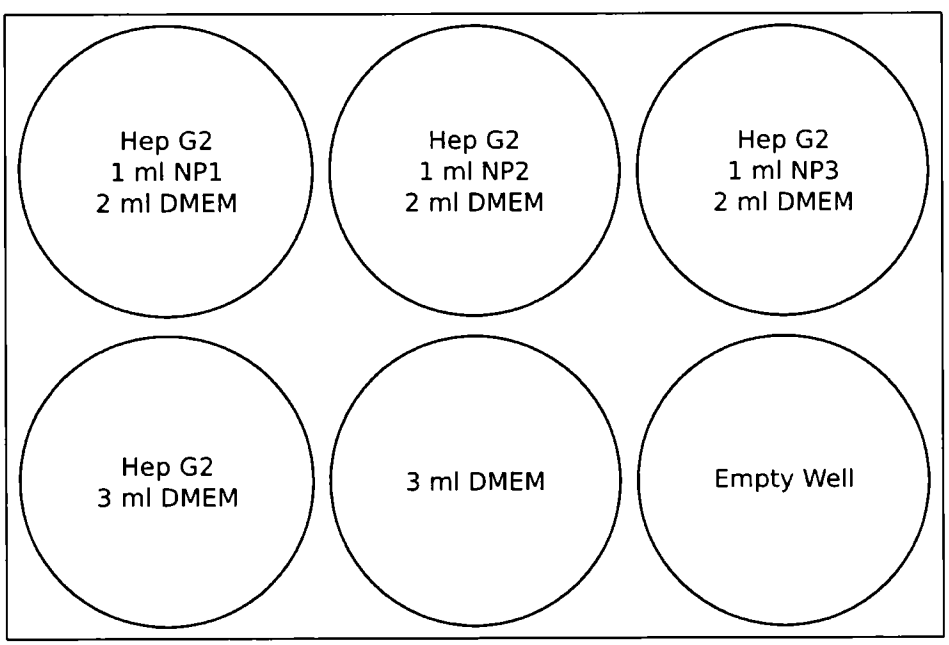

Figure 4.11: Schematic of cell culture plates and well contents

4.2.4.1 Cell viability

Cell viability after 4 and 7 days incubation was determined using the CellTiter 96® AQ_{ueous} Non-radioactive cell proliferation assay (MTS) from Promega. This is a modernised version of Mosmann's MTT assay that produces a water-soluble formazan product, removing the need to add DMSO to improve solubility (fig. 4.12). The results of the MTS assays are shown in figure 4.13. After 4 days it was clear that there was little difference in the viabilities of cells cultured with or without nanoparticles. Statistical analysis (Student t-test) gives a significant difference between cells incubated with the smallest particles (NP1) and the positive control ($p \leq 0.05$) but this difference is marginal. After 7 days all three nanoparticle solutions had significantly higher viabilities compared to the positive control; however the positive control is a similar level to the negative (i.e. no cells) suggesting that the control cells are dead. When culturing HepG2 cells the media is typically replaced every 3-4 days but due to the limited quantities of nanoparticles solutions available the media was not replaced for the duration of the experiments so it is unsurprising that after 7 days the control cells were unviable. It is unlikely that the nanoparticles had such a pronounced effect on cell viability and it is more likely that they instead interfere with the MTS assay. The formazan product formed during the assay was measured by UV-Visible spectroscopy at 490 nm and it is possible that residual particles in the media were increasing absorption at this wavelength; an effect that would be more pronounced when the level of formazan produced is low due to few viable cells. Other assays of cell viability, such as albumin determination may allow elucidation oof particle toxicity.

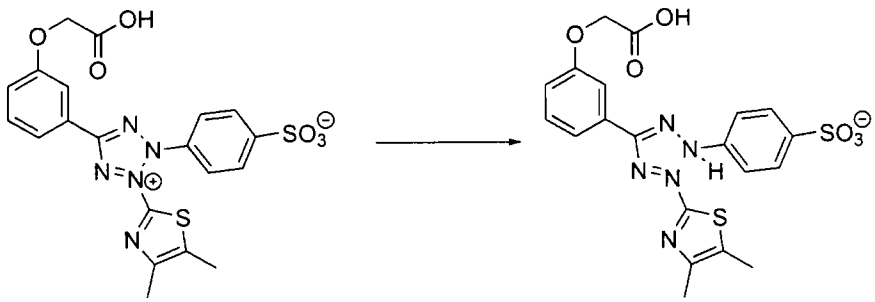

Figure 4.12: Formation of formazan dye from MTS substrate

4.2.4.2 TEM imaging of incubated cells

To further determine the condition of the cells and also determine whether nanoparticles could be visualised, the cells were analysed by TEM. After incubation for 7 days, cells were fixed, scraped from the plates and pelleted. The pellets were stained, dehydrated and then embedded in resin from which ultra-thin sections were produced after setting. The sections were then mounted on a TEM grid and imaged. Representative images of the four samples are shown in figure 4.14. The positive control (fig. 4.14a) and cells incubated with the smallest nanoparticles (fig. 4.14b) contain recognisable intracellular organelles including nuclei (**N**), mitochondria (**mt**) and the rough endoplasmic reticulum (**rER**); but overall cell condition is poor. The micrographs from the samples incubated with the two larger nanoparticle solutions also contain recognisable nuclei but other organelles are not easily identified. There are also areas of what appear to be aggregated nanoparticles (circled) as well as numerous small dark spots that may be the same. In these images the cells are clearly in very poor condition. Higher magnification images of the positive control and first nanoparticle solution cells are shown in figure 4.15. From these it is not possible to determine conclusively whether any nanoparticles are present. Figure

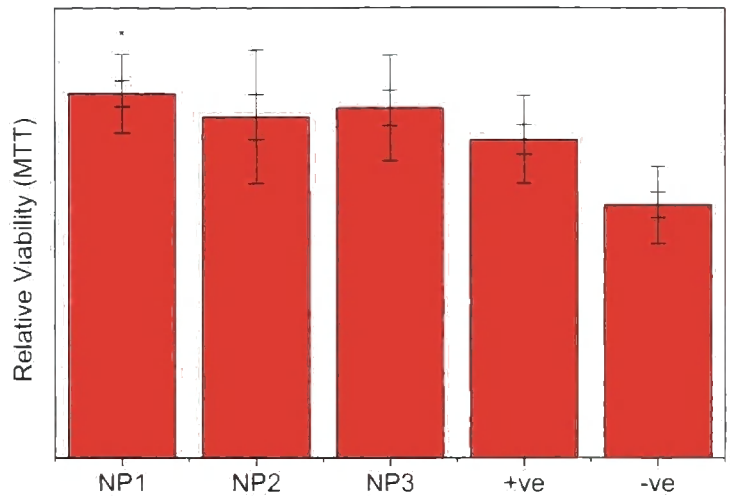

(a)

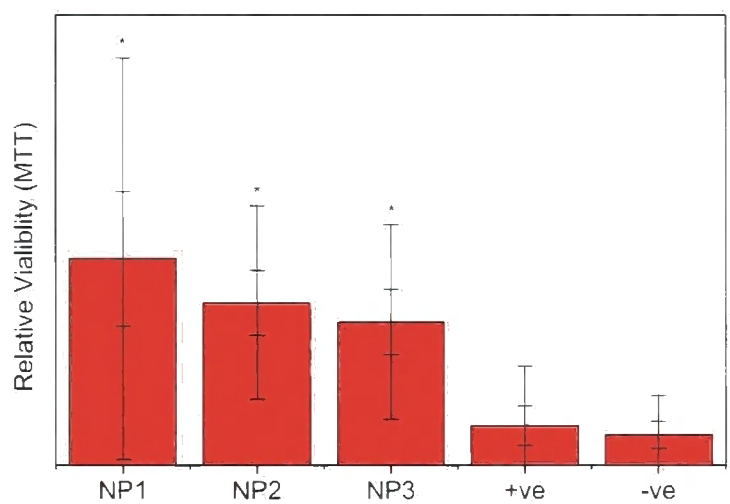

(b)

Figure 4.13: Cell viabilities after incubation with poly[GalEMA]-modified gold nanoparticles. (a) After 4 days; (b) after 7 days. Large error bars represent ±SD, small error bars ±SEM, * $p \leq 0.05$ compared to positive control.

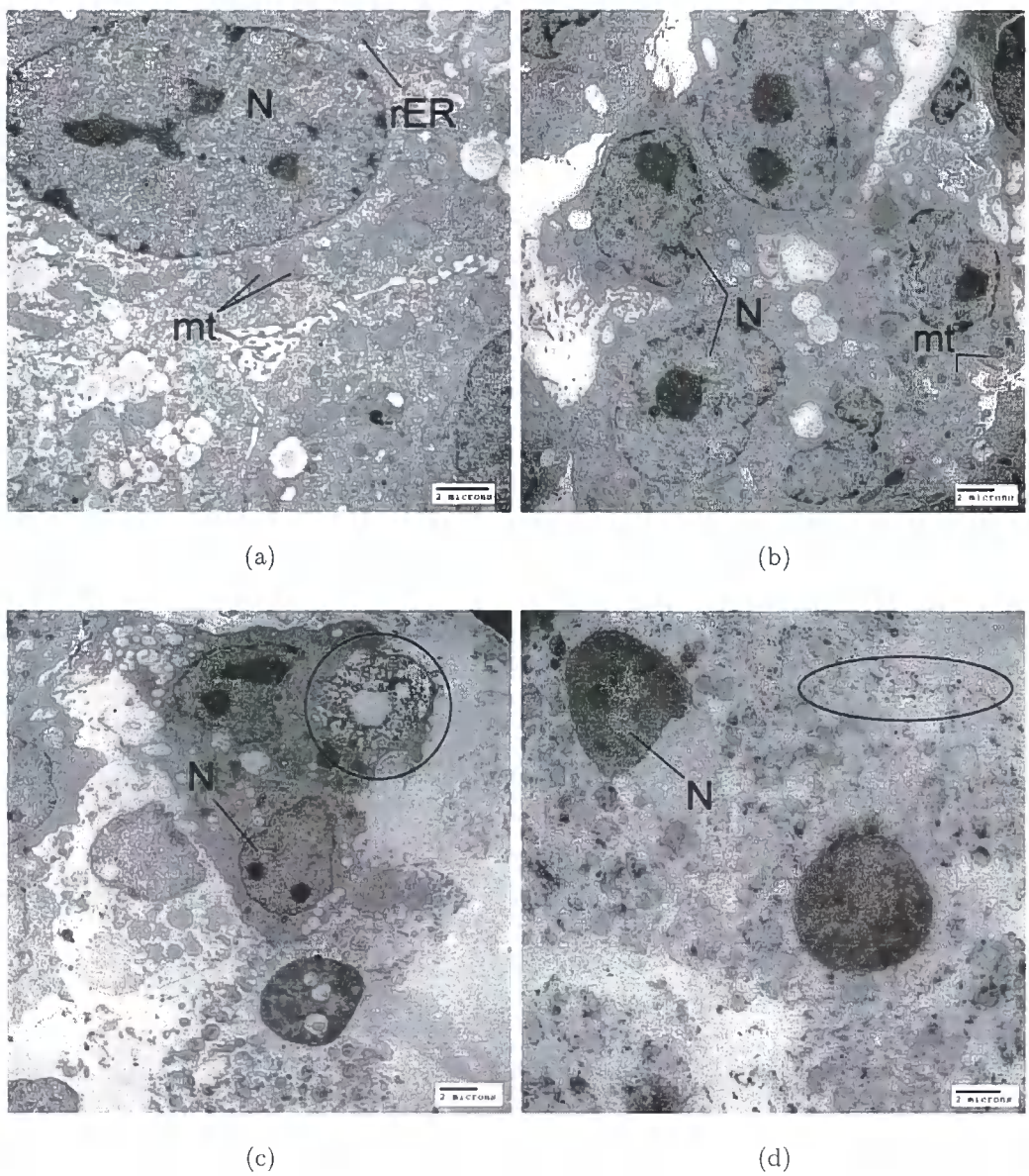

(a) (b)

(c) (d)

Figure 4.14: TEM micrographs of HepG2 cells cultured in the presence or absence of poly[GalEMA]-modified gold nanoparticles. (a) Positive control, cells only; (b) nanoparticle solution 1; (c) nanoparticle solution 2; (d) nanoparticle solution 3. Annotations: nuclei (N), mitochondria (mt), rough endoplasmic reticulum (rER). Circled areas denote possible aggregated nanoparticles.

4.15b does appear to contain more areas of high electron density (darkened areas) compared to the figure 4.15a. These areas appear to made up of small particles, but they are too large to be the particles under study and are probably a biological entity also evident in the control sample.

The condition of the cells in the TEM micrographs agrees well with the hypothesis that the MTS assay after 7 days does not determine accurately the viability of the cells. The control cells appear to be the most healthy by TEM but fair very poorly via MTS whereas the nanoparticle incubated cells appear to be of increasingly poor quality as the particle size increases yet the MTS assay places them approximately equal. This further supports the hypothesis that the nanoparticle solutions themselves are interfering with the measurement; either directly, by absorbing at the same wavelength, or indirectly, by somehow catalysing the production of the formazan product. The former is certainly feasible as these particle solutions were shown to absorb reasonably strongly at 490 nm (see fig. 4.6b). The magnitude of this absorption also increases with particle size and larger particles could make very poor condition cells appear as viable as reasonably healthy ones.

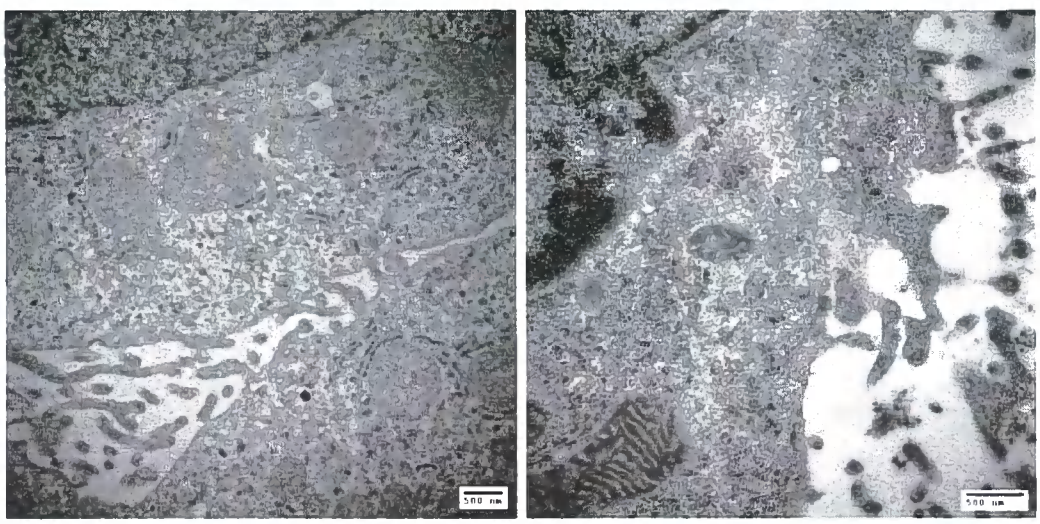

(a) (b)

Figure 4.15: High magnification TEM micrographs of HepG2 cells cultured (a) in the absence of nanoparticles, (b) in presence of nanoparticle solution 1.

4.3 Conclusions

The synthesis of multivalent carbohydrate-modified gold nanoparticles has been demonstrated by the simultaneous reduction of RAFTed glycopolymers and $HAuCl_4$. Some control of particle size has been demonstrated although, as has been seen in similar particle syntheses there appears to be a maximum limiting core size of ~ 3.5 nm. It may be possible to increase the core diameter of these particles through Ostwald ripening as has been demonstrated for alkanethiol-modified particles. [226] Particles synthesised in this manner retain their ability to bind specifically to lectins as demonstrated by a simple agglomeration assay. In vitro experiments were inconclusive with regard to the cytoxicity of such particles and further investigation is required. Additional imaging of cells cultured in the presence of gold nanoparticles using X-ray microanalysis TEM would enable detection of gold within the samples. [227] Additionally, comparative labelling of ASGPR positive and ASGPR negative cell lines without prior culture may be of interest. Use of an alternative labelling stategy, such as immunofluoresence, would allow elucidation of specificity by determining the localisation of ASGPRs for comparison.

4.4 Experimental

4.4.1 Materials and Methods

4.4.1.1 Materials

Hydrogen tetrachloroaurate (> 99.9 %, 49 % Au by mass) was purchased from Alfa Aesar. Sodium borohydride (> 98 %) was purchased from Sigma Aldrich and used without further purification. Poly[2-(β-D-galactosyloxy)ethyl methacrylate] was synthesised as described in chapter 2. RAFT synthesised poly(methyl 6-*O*-methacryloyl-α-D-glucoside) was kindly provided by Dr Luca Albertin. [132]

4.4.1.2 Methods

Dynamic light-scattering measurements were conducted using a Brookhaven Instruments 90 Zeta-Plus particle size analyser. Before analysis all samples were filtered through a 0.2 μm syringe filter to minimise contamination with dust. Transmission electron microscopy was conducted on a Hitachi 7600 instrument. Samples were prepared by deposition of a drop of the particle solution on to a carbon-coated copper grid and allowing the solvent to evaporate leaving a thin film of particles. Thermal gravimetric analyses were performed on a Perkin Elmer Pyris 1 TGA under nitrogen gas; heating from 20 °C to 800 °C at 10 °C/min

4.4.2 Synthesis of glycopolymer functionalised gold nanoparticles via modified Brust synthesis

Solutions of hydrogen tetrachloroaurate (0.5 mM), poly[2-(β-D-galactosyloxy)ethyl methacrylate] (M_n = 9.8 kDa, 5.0 mM) and sodium borohydride (50 mM) were prepared in UHQ water (resistivity > 18.0 MΩ). The $HAuCl_4$ and polymer solutions were combined and diluted to equal volume as described in table 4.3. With vigorous stirring, the $NaBH_4$ solution was added as 1 ml aliquots to each solution and stirring was continued for 2 h. After this time the particle solutions were initially filtered through a 0.2 μm syringe filter and then separated from any residual free polymer by repeated centrifugal filtration (Sartorious Vivaspin 15, MWCO 30 kDA) and washing with UHQ water.

Table 4.3: Experimental data for the synthesis of glycopolymer functionalised gold nanoparticles via modified Brust synthesis

#	Vol. $HAuCl_4$ (μl)[a]	Vol. Polymer (μl)[a]	Vol. Water (μl)	Vol. $NaBH_4$ (μl)[a]	[Au]/[polymer][b]
1	10000	400	0	2000	1.25
2	10000	200	200	2000	2.50
3	10000	100	300	2000	5.00
4	10000	50	350	2000	10.00
5	10000	25	375	2000	20.00

[a] $[HAuCl_4]$ = 0.5 mM; [Polymer] = 5.0 mM, M_n = 9.8 kDa; $[NaBH_4]$ = 50 mM. [b] Based on a Au content of 49 % for $HAuCl_4$

4.4.3 Agglutination assay

Prior to these experiments, the nanoparticles were analysed by SEC to confirm the absence of free polymer. A suspension of agarose beads coated with peanut agglutinin (PNA) (20 μl, 2-4 mg PNA/ml solution) was pipetted onto a microscope slide. 40 μl of p[GalEMA]-coated nanoparticle solution was added to the beads and the aggregation was monitored by optical microscopy; after 30 min. the beads appeared to agglomerate completely. Redispersion experiments were attempted by addition of 10 μl of a 0.072 M solution of methyl β-D-galactopyranoside or methyl β-D-glucopyranoside. A control experiment was also conducted in an identical manner using gold nanoparticles stabilized with poly[6-*O*-MAMGlc].

4.4.4 Cell viability and uptake studies on glycopolymer-AuNP conjugates

4.4.4.1 Preparation of particles

Gold nanoparticles were synthesised as described in previously. After synthesis the particles were purified and concentrated using centrifugal filtration (Sartorius Vivaspin 15 PES, 30 kDa MWCO) at 2000 *g* for 30 mins and repeated washing with UHQ water. After 4 washings the particles were concentrated once again and resuspended in 15 ml of DMEM. Nanoparticle suspensions were then filter sterilised by passing through a 0.2 μm membrane.

4.4.4.2 Hepatocyte Cell Culture

The human hepatic carcinoma cell line, Hep G2, was obtained from the American Type Culture Collection (ATCC) and maintained in DMEM. Confluent cultures of Hep G2 cells were washed with PBS, detached with trypsin/EDTA solution and counted with a hæmocytometer. Cell suspensions were then seeded in the 6-well plates (Nunc) at a density of 5×10^5 cells per well. Media and nanoparticle suspensions were added as detailed in fig. 4.11.

4.4.4.3 Determination of viable cell number

The viable cell number was determined using the commercially available colorimetric assay CellTiter 96® AQueous One Solution Cell Proliferation Assay (Promega®). Culture samples were incubated with the assay solution for 4 h before transferring to 96-well plates (Nunc); the viable cell number was then determined by measuring the absorbance of the formazan product at 490 nm.

4.4.4.4 Preparation of tissue samples for transmission electron microscopy

Culture samples were prepared for TEM by removal of the culture media, washing with PBS and fixing with 2 % paraformaldehyde and 2.5 % glutaraldehyde in Sorenson's phosphate buffer for 2 h at 4 °C. After this time the cells were scraped from the plates, pelleted at 10,000 *g* for 5 min. The pelleted cells were then washed with 0.1M phosphate buffer before staining with 1 % OsO_4 solution in 0.1 M phosphate buffer for 1 h. The stained pellets were then washed twice with 0.1 M phosphate buffer before dehydration in 25 %, 50 %, 95 % and 100 % ethanol solutions for 10 minutes;

each dehydration step was repeated three times. After dehydration, samples were immersed in a 50/50 mixture of ethanol/resin (Agar Scientific LR White) overnight. The resin solution was then replaced with pure resin and changed periodically over the following 2 days. The samples were then cured by placing in an oven overnight. Once set, the samples were cut into ultra-thin sections and imaged via TEM (Hitachi H6700).

I'm issuing a restraining order. Religion must stay 500 yards from Science at all times

Judge Roy Snider - *The Simpsons*

5

Concluding remarks

5.1 Conclusions

This thesis initially aimed to determine whether the synthesis of bioactive glycosylated polymers could be performed in a controlled manner. It has been demonstrated that reversible addition-fragmentation chain transfer polymerisation of 2-(D-glycosyloxy)ethyl methacrylates produces the corresponding glycopolymers with predictable molecular weight, narrow polydispersity and in high yield. Additionally, block and statistical copolymers have been synthesised. Despite these successes more study of the RAFT synthesis of glycopolymers is required. In addition to the glucosyl and galactosyl monomers described in Chapter 2 the α-mannosyl derivative was synthesised by identical methods. It was found that polymerisation under identical conditions did not yield any polymer and that conversions were limited to $\leq 10\%$. Owing to time constraints no further study of this monomer was possible, hence its exclusion from the bulk of this thesis, and so the reasons for its inactivity remain unknown.

Methods for producing glycopolymers of controlled, pre-defined structures allows the study of the effect said structure has on properties and here this has been investigated with respect to the cluster glycoside effect. Studies have confirmed previous findings that avidity scales with valency but in a non-linear manner and that there is a large increase in avidity once a ligand is able to bridge multiple binding sites on the same receptor. Additionally, combining the calorimetry and plasmon resonance data supports the hypothesis that avidity is increased through many, individual and sequential transient bindings between a receptor and several ligands, because of an increase of the local concentration of ligands, as well as

mulitple simultaneous bindings.

In order to further increase multivalency glycopolymer-coated nanoparticles have been synthesised in a facile way and found to maintain carbohydrate-specific binding to lectins. Unfortunately, it appears that, apart from in the smallest examples, they are of limited stability and have poor cytocompatibility, making them poor candidates as either imaging agents or therapeutics.

5.2 Future work

Although RAFT polymerisation has been shown to be a viable method for the synthesis of glycopolymers, the carbohydrates utilised in this study are simple and of little biological significance. If RAFT polymerisation is to be utilised for the production of biologically relevant glycopolymers (for example, polymers that display antigens such as sialyl-Lewis^x) then its applicability to the polymerisation of such moieties is required. The synthesis of complex oligosaccharides is non-trivial, usually resulting in low quantities of material (10–100s of milligrams), and is a challenge to be overcome if a thorough investigation of polymerisation is to be achieved.

To investigate further the factors affecting the multivalency effect a more thorough investigation is required. A comparative study, utilising both ITC and SPR, of a large range of polymers of different chain lengths and carbohydrate densities would allow further elucidation of the mechanisms by which multivalent ligands interact with multivalent receptors. This would also produce a 'map' of polymers that could be used to tailor polymers for a particular application.

Synthesis of glycoNPs from RAFTed glycopolymers is facile but is in need of

a far deeper investigation. The small core sizes synthesised here, and their high polydispersities, makes the particles unsuitable for use either in vitro, as labels, or in vivo, as pharmaceuticals. Synthesis of glycoNPs by two-step method where first a larger particle of controlled size is synthesised (e.g. by the Frens methodology) and this is functionalised by ligand transfer with a RAFTed glycopolymer should yield particles of greater potential. In fact, this methodology is routinely used by Brust for the synthesis of biologically relevant particles, [228–230] despite being the inventor of the alternative method.

Bibliography

[1] A. D. McNaught, *Pure and Appl. Chem.*, 1996, **68**, 1919–2008.

[2] W. M. Watkins and W. T. J. Morgan, *Nature*, 1952, **169**, 825–826.

[3] A. Dell, H. R. Morris, R. L. Easton, M. Patankar and G. F. Clark, *Biochim. Biophys. Acta*, 1999, **1473**, 196–205.

[4] G. Opdenakker, P. M. Rudd, C. P. Ponting and R. A. Dwek, *FASEB Journal*, 1993, **7**, 1330–1337.

[5] E. S. Trombetta and A. Helenius, *Curr. Opin. Struc. Biol.*, 1998, **8**, 587–592.

[6] A. Helenius and M. Aebi, *Science*, 2001, **291**, 2364–2369.

[7] O. Popescu and G. N. Misevic, *Nature*, 1997, **386**, 231–232.

[8] R. A. Laine, *Glycobiology*, 1994, **4**, 759–767.

[9] H. Lis and N. Sharon, *Chem. Rev.*, 1998, **98**, 637–674.

[10] Y. C. Lee and R. T. Lee, *Acc. Chem. Res.*, 1995, **28**, 321–327.

[11] O. Livnah, E. A. Bayer, M. Wilchek and J. L. Sussman, *PNAS*, 1993, **90**, 5076–5080.

[12] M. Ambrosi, N. R. Cameron and B. G. Davis, *Org. Biomol. Chem.*, 2005, **3**, 1593–1608.

[13] N. Yamazaki, S. Kojima, N. V. Bovin, S. Andre, S. Gabius and H. J. Gabius, *Adv. Drug Del. Rev.*, 2000, **43**, 225–244.

[14] Y. Lee, R. Townsend, M. Hardy, J. Lonngren, J. Arnarp, M. Haraldsson and H. Lonn, *J. Biol. Chem.*, 1983, **258**, 199–202.

[15] J. J. Lundquist and E. J. Toone, *Chem. Rev.*, 2002, **102**, 555–578.

[16] D. C. Wiley and J. J. Skehel, *Annu. Rev. of Biochem.*, 1987, **56**, 365–394.

[17] J. Rao, J. Lahiri, L. Isaacs, R. M. Weis and G. M. Whitesides, *Science*, 1998, **280**, 708–711.

[18] M. R. Villarreal, http://upload.wikimedia.org/wikipedia/commons/1/1a/Endocytosis_types.svg, retrieved 23rd February 2008.

[19] B. Alberts, D. Bray, A. Johnson, J. Lewis, M. Raff, K. Roberts and P. Walter, *Essential Cell Biology*, Garland Publishing, New York, 1998.

[20] B. G. Davis, *Chem. Rev.*, 2002, **102**, 579–601.

[21] R. Roy, F. D. Tropper and A. Romanowska, *Bioconjugate Chem.*, 1992, **3**, 256–261.

[22] S.-K. Choi, M. Mammen and G. M. Whitesides, *J. Am. Chem. Soc.*, 1997, **119**, 4103–4111.

[23] E. J. Gordon, L. E. Strong and L. L. Kiessling, *Bioorg. Med. Chem.*, 1998, **6**, 1293–1299.

[24] T. Yoshida, T. Akasaka, Y. Choi, K. Hattori, B. Yu, T. Mimura, Y. Kaneko, H. Nakashima, E. Aragaki, M. Premanathan, N. Yamamoto and T. Uryu, *J. Polym. Sci. Part A: Polym. Chem.*, 1999, **37**, 789–800.

[25] R. Roy and M.-G. Baek, *Rev. Molecul. Biotech.*, 2002, **90**, 291–309.

[26] J. Li, S. Zacharek, X. Chen, J. Wang, W. Zhang, A. Janczuk and P. G. Wang, *Bioorg. Med. Chem.*, 1999, **7**, 1549–1558.

[27] M. G. Garcia-Martin, C. Jimenez-Hidalgo, S. S. J. Al-Kass, M. Caraballo, V. de Paz and J. A. Galbis, *Polymer*, 2000, **41**, 821–826.

[28] A. C. Roche, I. Fajac, S. Grosse, N. Frison, C. Rondanino, R. Mayer and M. Monsigny, *Cell. Mol. Life Sci.*, 2003, **60**, 288–297.

[29] Y. H. Yun, D. J. Goetz, P. Yellen and C. Weiliam, *Biomaterials*, 2004, **25**, 147–157.

[30] S. J. Novick and J. S. Dordick, *Chem. Mat.*, 1998, **10**, 955–958.

[31] T. Miyata, T. Uragami and K. Nakamae, *Adv. Drug Del. Rev.*, 2002, **54**, 79–98.

[32] E. Karamuk, J. Mayer, E. Wintermantel and T. Akaike, *Artif. Organs*, 1999, **23**, 881–887.

[33] S.-H. Kim, J.-H. Kim and T. Akaike, *FEBS Lett.*, 2003, **553**, 433–439.

[34] T. Taguchi, A. Kishida, N. Sakamoto and M. Akashi, *J. Biomed. Mat. Res.*, 1998, **41**, 386–391.

[35] W. W. Thompson, D. K. Shay, E. Weintraub, L. Brammer, N. Cox, L. J. Anderson and K. Fukuda, *J. Am. Med. Assoc.*, 2003, **289**, 179–186.

[36] N. K. Sauter, M. D. Bednarski, B. A. Wurzburg, J. E. Hanson, G. M. Whitesides, J. J. Skehel and D. C. Wiley, *Biochemistry*, 1989, **28**, 8388–8396.

[37] M. N. Mastrovich, L. V. Mochalova, V. P. Marinina, N. E. Byramova and N. V. Bovin, *FEBS Lett.*, 1990, **272**, 209–212.

[38] A. Spaltenstein and G. M. Whitesides, *J. Am. Chem. Soc.*, 1991, **113**, 686–687.

[39] M. A. Sparks, K. W. Williams and G. M. Whitesides, *J. Med. Chem.*, 1993, **36**, 778–783.

[40] W. J. Lees, A. Spaltenstein, J. E. Kingery-Wood and G. M. Whitesides, *J. Med. Chem.*, 1994, **37**, 3419–3433.

[41] M. Mammen, G. Dahmann and G. M. Whitesides, *J. Med. Chem.*, 1995, **38**, 4179–4190.

[42] S.-K. Choi, M. Mammen and G. M. Whitesides, *Chem. Biol.*, 1996, **3**, 97–104.

[43] G. B. Sigal, M. Mammen, G. Dahmann and G. M. Whitesides, *J. Am. Chem. Soc.*, 1996, **118**, 3789–3800.

[44] J. E. Kingery-Wood, K. W. Williams, G. B. Sigal and G. M. Whitesides, *J. Am. Chem. Soc.*, 1992, **114**, 7303–7305.

[45] T. Pritchett and J. Paulson, *J. Biol. Chem.*, 1989, **264**, 9850–9858.

[46] S. L. Johnston, *Virus Res.*, 2002, **82**, 147–152.

[47] R. Wagner, M. Matrosovich and H.-D. Klenk, *Rev. Med. Virology*, 2002, **12**, 159–166.

[48] Q. Wang, J. S. Dordick and R. J. Linhardt, *Org. Lett.*, 2003, **5**, 1187–1189.

[49] K. Matsuoka, C. Takita, T. Koyama, D. Miyamoto, S. Yingsakmongkon, K. I. P. J. Hidari, W. Jampangern, T. Suzuki, Y. Suzuki, K. Hatano and D. Terunuma, *Bioorg. Med. Chem. Lett.*, 2007, **17**, 3826–3830.

[50] J.-I. Sakamoto, T. Koyama, D. Miyamoto, S. Yingsakmongkon, K. I. P. J. Hidari, W. Jampangern, T. Suzuki, Y. Suzuki, Y. Esumi, K. Hatano, D. Terunuma and K. Matsuoka, *Bioorg. Med. Chem. Lett.*, 2007, **17**, 717–721.

[51] United Nations 2006 Report on the global AIDS epidemic.

[52] K. D. McReynolds and J. Gervay-Hague, *Chem. Rev.*, 2007, **107**, 1533–1552.

[53] C. P. Ferri, M. Prince, C. Brayne, H. Brodaty, L. Fratiglioni, M. Ganguli, K. Hall, K. Hasegawa, H. Hendrie, Y. Huang, A. Jorm, C. Mathers, P. R. Menezes, E. Rimmer and M. Scazufca, *The Lancet*, 2005, **366**, 2112–2117.

[54] J. Hardy and D. J. Selkoe, *Science*, 2002, **297**, 353–356.

[55] S. T. Ferreira, M. N. N. Vieira and F. G. De Felice, *IUBMB Life*, 2007, **59**, 332–345.

[56] J. McLaurin, T. Franklin, P. E. Fraser and A. Chakrabartty, *J. Biol. Chem.*, 1998, **273**, 4506–4515.

[57] J. McLaurin, T. Franklin, X. Zhang, J. Deng and P. E. Fraser, *Eur. J. Biochem.*, 1999, **266**, 1101–1110.

[58] A. Kakio, S.-I. Nishimoto, K. Yanagisawa, Y. Kozutsumi and K. Matsuzaki, *J. Biol. Chem.*, 2001, **276**, 24985–24990.

[59] J. Diaz-Nido, F. Wandosell and J. Avila, *Peptides*, 2002, **23**, 1323–1332.

[60] A. Kakio, S.-I. Nishimoto, K. Yanagisawa, Y. Kozutsumi and K. Matsuzaki, *Biochemistry*, 2002, **41**, 7385–7390.

[61] Y. Miura, K. Yasuda, K. Yamamoto, M. Koike, Y. Nishida and K. Kobayashi, *Biomacromolecules*, 2007, **8**, 2129–2134.

[62] B. C. Widemann and P. C. Adamson, *The Oncologist*, 2006, **11**, 694–703.

[63] W. M. Pardridge, *NeuroRx*, 2005, **2**, 3–14.

[64] R. Polt, M. Dhanasekaran and C. M. Keyari, *Med. Res. Rev.*, 2005, **25**, 557–585.

[65] H. Ringsdorf, *J. Polym. Sci. Polym. Symp.*, 1975, **51**, 135–153.

[66] G. Parut and F. M. Veronese, *Prog. Polym. Sci.*, 2007, **32**, 933–961.

[67] R. Duncan, J. Kopeček, P. Rejmanová and J. B. Lloyd, *Biochim. Biophys. Acta*, 1983, **755**, 518–521.

[68] R. Duncan, L. W. Seymour, L. Scarlett, J. B. Lloyd, P. Rejmanová and J. Kopeček, *Biochim. Biophys. Acta*, 1986, **880**, 62–71.

[69] R. Duncan, I. C. Hume, P. Kopečková, K. Ulbrich, J. Strohalm and J. Kopeček, *J. Control. Release*, 1989, **10**, 51–63.

[70] J. Kopeček and R. Duncan, *J. Control. Release*, 1987, **6**, 315–327.

[71] P. J. Julyan, L. W. Seymour, D. R. Ferry, S. Daryani, C. M. Boivin, J. Doran, M. David, D. Anderson, C. Christodoulou, A. M. Young, S. Hesslewood and D. J. Kerr, *J. Control. Release*, 1999, **57**, 281–290.

[72] L. W. Seymour, D. R. Ferry, D. Anderson, S. Hesslewood, P. J. Julyan, R. Poyner, J. Doran, A. M. Young, S. Burtles and D. J. Kerr, *J. Clin. Oncol.*, 2002, **20**, 1668–1676.

[73] K. Greish, *J. Drug Target.*, 2007, **15**, 457–464.

[74] K. G. Mann, *Thrombosis and Haemostasis*, 1999, **82**, 165–174.

[75] H. Dam, *Biochem. J.*, 1935, **29**, 1273–1285.

[76] R. M. Puckett and M. Offringa, *Cochrane Database of Systematic Reviews*, 2000, CD002776.

[77] M. Hashida, H. Hirabayashi, M. Nishikawa and Y. Takakura, *J. Control. Release*, 1997, **46**, 129–137.

[78] C. Fleming, A. Maldjian, D. D. Costa, A. K. Rullay, D. M. Haddleton, J. St John, P. Penny, R. C. Noble, N. R. Cameron and B. G. Davis, *Nat. Chem. Biol.*, 2005, **1**, 270–274.

[79] M. E. Davis, *Curr. Opin. Biotech.*, 2002, **13**, 128–131.

[80] J. D. Druliner, *Macromolecules*, 1991, **24**, 6079–6082.

[81] Y. Gnanou, D. Grande and R. Guerrero, *Polymer Preprints*, 1999, **40**, 99–100.

[82] D. Grande, S. Baskaran, C. Baskaran, Y. Gnanou and E. L. Chaikof, *Macromolecules*, 2000, **33**, 1123–1125.

[83] D. Grande, S. Baskaran and E. L. Chaikof, *Macromolecules*, 2001, **34**, 1640–1646.

[84] S. Baskaran, D. Grande, X.-L. Sun, A. Yayon and E. L. Chaikof, *Bioconjugate Chem.*, 2002, **13**, 1309–1313.

[85] X.-L. Sun, D. Grande, S. Baskaran, S. R. Hanson and E. L. Chaikof, *Biomacromolecules*, 2002, **3**, 1065–1070.

[86] O. Saksela, D. Moscatelli, A. Sommer and D. B. Rifkin, *J. Cell Biol.*, 1988, **107**, 743–751.

[87] R. Guan, X.-L. Sun, S. Hou, P. Wu and E. L. Chaikof, *Bioconjugate Chem.*, 2004, **15**, 145–151.

[88] K. Nakamae, M. Takashi, A. Jikihara and A. S. Hoffman, *J. Biomat. Sci., Polym. Ed.*, 1995, **6**, 79–90.

[89] T. Miyata, A. Jikihara and K. Nakamae, *Macromol. Chem. Phys.*, 1997, **197**, 1135–1146.

[90] Y. Zhang, Q. Yao, C. Xia, X. Jiang and P. G. Wang, *ChemMedChem*, 2006, **1**, 1361 – 1366.

[91] K. Matyjaszewski and A. H. E. Müller, *Polymer Preprints*, 1997, **38**, 6–9.

[92] T. Otsu and M. Yoshida, *Macromol. Rapid Comm.*, 1982, **3**, 127–132.

[93] T. Otsu, *J. Polym. Sci. Part A: Polym. Chem.*, 2000, **38**, 2121–2136.

[94] C. J. Hawker, A. W. Bosman and E. Harth, *Chem. Rev.*, 2001, **101**, 3661–3688.

[95] K. Matyjaszewski and J. Xia, *Chem. Rev.*, 2001, **101**, 2921–2990.

[96] S. Perrier and P. Takolpuckdee, *J. Polym. Sci. Part A: Polym. Chem.*, 2005, **43**, 5347–5393.

[97] J. Chiefari, Y. K. Chong, F. Ercole, J. Krstina, J. Jeffery, T. P. T. Le, R. T. A. Mayadunne, G. F. Meijs, C. L. Moad, G. Moad, E. Rizzardo and S. H. Thang, *Macromolecules*, 1998, **31**, 5559–5562.

[98] Y. K. Chong, T. P. T. Le, G. Moad, E. Rizzardo and S. H. Thang, *Macromolecules*, 1999, **32**, 2071–2074.

[99] A. Goto, K. Sato, T. Fukuda, G. Moad, E. Rizzardo and S. H. Thang, *Polymer Preprints*, 1999, **40**, 397–398.

[100] H. D. Brouwer, M. A. J. Schellekens, B. Klumperman, M. J. Monteiro and A. L. German, *J. Polym. Sci. Part A: Polym. Chem.*, 2000, **38**, 3596–3603.

[101] G. Moad, J. Chiefari, Y. K. Chong, J. Krstina, R. T. A. Mayadunne, A. Postma, E. Rizzardo and S. H. Thang, *Polym. Int.*, 2000, **49**, 993–1001.

[102] M. S. Donovan, A. B. Lowe, T. A. Sanford and C. L. McCormick, *J. Polym. Sci. Part A: Polym. Chem.*, 2003, **41**, 1262–1281.

[103] D. B. Thomas, B. S. Sumerlin, A. B. Lowe and C. L. McCormick, *Macromolecules*, 2003, **36**, 1436–1439.

[104] M. H. Stenzel, L. Cummins, G. E. Roberts, T. P. Davis, P. Vana and C. Barner-Kowollik, *Macromol. Chem. Phys.*, 2003, **204**, 1160–1168.

[105] A. A. Toy, P. Vana, T. P. Davis and C. Barner-Kowollik, *Macromolecules*, 2004, **37**, 744–751.

[106] J. B. McLeary and B. Klumperman, *Soft Matter*, 2006, **2**, 45–53.

[107] S. Perrier, T. P. Davis, A. J. Carmichael and D. M. Haddleton, *Chem. Commun.*, 2002, 2226–2227.

[108] K. Thurecht, A. M. Gregory, S. Villarroya, J. Zhou, A. Heise and S. M. Howdle, *Chem. Commun.*, 2006, 4383–4385.

[109] K. J. Thurecht, A. M. Gregory, W. Wang and S. M. Howdle, *Macromolecules*, 2007, **40**, 2965–2967.

[110] A. B. Lowe and C. L. McCormick, *Prog. Polym. Sci.*, 2007, **32**, 283–351.

[111] H. Yin, H. Zheng, L. Lu, L. Pengsheng and Y. Cai, *J. Polym. Sci. Part A: Polym. Chem.*, 2007, **45**, 5091–5102.

[112] H. Zhang, J. Deng, L. Lu and Y. Cai, *Macromolecules*, 2007, **40**, 9252–9261.

[113] S. L. Brown, C. M. Rayner and S. Perrier, *Macromol. Rapid Comm.*, 2007, **28**, 478–483.

[114] S. L. Brown, C. M. Rayner, S. Graham, A. Cooper, S. Rannard and S. Perrier, *Chem. Commun.*, 2007, 2145–2147.

[115] V. Ladmiral, E. Melia and D. M. Haddleton, *Eur, Polym. J.*, 2004, **40**, 431–449.

[116] A. J. Varma, J. F. Kennedy and P. Galgali, *Carbohyd. Polym.*, 2004, **56**, 429–445.

[117] H. C. Kolb, M. G. Finn and K. B. Sharpless, *Angew. Chem. Int. Edit.*, 2001, **40**, 2004–2021.

[118] M. Ambrosi, A. S. Batsanov, N. R. Cameron, B. G. Davis, J. A. K. Howard and R. Hunter, *J. Chem. Soc. Perkin Trans. 1*, 2002, 45–52.

[119] M. Minoda, K. Yamaoka, K. Yamada, A. Takaragi and T. Miyamoto, *Macromol. Symp.*, 1995, **99**, 169–177.

[120] K. Yamada, K. Yamaoka, M. Minoda and T. Miyamoto, *J. Polym. Sci. Part A: Polym. Chem.*, 1997, **25**, 255–261.

[121] K. Yamada, M. Minoda and T. Miyamoto, *Macromolecules*, 1999, **32**, 3553–3558.

[122] K. Yamada, M. Minoda, T. Fukuda and T. Miyamoto, *J. Polym. Sci. Part A: Polym. Chem.*, 2001, **39**, 459–467.

[123] S. Loykulnant, M. Hayashi and A. Hirao, *Macromolecules*, 1998, **31**, 9121–9126.

[124] S. Loykulnant and A. Hirao, *Macromolecules*, 2000, **33**, 4757–4764.

[125] G. Descotes, J. Ramza, J.-M. Basset and S. Pagano, *Tetrahedron Lett.*, 1994, **35**, 7379–7382.

[126] K. H. Mortell, M. Gingras and L. L. Kiessling, *J. Am. Chem. Soc.*, 1994, **116**, 12053–12054.

[127] C. Fraser and R. H. Grubbs, *Macromolecules*, 1995, **28**, 7248–7255.

[128] S. Kitazawa, M. Okumura, K. Kinomura and T. Sakakibara, *Chemistry Lett.*, 1990, 1733–1736.

[129] T. Nakaya, K. Nishio, M. Memita and M. Imoto, *Makromol. Chem. Rapid Comm.*, 1993, **14**, 77–83.

[130] T. Mori, S. Fujita and Y. Okahata, *Carbohyd. Res.*, 1997, **298**, 65–73.

[131] M. Santin, F. Rosso, A. Sada, G. Peluso, R. Improta and A. Trincone, *Biotech. Bioeng.*, 1996, **49**, 217–222.

[132] L. Albertin, M. Stenzel, C. Barner-Kowollik, L. J. R. Foster and T. P. Davis, *Macromolecules*, 2004, **37**, 7530–7537.

[133] A. B. Lowe, B. S. Sumerlin and C. L. McCormick, *Polymer*, 2003, **44**, 6761–6765.

[134] L. Albertin, M. H. Stenzel, C. Barner-Kowollik and T. P. Davis, *Polymer*, 2006, **47**, 1011–1019.

[135] L. Albertin, C. Kohlert, M. Stenzel, L. J. R. Foster and T. P. Davis, *Biomacromolecules*, 2004, **5**, 255–260.

[136] J. Bernard, A. Favier, L. Zhang, A. Nilasaroya, T. P. Davis, C. Barner-Kowollik and M. H. Stenzel, *Macromolecules*, 2005, **38**, 5475–5484.

[137] S. R. S. Ting, A. M. Granville, D. Quémener, T. P. Davis, M. H. Stenzel and C. Barner-Kowollik, *Aust. J. Chem.*, 2007, **60**, 405–409.

[138] J. Bernard, X. Hao, T. P. Davis, C. Barner-Kowollik and M. Stenzel, *Biomacromolecules*, 2006, **7**, 232–238.

[139] Y. Tsujii, M. Ejaz, K. Sato, A. Goto and T. Fukuda, *Macromolecules*, 2001, **34**, 8872–8878.

[140] M. H. Stenzel, L. Zhang and W. T. S. Huck, *Macromol. Rapid Comm.*, 2006, **27**, 1121–1126.

[141] A. Housni, H. Cai, S. Liu, S. H. Pun and R. Narain, *Langmuir*, 2007, **23**, 5056–5061.

[142] R. Narain, A. Housni, G. Gody, P. Boullanger, M.-T. Charreyre and T. Delair, *Langmuir*, 2007, **23**, 12835–12841.

[143] D. R. Mootoo, P. Konradsson, U. Udodong and B. Fraser-Reid, *J. Am. Chem. Soc.*, 1988, **110**, 5583–5584.

[144] S. Deng, U. Gangadharmath and C.-W. Chang, *J. Org. Chem.*, 2006, **71**, 5179–5185.

[145] G. Widmalm, *Physical methods in carbohydrate research*, in *Carbohydrate Chemistry*, ed. G.-J. Boons, Blackie Academic and Professional, London, 1998, pp. 448–502.

[146] C. A. Wamser, *J. Am. Chem. Soc.*, 1951, **73**, 409–416.

[147] R. T. Lee and Y. C. Lee, *Carbohyd. Res.*, 1995, **271**, 131–136.

[148] M.-Z. Liu, H.-N. Fan, Z.-W. Guo and Y.-Z. Hui, *Carbohyd. Res.*, 1996, **290**, 233–237.

[149] K. Toshima and K. Tatsuta, *Chem. Rev.*, 1993, **93**, 1503-1531 and references therein.

[150] V. Vázquez-Dorbatt and H. D. Maynard, *Biomacromolecules*, 2006, **7**, 2297–2302.

[151] F. M. Lewis and M. S. Matheson, *J. Am. Chem. Soc.*, 1949, **71**, 747–748.

[152] D. C. Blackley and A. C. Haynes, *J. Chem. Soc. Faraday Trans. 1*, 1979, **75**, 935–941.

[153] F. Ganachaud, A. Theretz, M. N. Erout, M. F. Llauro and C. Pichot, *J. Appl. Polym. Sci.*, 1995, **58**, 1811–1824.

[154] C. Barner-Kowollik, M. Buback, B. Charleux, M. L. Coote, M. Drache, T. Fukuda, A. Goto, B. Klumperman, A. B. Lowe, J. B. McLeary, G. Moad, M. J. Monteiro, R. D. Sanderson, M. P. Tonge and P. Vana, *J. Polym. Sci. Part A: Polym. Chem.*, 2006, **44**, 5809–5831.

[155] L. Albertin and N. R. Cameron, *Macromolecules*, 2007, **40**, 6082–6093.

[156] E. T. A. Van Den Dungen, H. Matahwa, J. B. McLeary, R. D. Sanderson and B. Klumperman, *J. Polym. Sci. Part A: Polym. Chem.*, 2008, **46**, 2500–2509.

[157] Y. Chen and G. Wulff, *Macromol. Chem. Phys.*, 2001, **202**, 3426–3431.

[158] K. Ohno, Y. Tsujii and T. Fukuda, *J. Polym. Sci. Part A: Polym. Chem.*, 1998, **36**, 2473–2481.

[159] M. U. Beer, P. J. Wood and J. Weisz, *Carbohyd. Polym.*, 1999, **39**, 377–380.

[160] J. F. J. Coelho, P. M. F. O. Gonçalves, D. Miranda and M. H. Gil, *Eur, Polym. J.*, 2006, **42**, 751–763.

[161] C. M. Fernyhough, R. N. Young, A. J. Ryan and L. R. Hutchings, *Polymer*, 2006, **47**, 3455–3463.

[162] L. Albertin, M. H. Stenzel, C. Barner-Kowollik, L. J. R. Foster and T. P. Davis, *Macromolecules*, 2005, **38**, 9075–9084.

[163] J. V. M. Weaver, B. I, K. L. Robinson, X. Bories-Azeau, S. P. Armes, M. Smallridge and P. McKenna, *Macromolecules*, 2004, **37**, 2395–2403.

[164] M. Ambrosi, N. R. Cameron, B. G. Davis and S. Stolnik, *Org. Biomol. Chem.*, 2005, **3**, 1476–1480.

[165] T. Wiseman, S. Williston, J. F. Brandts and L.-N. Lin, *Anal. Biochem.*, 1989, **179**, 131–137.

[166] http://www.opcw.org/html/db/cwc/eng/cwc_annex_on_chemicals.html.

[167] L. M. Roberts, F. I. Lamb, D. J. C. Pappin and J. M. Lord, *J. Biol. Chem.*, 1985, **260**, 15682–15686.

[168] E. Saltvedt, *Biochim. Biophys. Acta*, 1976, **451**, 536–548.

[169] D. B. Cawley, M. L. Hedblom and L. L. Houston, *Arch. Biochem. Biophys*, 1978, **190**, 744–755.

[170] M. O'Hare, L. M. Roberts and J. M. Lord, *FEBS Lett.*, 1992, **299**, 209–212.

[171] J. Adam, M. Pokorná, C. Sabin, E. P. Mitchell, A. Imberty and M. Wimmerová, *BMC Struct. Biol.*, 2007, **7**, 36.

[172] K. M. Halkes, A. C. d. Souza, C. E. P. Maljaars, G. J. Gerwig and J. P. Kamerling, *Eur. J. Org. Chem.*, 2005, 3650–3659.

[173] S. Sharma, S. Bharadwaj, A. Surolia and S. K. Podder, *Biochem. J.*, 1998, **333**, 539–542.

[174] T. K. Dam, R. Roy, D. Pagé and C. F. Brewer, *Biochemistry*, 2002, **41**, 1351–1358.

[175] T. K. Dam, H.-J. Gabius, S. André, H. Kaltner, M. Lensch and C. F. Brewer, *Biochemistry*, 2005, **44**, 12564–12571.

[176] C. Zentz, J.-P. Frenoy and R. Bourrillon, *Biochimie*, 1979, **61**, 1–6.

[177] D. A. Mann, M. Kanai, D. J. Maly and L. L. Kiessling, *J. Am. Chem. Soc.*, 1998], **120**, 10575–10582.

[178] Jmol: an open-source Java viewer for chemical structures in 3D. http://www.jmol.org/.

[179] A. Herráez, *Biochemistry and Molecular Biology Education*, 2006, **34**, 255–261.

[180] A. G. Gabdoulkhakov, Y. Savochkina, N. Konareva, R. Krauspenhaar, S. Stoeva, S. V. Nikonov, W. Voelter, C. Betzel and A. M. Mikhailov, *Agglutinin from Ricinus communis with galactoaza*, PDB ID: 1RZO, 2004.

[181] M. Mammen, S.-K. Choi and G. M. Whitesides, *Angew. Chem. Int. Edit.*, 1998, **37**, 2754–2794.

[182] D. K. Mandal, N. Kishore and C. F. Brewer, *Biochemistry*, 1994, **33**, 1149–1156.

[183] B. Perlmutter-Hayman, *Acc. Chem. Res.*, 1986, **19**, 90–96.

[184] P. I. Kitov and D. R. Bundle, *J. Am. Chem. Soc.*, 2003, **125**, 16271–16284.

[185] S. A. Bernhard, *J. Biol. Chem.*, 1956, **218**, 961–969.

[186] Y.-Z. Liang, Z.-C. Li and F.-M. Li, *J. Colloid and Interf. Sci.*, 2000, **224**, 84–90.

[187] T. K. Dam, R. Roy, S. K. Das, S. Oscarson and C. F. Brewer, *J. Biol. Chem.*, 2000, **275**, 14223–14230.

[188] H. Uzawa, H. Ito, P. Neri, H. Mri and Y. Nishida, *ChemBioChem*, 2007, **8**, 2117–2124.

[189] J. Geng, G. Mantovani, L. Tao, J. Nicolas, G. Chen, R. Wallis, D. A. Mitchell, R. G. Johnson Benjamin, S. D. Evans and D. M. Haddleton, *J. Am. Chem. Soc.*, 2007, **129**, 15156–15163.

[190] L. Yu, M. Huang, P. G. Wnag and X. Zeng, *Anal. Chem.*, 2007, **79**, 8979–8986.

[191] A. Alexeev, R. Verberg and A. C. Balazs, *Langmuir*, 2007, **23**, 983–987.

[192] A. Alexeev, R. Verberg and A. C. Balazs, *Phys. Rev. Lett.*, 2006, **96**, 148103.

[193] C. Dong, J. Cao, E. J. Struble and H. H. Lipowsky, *Ann. Biomed. Eng.*, 1999, **27**, 298–312.

[194] E. F. Krasik and D. A. Hammer, *Biophys. J.*, 2004, **87**, 2912–2930.

[195] M. Faraday, *Phil. Trans. Royal Soc. London*, 1857, **147**, 145–181.

[196] http://www.rigb.org/heritage/popups/gold.jsp.

[197] P. P. Edwards and J. M. Thomas, *Angew. Chem. Int. Edit.*, 2007, **46**, 5480–5486.

[198] J. Turkevich, P. C. Stevenson and J. Hillier, *Discuss. Faraday Soc.*, 1951, **11**, 55–75.

[199] B. V. Enüstün and J. Turkevich, *J. Am. Chem. Soc.*, 1963, **85**, 3317–3328.

[200] J. Turkevich, *Gold Bull.*, 1985, **18**, 87–91.

[201] J. Turkevich, *Gold Bull.*, 1985, **18**, 125–131.

[202] G. Frens, *Nature Phys. Sci.*, 1973, **241**, 20–22.

[203] M. Brust, M. Walker, D. Bethell, D. J. Schiffrin and R. Whyman, *Chem. Commun.*, 1994, 801–802.

[204] J. De la Fuente and S. Penadés, *Biochim. Biophys. Acta*, 2006, **1760**, 636–651.

[205] J. M. de la Fuente, A. G. Barrientos, T. C. Rojas, J. Rojo, J. Cañada, A. Fernández and S. Penadés, *Angew. Chem. Int. Edit.*, 2001, **40**, 2257–2261.

[206] J. M. de la Fuente, P. Eaton, A. G. Barrientos, M. Menésndez and S. Penadés, *J. Am. Chem. Soc.*, 2005, **127**, 6192–6197.

[207] T. C. Rojas, J. M. de la Fuente, A. G. Barrientos, S. Penadés, L. Ponsonnet and A. Fernández, *Adv. Mater.*, 2002, **14**, 585–588.

[208] B. Nolting, J.-J. Yu, G.-y. Liu, S.-J. Cho, S. Kauzlarich and J. Gervay-Hague, *Langmuir*, 2003, **19**, 6465–6473.

[209] J. Rojo, V. Diaz, J. M. de la Fuente, I. Segura, A. G. Barrientos, H. H. Riese, A. Bernade and S. Penadés, *Chembiochem*, 2004, **5**, 291–297.

[210] R. Ojeda, J. L. de Paz, A. G. Barrientos, M. Martín-Lomas and S. Penadés, *Carbohyd. Res.*, 2007, **342**, 448–459.

[211] S. A. Svarovsky, Z. Szekely and J. J. Barchi, *Tetrahedron: Asymm.*, 2005, **16**, 587–598.

[212] A. Sundgren and J. J. Barchi, *Carbohyd. Res.*, 2008, **343**, 1594–1604.

[213] D. C. Hone, A. H. Haines and D. A. Russell, *Langmuir*, 2003, **19**, 7141–7144.

[214] C. L. Schofield, R. A. Field and D. A. Russell, *Anal. Chem.*, 2007, **79**, 1356–1361.

[215] C. A. Schofield, B. Mukhopadhyay, S. M. Hardy, M. B. McDonnell, R. A. Field and D. A. Russell, *The Analyst*, 2008, **133**, 626–634.

[216] A. B. Lowe, B. S. Sumerlin, M. S. Donovan and C. L. McCormick, *J. Am. Chem. Soc.*, 2002, **124**, 11562–11563.

[217] J. Shan, M. Nuopponen, H. Jiang, E. Kauppinen and H. Tenhu, *Macromolecules*, 2003, **36**, 4526–4533.

[218] J. Shan, M. Nuopponen, H. Jiang, T. Viitala, E. Kauppinen, K. Kontturi and H. Tenhu, *Macromolecules*, 2005, **38**, 2918–2926.

[219] K. L. McGilvray, M. R. Decan, D. Wang and J. C. Scaiano, *J. Am. Chem. Soc.*, 2006, **128**, 15980–15981.

[220] M. Brust and C. J. Kiely, *Colloid. Surface. A*, 2002, **202**, 175–186.

[221] I. Hussain, S. Graham, Z. Wang, B. Tan, D. C. Sherrington, S. P. Rannard, A. I. Cooper and M. Brust, *J. Am. Chem. Soc.*, 2005, **127**, 16398–16399.

[222] M. D. Abramoff, P. J. Magelhaes and S. J. Ram, *Biophotonics International*, 2004, **11**, 36–42.

[223] W. S. Rasband, ImageJ, US National Institutes of Health, Bethesda. http://rsb.info.nih.gov/ij/, 1997-2007.

[224] M. J. Hostetler, J. E. Wingate, C.-J. Zhong, J. E. Harris, R. W. Vachet, M. R. Clark, J. D. Londono, S. J. Green, J. J. Stokes, G. D. Wignall, G. L. Glish, M. D. Porter, N. D. Evans and R. W. Murray, *Langmuir*, 1998, **14**, 17–30.

[225] D. J. Shaw, *Introduction to Colloid and Surface Chemistry*, Butterworth-Heinemann, fourth edn., 1992.

[226] N. R. Jana, L. Gearheart and C. J. Murphy, *Langmuir*, 2001, **17**, 6782–6786.

[227] T. Negata, *Progress in Histochemistry and Cytochemistry*, 2004, **39**, 185–319.

[228] Z. Krpetić, P. Nativo, F. Porta and M. Brust, *Bioconjugate Chem.*, 2009, **20**, 619–624.

[229] P. Nativo, I. A. Prior and M. Brust, *ACS Nano*, 2008, **2**, 1639–1644.

[230] A. Kanaras, Z. Wang, M. Brust, R. Cosstick and A. Bates, *Small*, 2007, **3**, 590–594.

Publications and Presentations

Publications

1. M. I. Gibson; C. A. Barker; S. G. Spain; L. Albertin and N. R. Cameron, "Inhibition of Ice Crystal Growth by Synthetic Glycopolymers; Implications for the Rational Design of Antifreeze Glycoprotein Mimics" *Biomacromolecules* 2009, **10**, 328-333.

2. N. R. Cameron; S. G. Spain; J. A. Kingham et al, "Synthesis of well-defined glycopolymers and some studies of their aqueous solution behaviour" *Faraday Discussions* 2008, **139**, 359-368.

3. A. L. Parry; S. G. Spain; J. Ellis; B. G. Davis and N. R. Cameron, "Multivalent glyconanoparticles from RAFT polymers: synthesis and characterization" *Polym. Prepr.* 2008, **49**, 587-588.

4. S. G. Spain; M. I. Gibson and N. R. Cameron, "Recent advances in the synthesis of well-defined glycopolymers" *J. Polym. Sci. Part. A. Polym. Chem.*

2007, **45**, 2059-2072.

5. S. G. Spain; L. Albertin and N. R. Cameron, "Facile *in situ* preparation of biologically active multivalent glyconanoparticles" *Chem. Commun.* 2006, 4198-4200.

   Selected for publication in the RSC's Chemical Biology Virtual Journal and one of the Top Ten Accessed Chemical Biology articles for October 2006.

6. A. Dureault, S. G. Spain, J. P. M. Bayley, H. Watson, N. R. Cameron, J. M. Sanderson, J. Thies, L. Ayres and J. C. M. van Hest, "Well defined bioactive polymers by RAFT polymerization" *Polym. Prepr.* 2005, **46**, 492-493.

Conference Presentations

Oral

1. Sept. 2007 — 14^{th} European Carbohydrate Symposium

   "A Versatile Synthesis of Multifunctional Bioactive Glycopolymers"

2. Dec. 2006 — RSC Bio-organic Group Postgraduate Meeting

   "Controlled glycopolymer synthesis for the functionalization of surfaces"

Poster

1. March 2007 — Nanoparticles: New Opportunities and Challenges for Colloid Scientists

   "Synthesis of Bioactive Nanoparticles for Glycosylated Polymers"

2. Aug. 2006 Macro Group UK International Conference on Polymer Synthesis
   "Controlled Glycopolymer Synthesis for Surface Functionalization"

3. July 2006 23^{rd} International Carbohydrate Symposium
   "Controlled Glycopolymer Synthesis for Surface Functionalization"

4. Sept. 2005 UK Polymer Showcase 2005
   "Synthesis of gold nanoparticles functionalised with biologically active polymers for potential biomedical applications"

5. July 2005 MC7: Functional Materials for the 21st Century
   "Controlled Synthesis of Glycopolymers via RAFT Polymerisation"

6. June 2005 Macro Group UK: Innovative Polymer Synthesis - From Molecules to Microns
   "Controlled Synthesis of Glycopolymers for the Surface Functionalisation of Gold Particles"